Dissertation zur Erlangung des Doktorgrades

der Fakultät für Chemie und Pharmazie

der Ludwig-Maximilians-Universität München

Oligoaminoamide-Based siRNA Formulations for Folate Receptor-Directed Tumor Targeting and Gene Silencing

Dian-Jang Lee

aus

Taipeh, Taiwan

2016

Erklärung

Diese Dissertation wurde im Sinne von § 7 der Promotionsordnung vom 28. November 2011 von Herrn Prof. Dr. Ernst Wagner betreut.

Eidesstattliche Versicherung

Diese Dissertation wurde eigenständig und ohne unerlaubte Hilfe erarbeitet.

München, 03.11.2016

.....……

Dian-Jang Lee

Dissertation eingereicht am 03.11.2016

1. Gutachter: Prof. Dr. Ernst Wagner
2. Gutachter: Prof. Dr. Gerhard Winter

Mündliche Prüfung am 20.12.2016

Meiner Familie

“Wir müssen lernen, magische Kugeln zu gießen, die gleichsam wie Zauberkugeln des Freischützen nur die Krankheitserreger treffen.”
(We have to learn how to cast magic bullets, which behave like the magic bullets of a marksman and exclusively hit pathogens).

Paul Ehrlich
Nobel Prize in Physiology or Medicine, 1908

Table of Contents

1 Introduction

Since the discovery of RNA interference (RNAi), small interfering RNA (siRNA) provides a promising option for drug development in oncology over the past decade [1]. RNAi is an evolutionarily conserved phenomenon for sequence-specific gene silencing among multicellular organisms as diverse as plants, worms, yeast and humans, in which double-stranded RNA triggers specific degradation of the complementary mRNA sequence to silence the expression of target gene [2]. Since it was found that siRNA can also invoke RNAi responses in mammalian cells [3], this novel strategy has rapidly become a powerful tool for sequence-specific gene silencing, with many lead compounds in various stages of clinical development [4]. As viral vectors are not compatible with the delivery of synthetic siRNA, different non-viral delivery systems have sparkled intense investigations [5].

1.1 RNAi machinery

In mammalian cells, siRNA sequences are produced by the ribonuclease Dicer [6]. Dicer, an endonuclease of the RNase III family, precisely produces RNA duplexes ~21-23 nucleotides in length with a dinucleotide overhang at 3' end and a monophosphate group at 5' end [7]. The siRNA duplex length and characteristic termini are required for efficient recognition by and integration into the RNA-Induced Silencing Complex (RISC) [8]. RNAi is processed when siRNA is loaded into RISC [8], where the strands are separated, and the antisense strand (guide strand) directs sequence-specific cleavage of target mRNA in a manner of Watson-Crick base pairing [9]. The core of the RISC complex and crucial processor of RNAi is the Argonaute protein. There are four human Argonaute proteins (AGO 1-4), and siRNA-induced gene silencing is mediated *via* AGO2 [10]. AGO2 attaches the guide siRNA strand, extrudes the passenger strand, and then repeats target mRNA recognition, cleavage, and release [7]. Structurally, AGO2 has three functional domains: PAZ, MID, and PIWI. PIWI docking an RNase H fold is the motor for RISC's slice activity [11]. For RISC loading, PAZ domain is able to specifically recognize the 3' dinucleotide of siRNA, and such overhang enters deep into a hydrophobic pocket of the domain [12]. At the same time, the 5' phosphate group inserts between the MID and PIWI domains, binding to a magnesium ion [13]. For guide-strand selection, both the absolute and relative stabilities of the base pairs at the 5' end of the two siRNA strands determine which strand participates in the RNAi pathway, herein Argonaute selects the one with the less thermodynamically stable 5' end as the guide strand and cleaves the other one. Moreover, the guide siRNA strand inside RISC can be repeatedly used to target other complementary mRNA sequences. Such remarkable properties

have rendered the synthetic siRNA molecules for the therapeutic knockdown of endogenous mRNA [14].

1.2 Antitumoral siRNA therapeutics

Recently, numerous novel RNAi targets for malignancies have been identified, such as for breast cancer (WEE1) [15], glioma (PFKFB4) [16], multiple myeloma (GSK3) [17], and pancreatic cancer (CHK1) [18]. By silencing important oncogene targets in cancer cells, the siRNA therapeutics are showing impressive potential with several clinical trials are underway [19]. These include TKM-080301, siG12D LODER, siRNA–EphA2–DOPC, DCR-MYC, ALN–VSP02 and Atu027 (Table 1.2.1), providing hope to those with limited options for cancer survival. For examples, the company Arbutus developed TKM-PLK1 for hepatocellular carcinoma (HCC), using LNPs to deliver siRNA against polo-like kinase (PLK) [20]. PLK is mostly overexpressed in malignant cells, and inhibition of PLK results in reduced cell division [21]. Phase I trials indicated a dose-dependent effect and 19.3% reduction in tumor size [22]. Moreover, KRAS gene is overexpressed in more than 90% of pancreatic ductal adenocarcinomas [22]. To downregulate the KRAS gene, the company Silenseed's siG12D LODER is composed of polylactic glycolic acid as polymer matrix and an unmodified siRNA against a mutant KRAS gene, KRAS-G12D [22]. Phase I trials that combined siG12D LODER with chemotherapy resulted in a median survival of 16 months, compared with a median survival of 10–13 months for patients treated with only chemotherapy. More encouragingly, two patients have survived beyond 2 years [22]. siG12D LODER has now initiated Phase II/III trials of repeated doses every 4 months combined with chemotherapy [20]. As another example, EphA2 gene encoding the epithelial cell receptor protein–tyrosine kinase is frequently overexpressed in cancer cells and its expression level is related to tumor aggressiveness, tumor recurrence and survival [23]. In MD Anderson Cancer Center, Phase I study in 40 advanced solid tumors with a liposome-based siRNA therapeutic, siRNA-EphA2-DOPC, is currently ongoing to determine the maximum tolerated dose and efficacy of EphA2 gene silencing [20]. In addition, the company Dicerna has launched Phase II trials with DCR-MYC, a Dicer substrate–based RNAi therapeutic targeting the MYC oncogene in solid tumors (especially HCC), multiple myeloma and lymphoma [20].

One implicated oncological target gene is eglin 5 (EG5, also known as Kif11, KSP), a member of the Kinesin-5 subclass of kinesins, which is involved in the assembly and organization of the mitotic spindle apparatus, and is responsible for centrosome separation in cell division [24]. Thus, targeting siRNA against EG5 (siEG5) that corresponds to a sequence of the EG5 coding region

conserved between human and mouse, would represent an excellent strategy to hinder mitosis, leading to G2 arrest and eventually cell death of cancer cells [25-27]. However, early *in vivo* studies with siRNA described nuclease sensitivity and undesirable immunostimulatory effects [28]. For this, Judge *et al*. used 2' OMe-modified siRNA to prevent the recognition by the innate immune system [29, 30].

Table 1.2.1. RNAi-based drugs in clinical trials.[a]

Drug	Target	Delivery system	Disease	Phase	Company	NCT No.
TKM-080301	PLK1	LNP	HCC	I/II	Arbutus	NCT01262235
siG12D LODER	KRAS-G12D	Polymer (local administration)	Pancreatic cancer	I	Silenseed	NCT01188785 NCT01676259
siRNA–EphA2–DOPC	EphA2	LNP	Advanced cancers	I	MD Anderson	NCT01591356
DCR-MYC	MYC	LNP	Solid tumors, Multiple myeloma, Lymphoma	I I/II	Dicerna	NCT02110563 NCT02314052
ALN–VSP02	KSP & VEGF	LNP	Solid tumors	I	Alnylam	NCT01158079
Atu027	PKN3	LNP	Pancreatic cancer	II	Silence Therapeutics	NCT01808638

[a]Abbreviations: LNP, lipid nanoparticle; HCC, hepatocellular carcinoma; PLK1, polo-like kinase 1; LODER, local drug eluter; DOPC, 1,2-dioleoyl-sn-glycero-3-phosphocholine; EphA2, ephrin type-A receptor 2; KRAS-G12D, Kirsten rat sarcoma viral oncogene homolog G12D mutation. The information for clinical trials are published by U.S. National Institutes of Health [20].

1.3 Sequence-defined oligomers for siRNA delivery

The main hurdles against efficient cytosolic siRNA delivery include: (i) high charge distribution and size of siRNA impede its translocation through the cell membrane [31]; (ii) siRNA is biologically fragile and is actively targeted by nucleases for degradation in extracellular and intracellular environments [32]; (iii) upon systemic administration, negative charge of siRNA may be recognized by pattern recognition receptors (PRRs) triggering the innate immune response [5]; and naked siRNA is subject to rapid elimination by renal clearance [33]. It is generally realized that transforming siRNA from valuable research tool to clinical application is highly dependent on the development of safe and efficient delivery systems.

siRNA carriers have recently shown great potential for low toxicity and effective delivery to target cells/tissues [31, 34]. Recently, our laboratory, has developed a solid phase supported synthesis method [35], where oligoamidoamine building blocks (as proton sponge motifs) were applied together with lysines (as branching units), various fatty acids (as stabilizing hydrophobic domains), and cysteines (as bioreversible disulfide-forming units) to generate sequence-defined monodisperse peptide-like oligomers [26, 36, 37].

It is widely recognized that different non-viral vectors utilize different endocytic pathways in order to gain access to the cells [38]. Consequently, both vectors and their respective cargo remain to high extent entrapped in endosomal compartments and this endosomal entrapment serves as the main limiting factors in their efficient delivery. Many different strategies have been investigated aiming to induce endosomal escape [39]. Above-mentioned oligoamidoamine-based building blocks such as succinoyl-tetraethylene pentamine (Stp) and succinoyl-pentaethylene hexamine (Sph) [40] are designed in the way that they would act as proton sponge motifs, which express about 20% protonation of nitrogens at neutral pH and would become increasingly protonated with endolysosomal acidification. The influx of protons is followed by subsequent rupture of the endosomal membrane and release of the polyplexes [36, 39].

It is believed that polyplex formation between the cationic carriers and nucleic acids, *i.e.* siRNA, takes place due to the electrostatic interaction between the nitrogens of the oligomers and the phosphates of the siRNA [41]. In addition to electrostatic interaction, hydrogen bonding and hydrophobic interactions can increase polyplexes stability [39]. For example, lipid moieties can be incorporated to increase hydrophobicity, improve polyplex stability and also introduce pH-dependent lytic activity, leading to enhanced membrane destabilization with endosomal acidification [35, 36]. Moreover, the introduction of cysteines that allows disulfide crosslinking has been shown to increase particle stability during polyplex formation [36, 42]. In this case, it has been hypothesized that siRNA might help bringing the positively charged oligomer molecules together into close distance by charge neutralization, followed by disulfide formation to fix the nanostructure. Disulfide bonds are stable in the bloodstream but cleaved in the reducing environment of the cytosol [39], facilitating dissociation of the particle and release of the siRNA. Furthermore, these oligomers could be synthesized with very diverse molecular topologies such as i-shape, T-shape, U-shape or branched configurations. Promising candidates of the library such as oligomers **49**, **229**, **278**, **386** and **454** (Figure 1.3.1) have shown high activity for siRNA delivery, enabling successful silencing of target genes of interest in both *in vitro* and *in vivo* settings [35-37]. The addition of tyrosines to the terminal cysteines of **454** has rendered the carrier even more potent in terms of gene silencing efficiency [37]. From *in vivo* perspective, the three-arm oligomer **386** has displayed the fastest onset of protein knockdown and highest *in vivo* antitumoral effect [26]. These oligoamidoamine-based oligomers are also flexible for further functional modifications, as targeting and shielding moieties have been successfully incorporated into such oligomers [33].

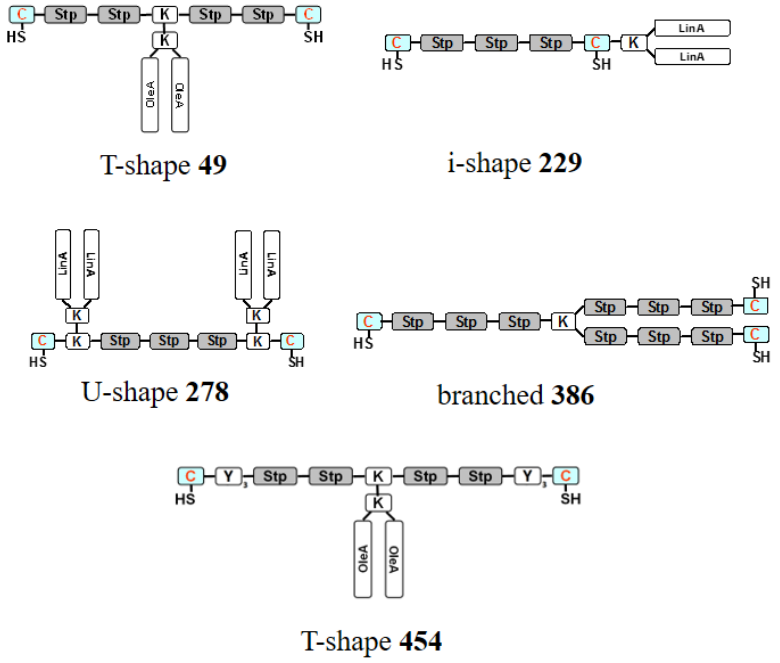

Figure 1.3.1. The structures of oligomers **49**, **229**, **278**, **386** and **454**. Apart from **386**, these oligomers are modified with lipid moieties and contain terminal cysteines, which form intermolecular disulfide bonds after siRNA polyplex formation. The oligotyrosines are added to the terminal cysteines of oligomer **454** as stabilizing components for siRNA polyplex formation.

1.3.1 Oligoglutamyl-methotrexate (MTX) as bifunctional targeting ligand

To improve the tissue selectivity and cellular uptake, *i.e.* to achieve targeted delivery, cationic oligomers could be modified with targeting motifs such as antibodies, antibody fragments, small molecules, and peptides [33, 43]. As previously reported, oligomer **356** (Figure 1.3.2) contains a electrostatic nucleic acid binding core consisted of a branched two-arm structure comprising eight Stp units providing the positive charge for siRNA binding, and two cysteines for disulfide-based polyplex stabilization [33]. Polyethylene glycol (PEG) comprising 24 ethylene oxide units are positioned in the center of the cationic two-arm cores for shielding of the positive surface charge and preventing unspecific protein bindings. Moreover, the folate is attached to the exposed part of the PEG segment, as targeting ligand for FR-overexpressing tumors. As a result, this folate-conjugated PEGylated oligomer can formulate siRNA as neutrally-charged monomolecular nanoplexes with hydrodynamic diameter of ~6 nm, successfully exhibiting FR-specific cellular uptake and gene silencing *in vitro* and *in vivo*.

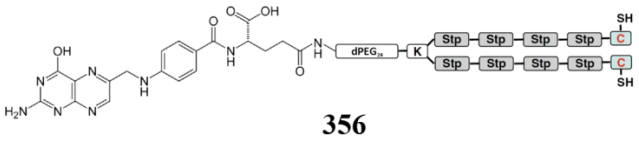

356

Figure 1.3.2. The structure of folate-conjugated PEGylated oligomer **356**.

An interesting strategy is to use a ligand that would be multifunctional, for example combining targeting capacity with chemotherapeutic activity. One molecule that could act in this manner is the widely used antifolate drug, methotrexate (MTX). MTX and folate (Figure 1.3.3) enter cells *via* two major transport systems: folate receptors (FR) and reduced folate carrier (RFC) [44]. The folate receptors consist of several isoforms. FR-α alone is expressed in normal epithelial cells and is frequently overexpressed in numerous carcinomas [45]; while RFC is ubiquitously distributed [46]. A broad variety of FR-targeted experimental therapies have focused on FR-α, which has thus served as a golden standard for targeted drug delivery [47]. Mostly, transport of low molecular weight (LMW) MTX occurs *via* the RFC (K_m~1–5 μM); however, LMW MTX also binds to the FR-α in the cells with FR-α upregulation [48]. After entering cells, glutamic acid residues are attached to MTX by the folylpolyglutamyl synthetase (FPGS), producing MTX polyglutamates which are retained in the cytosol and represent the more pharmacologically active form [49]. Polyglutamylated MTX inhibits dihydrofolate reductase (DHFR), resulting in inhibition of *de novo* thymidylate and purine synthesis, and consequently DNA and RNA synthesis [46]. Previous studies from our lab involving modification of polyglutamylation in covalent MTX-PEG-STP conjugates (**638**-**641**, see Figure 1.3.4) gave critical evidence that the glutamylation degree is closely related to DHFR inhibition potency, cytotoxicity, and cellular uptake [50]. In that work, a library of targeted PEGylated oligomers with bifunctional MTX ligands, in order to mediate FR-specific cellular delivery and augmented tumor suppression was designed and synthesized.

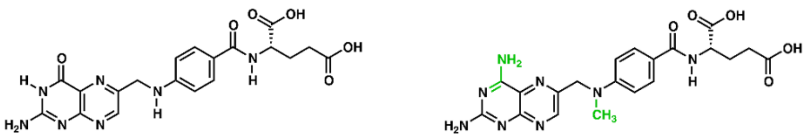

Folate Methotrexate (MTX)

Figure 1.3.3. The structures of folate and methotrexate (MTX). The structural differences between two compounds are highlighted in green.

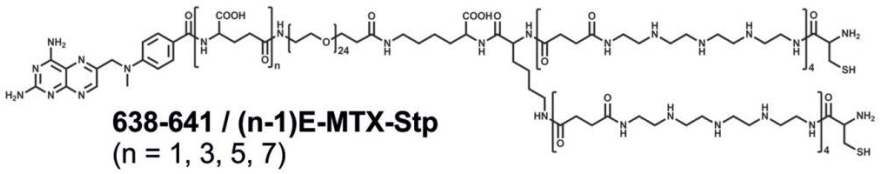

Figure 1.3.4. The structures of MTX-conjugated PEGylated oligomer **638**-**641**.

1.3.2 Combinatorial optimization of oligomers by covalent coupling

Successful applications of RNAi-based cancer therapy require sufficient intracellular delivery of siRNA to the site of action and effective knockdown of targeted transcripts. Thus, an ideal siRNA delivery system should possess multifunctionalities to conquer multiple barriers all the way to its target site [31]. Generally, the siRNA carrier needs to incorporate siRNA into nanoparticles of suitable size to protect siRNA from nucleases and renal clearance, and also enables passive targeting to tumor by enhanced permeability and retention (EPR) effect [51].

Combination of two different oligomers by covalent coupling provides an efficient alternative to obtain a multifunctional carrier, which may formulate therapeutic nucleic acids and overcome possible disadvantages of single oligomers. For example, a c-Met targeting PEGylated oligomer, which is deficient in DNA condensation, was combined in a 7/3 ratio with a 3-arm oligomer to facilitate nucleic acid compaction, and such compaction was critically required for efficient intravenous gene delivery, and resulted in greatly enhanced ligand-dependent gene expression in the distant tumor [52].

1.3.3 siRNA lipopolyplexes

As explained above, oligomer **356** (Figure 1.3.2.) successfully exhibited FR-specific cellular uptake and gene silencing *in vitro* and *in vivo* [33] . However, some limitations remained to be overcome. First, because of small particle size, **356** siRNA nanoplexes displayed a short circulation time of 15 min followed by renal excretion after systemic administration. Second, since **356** siRNA nanoplexes lack robust endosomal escape capacity, modification of siRNA with an endosomolytic Inf7 peptide is necessary for potent gene suppression [33, 53]. For systemic siRNA administration, an established strategy is to formulate various combinations of lipids and polycations to generate lipopolyplexes [54-56]. Hitherto, sorts of cationic polymers were utilized in lipopolyplexes such as branched polyethylenimine (bPEI), linear polyethylenimine (lPEI), poly-L-lysine (PLL), poly (beta-amino ester), protamine, chitosan, polyallylamine (PAA) and other constructs [57-59]. Low molecular weight polyethylenimine (PEI F25-LMW) and various lipid combinations are formulated as optimized lipopolyplexes for siRNA delivery [55]. Addition of negatively charged and rigid liposomes to pre-condensed polyplexes decreased intrinsic cytotoxicity of PEI [55]. Moreover, combination of PEI (2 kDa) and various cationic liposomes with or without transferrin was developed by Penacho *et al.* [60]. Among these transferrin-modified formulations lipopolyplexes composed of DOTAP/Chol showed the upmost transfection efficiency [60]. These results showed that the combination of the polyplexes with fatty acids renders DNA/siRNA carriers desirable physicochemical and pharmacological characteristics for a more efficient cargo delivery.

1.4 Aim of the thesis

Potent sequence-selective gene silencing by siRNA therapeutics is promising in cancer treatment, and the goal of this thesis was to optimize nanosized siRNA delivery system for *in vivo* application evaluated using antitumoral siRNA in the FR-overexpressing tumor models. Through various experiments we expected to achieve the following aims:

(i) The first aim was to evaluate a library of PEGylated Stp oligomers with bifunctional MTX ligands for siRNA delivery. It had to be investigated whether these siRNA polyplexes can access tumor cells specifically through the FR, and to be evaluated if Inf7-modified siEG5 (siEG5-Inf7) can be formulated with MTX-linked oligomers to mediate tumor cell-specific cytotoxicity *in vitro*. It also had to be examined if the transfection efficiency was elevated with an increasing degree of polyglutamylation of MTX-conjugated oligomers. Eventually, intratumoral treatment in KB tumor-bearing mice had to be performed, in order to find out whether these siRNA polyplexes can prolong tumoral retention time and enhance antitumoral effect *via* dual mechanisms.

(ii) Since systemic delivery of siRNA directed to the tumor site remains a major limitation, this thesis (together with the thesis of my colleague Dr. Dongsheng He) also aimed to optimize the physicochemical properties of polyplexes by combinatorial optimization of PEGylated folate-conjugated oligomer and 3-arm oligomer to generate targeted combinatorial polyplexes (TCPs). For uni-directional fast coupling between the two groups of oligomers, the cysteine thiol groups of one of the oligomers ought to be activated with 5,5'-dithio-bis(2-nitrobenzoic acid) to achieve a fast chemical linkage through disulfide formation with the free thiol groups of the other oligomer. The particle size, surface charge and siRNA binding activity of TCPs had to be assessed. By immuno-TEM in collaboration with Prof. Margus Pooga's lab (Institute of Molecular and Cell Biology, University of Tartu), we sought to confirm the involvement of FR in the cellular uptake of TCPs, and to gain more detailed insight into how these polyplexes associate with receptors and how they are endocytosed by cells. Finally, by *i.v.* administration of such formulation in L1210 tumor-bearing mice, we had to examine if siEG5-Inf7 TCPs were able to induce siRNA delivery and subsequent gene silencing in the tumors.

(iii) Next, siRNA polyplexes had to be optimized by co-formulating with a PEGylated folate-conjugated oligoaminoamide and one of several lipo-oligoaminoamides to develop targeted lipopolyplexes (TLPs), in which terminal cysteines of carriers stabilized TLPs by disulfide cross-linkage. This strategy was applied to render TLPs tunable sizes, surface shielding and improved

siRNA binding. In collaboration with Prof. Kazunori Kataoka's lab (Innovation Center of NanoMedicine and University of Tokyo), time-lapse confocal microscopy was used to investigate the colocalization of TLPs with endosomes and lysosomes and the onset of siRNA release from late endosomes. In addition, double-labeled siRNA had to be applied to analyze intracellular stability by FRET analysis. As to be tested by systemic administration in L1210 tumor-bearing mice, TLPs were anticipated to improve pharmacokinetic profile and mediate tumoral gene silencing efficiency with siEG5.

2 Materials and Methods

2.1 Materials

2.1.1 Chemicals and reagents

Inf7 peptide (GLFEAIEGFIENGWEGMIDGWYGC-amide) was obtained from Biosyntan (Berlin, Germany). 2-Chlorotrityl chloride resin, all Fmoc or Boc protected α-amino acids, peptide grade dimethylformamide (DMF), *N*-methyl-2-pyrrolidone (NMP), *N*,*N*-diisopropylethylamine (DIPEA), piperidine and trifluoroacetic acid (TFA) were purchased from Iris Biotech (Marktredwitz, Germany). Benzotriazol-1-yl-oxy-tris-pyrrolidino-phosphonium hexafluorophosphate (PyBOP) and syringe microreactors were obtained from Multisyntech GmbH (Witten, Germany). Folate, methotrexate, 1-hydroxy-benzotriazole (HOBt), triisopropylsilane (TIS), tris(2-carboxyethyl)phosphine (TCEP), 5,5'-dithio-bis(2-nitrobenzoic acid) (DTNB), 1,8-diazabicyclo[5.4.0]undec-7-ene (DBU), 3,6-dioxa-1,8-octanedithiol (DODT), dimethylsulfoxide (DMSO) and 3-(4,5-dimethylthiazol-2-yl)-2,5-diphenyltetrazolium bromide (MTT) were purchased from Sigma-Aldrich (Munich, Germany); hydrazine hydrate solution from Merck (Darmstadt, Germany), and 25% ammonia solution from Carl Roth (Karlsruhe, Germany). N^{10}-(trifluoroacetyl) pteroic acid was obtained from Niels Clauson-Kaas A/S (Farum, Denmark), and Fmoc-N-amido-dPEG$_{24}$-acid from Quanta Biodesign (Plain City, OH, USA). Fetal bovine serum (FBS) was purchased from Invitrogen (Karlsruhe, Germany), glucose from Merck (Darmstadt, Germany), and HEPES from Biomol GmbH (Hamburg, Germany). All other solvents were purchased from Sigma-Aldrich (Steinheim, Germany), Iris Biotech (Marktredwitz, Germany), Merck (Darmstadt, Germany), Bernd Kraft (Duisburg, Germany) or AppliChem (Darmstadt, Germany).

2.1.2 siRNA duplexes

For flow cytometry, Cy5-labeled siAHA1 was used:
sense: 5′-(Cy5)(NHC$_6$)-GGAuGAAGuGGAGAuuAGudTsdT-3′; antisense: 5′-ACuAAUCUCcACUUcAUCCdTsdT-3′ (Axolabs GmbH, Kulmbach, Germany).

For immuno-TEM, biotinylated siRNA was used:
sense: 5'-(biotinP)GAAAUCGCUGAUUUGUGUAdTdT-3'; antisense: 5'-UACACAAAUCAGCGAUUUCdTdT-3′ (P: phosphodiester) (Axolabs GmbH, Kulmbach, Germany).

For CLSM, Alexa Fluor (AF) 647-labeled siRNA was applied:
sense: 5'-AF 647-NH_2C_6-CUUACGCUGAGUACUUCGAdTdT-3'; antisense: 5'-UCGAAG UACUCAGCGUAAGdTdT-3' (Gene Design, Ibaraki, Japan).

For gene silencing studies, siRNA sequences were modified with Inf7 peptide: siGFP-Inf7 (sense: Inf7-ss-C_6-5′-AuAucAuGGccGAcAAGcAdTsdT-3′; antisense: 5′-UGCUUGUCGGC cAUGAuAUdTsdT-3′), siEG5-Inf7 (sense: Inf7-ss-C_6-5′-ucGAGAAucuAAAcu AAcudTsdT-3′; antisense: 5′-AGUuAGUUuAGAUUCUCGAdTsdT-3′) and control sequence siCtrl-Inf7 (sense: Inf7-ss-C_6-5′-AuGuAuuGGccuGuAuuAGdTsdT-3′; antisense: 5′-CuAAuAcAGGCcAAuAcA UdTsdT-3′). Unmodified siRNA sequences were exploited as comparison: siGFP (sense: 5'-AuAucAuGGccGAcAAGcAdTsdT-3'; antisense: 5'-UGCUUGUCGGCcAUGAuAUdTsdT-3') and siCtrl (sense: 5'-AuGuAuuGGccuGuAuuAGdTsdT-3'; antisense 5'-CuAAuAcAGGCcAAu AcAU dTsdT-3'); (Axolabs GmbH, Kulmbach, Germany).

For FRET study, Cy5/TAMRA double labeled siRNA was used (sense: 5'-Cy5-NH_2C_6-CUU ACGCUGAGUACUUCGAdTdT-NH_2C_6-TAMRA-3'; antisense: 5'-UCGAAGUACUCA GCGUAAGdTdT-3'); (Hokkaido System Science, Sapporo, Japan).

To evaluate *in vivo* biodistribution, we used Cy7-labeled siAHA1 (sense: C_6-ss-C_6-5′- GGAuGA AGuGGAGAuuAGudTsdT-3′; antisense: 5′-(Cy7)(NHC_6)ACuAAUCUCcACUUcAUCCdT sdT-3′); (Axolabs GmbH, Kulmbach, Germany) .
small letters: 2′-methoxy-RNA; s: phosphorothioate

2.1.3 Oligomers

Oligomers A-PEG_{24}-K(Stp_4-C)$_2$ (**188**), K(PEG_{24}-MTX)-K(Stp_4-C)$_2$ (**638**), K(PEG_{24}-E_2-MTX)-K(Stp_4-C)$_2$ (**639**), K(dPEG_{24}-E_4-MTX)-K(Stp_4-C)$_2$ (**640**), K(PEG_{24}-E_6-MTX)-K(Stp_4-C)$_2$ (**641**) and K(PEG_{24}-αMTX)-K(Stp_4-C)$_2$ (**642**) were provided by Dr. Ulrich Lächelt [50, 53], C-Stp_4-K(Stp_4-C)-dPEG_{24}-Folate (**356**) was provided by Dr. Dongsheng He and Philipp Klein [33], C-Stp_3-K-(Stp_3-C)$_2$ (**386**), C-H-(Stp-H)$_3$-K-[(H-Stp)$_3$-H-C]$_2$ (**689**), K-(PEG_{24}-Folate)-K-[K-(Sph_4-C)$_2$]$_2$ (**709**), K-(PEG_{24}-Folate)-K-(Sph_4-Y_3-C)$_2$ (**717**), TNB-C-Stp_3-K-(Stp_3-C-TNB)$_2$ (**769**), TNB-C-H-(Stp-H)$_3$-K-[(H-Stp)$_3$-H-C-TNB]$_2$ (**770**), K-(PEG_{24}-Folate)-K-[K-(Sph_4-C-TNB)$_2$]$_2$ (**873**) and K-(PEG_{24}-Folate)-K-(Sph_4-Y_3-C-TNB)$_2$ (**874**) were provided by Dr. Dongsheng, C-Y_3-Stp_2-[(OleA)$_2$-K]K-Stp_2-Y_3-C (**454**), C-Stp_2-[(OleA)$_2$-K]K-Stp_2-C (**49**) and (LinA)$_2$-K-C-Stp_3-C (**229**) were provided by Dr. Dongsheng and Sören Reinhard [36, 37].

2.2 Methods

2.2.1 siRNA polyplex formation

The amount of oligomer (n_{oligomer}, nmole) for the fixed amount of nucleic acid is calculated *via* N/P (pronatable amines of the oligomer/phosphates of the siRNA) ratio:

$$n_{\text{oligomer}}(nmole) = \frac{\text{m}_{\text{siRNA}}(\text{ng})}{\text{M}_{\text{siRNA}}} \cdot \text{P}_{\text{siRNA}} \cdot \frac{\text{N/P}}{\text{N}_{\text{oligomer}}}$$

m_{siRNA}: weight of siRNA (ng); M_{siRNA}: molecular weight of siRNA; P_{siRNA}: amount of phosphates of siRNA; $N_{oligomer}$: amount of pronatable amines of oligomer.

Polyplexes for transfections were prepared (unless otherwise mentioned) as follows: 500 ng of siRNA and the calculated amount of oligomer at the indicated N/P ratios were separately diluted in 10 µL of 20 mM HEPES buffered 5% glucose pH 7.4 (HBG). The oligomer solution was added to the nucleic acid solution and mixed by rapid pipetting (at least 5 times) to obtain totally 20 µL of polyplex solution. The polyplexes were allowed to form for 40 min under exposure to air oxidation at room temperature in the closed Eppendorf tube.

2.2.2 Formulation of targeted combinatorial polyplexes (TCPs)

Calculations of the individual two oligomers used at N/P 16 in formation of TCPs at indicated molar ratios were made as follows.

- Protonatable nitrogens (N) for the applied oligomers in the current work were calculated excluding histidine Ns (defined as unprotonated at pH 7.4): N = 29 for **386/769**, N = 29 for **689/770**, N = 68 for **709/873**, N = 34 for **717/874.**
- The required molar amine amounts of oligomers at N/P 16 were calculated, which are 24.88 nmol nitrogens (N) for 500 ng of siRNA (in transfection). For size measurements 10 µg of siRNA were used, corresponding to 498 nmol N.
- For the following calculation of the molar amount of each oligomer, general formulas were applied as follows:

1) $N/P_{total} = 16 = N/P_a + N/P_b$ ("a" and "b" to stand for the two oligomers).
2) Total molar amount of nitrogen $M_{total} = N_a \times M_a + N_b \times M_b$, here N stands for the number of protonatable nitrogens, while M stands for the molar amount.
3) The molar ratio of oligomers $M_a/M_b = R_a/R_b$.
   R stands for the ratio of each oligomer (1:1 in the majority of cases).
4) Calculation of the molar amount of each oligomer:

$M_a = 16 \times M_{total} \times N_a/(N_a + N_b \times R_b/R_a)$, and $M_b = 16 \times M_{total} \times N_b/(N_a \times R_a/R_b + N_b)$.

5) The individual N/P ratio for each oligomer (at $N/P_{total} = 16$):
   $N/P_a = 16 \times N_a/(N_a + N_b \times R_b/R_a)$, and $N/P_b = 16 \times N_b/(N_a \times R_a/R_b + N_b)$.

- As an example of TCP1 **386/873** at molar ratio 40:60, the individual N/P for **386** is 16 × 29/(29 + 68 × 60/40) = 3.5, for **873** it is 16 × 68/(29 × 40/60 + 68) = 12.5, and the molar amount M for **386** is 24.88 × 29/(29 + 68 × 60/40) = 5.45 nmol for 500 ng of siRNA.

Please note that, depending on the selected molar ratios and TCPs, the final molar ratios of thiol SH / TNB will differ. At oligomer molar ratio of 1:1, SH / TNB is 3:4 for TCP1, 2:3 for TCP2, 4:3 for TCP3, and 3:2 for TCP4.

siRNA polyplexes were prepared (unless otherwise mentioned) as follows: at the indicated N/P ratios, 500 ng of siRNA was diluted in 10 µL of HBG, and the calculated amount of the two oligomers for the designated [TNB-modified oligomer / unmodified mercapto-form of oligomer] molar ratio, were separately diluted in 5 µL of HBG. The solution of the first TNB-modified oligomer was added to the siRNA solution and mixed by rapid pipetting (at least 5 times) to obtain 15 µL of binary siRNA polyplex solution. After 30 min in the closed Eppendorf reaction tube at room temperature, the solution of the second oligomer was added to the siRNA polyplex solution, to obtain 20 µL of siRNA polyplex solution in total. The solution was placed for further 40 min at room temperature for disulfide formation.

2.2.3 Formulation of targeted lipopolyplexes (TLPs)

The individual two oligomers at N/P 16 in preparation of TLPs at indicated molar ratios were calculated as follows:

- Protonatable nitrogens (N) for the applied oligomers: N = 25 for **356**, N = 13 for **49**, N = 9 for **229**, N = 13 for **454**.
- The required molar amine amounts of oligomers at N/P 16 were calculated, which are 24.88 nmol nitrogens (N) for 500 ng of siRNA.
- For the following calculation of the molar amount of each oligomer, general formulas were applied as follows:

1) $N/P_{total} = 16 = N/P_a + N/P_b$ ("a" and "b" to stand for the two oligomers).
2) Total molar amount of nitrogen $M_{total} = N_a \times M_a + N_b \times M_b$, here N stands for the number of protonatable nitrogens, while M stands for the molar amount.
3) The molar ratio of oligomers $M_a/M_b = R_a/R_b$
   R stands for the ratio of each oligomer (*e.g.* **356**:**454** = 30%:70% for TLP1 and **356**:**49** =

30%:70% for TLP2).

4) Calculation of the molar amount of each oligomer:
   $M_a = 16 \times M_{total} \times N_a/(N_a + N_b \times R_b/R_a)$, and $M_b = 16 \times M_{total} \times N_b/(N_a \times R_a/R_b + N_b)$.
5) The individual N/P ratio for each oligomer (at $N/P_{total} = 16$):
   $N/P_a = 16 \times N_a/(N_a + N_b \times R_b/R_a)$, and $N/P_b = 16 \times N_b/(N_a \times R_a/R_b + N_b)$.

- As an example of TLP1 containing **356**:**454** at molar ratio of 30%:70%, the individual N/P for **356** is 16 × 25/(25 + 13 × 70/30) = 7.2, for **454** it is 16 × 13/(25 × 30/70 + 13) = 8.8, and the molar amount M for **356** is 24.88 × 25/(25 + 13 × 70/30) = 11.25 nmol for 500 ng siRNA.

siRNA polyplexes were prepared (unless otherwise mentioned) as follows: at the indicated N/P ratios, 500 ng of siRNA was diluted in 10 µL of HBG, and the calculated amount of the two oligomers for the designated [targeted PEG oligomer / lipo-oligomer] molar ratio at N/P 16 were diluted in 10 µL of HBG. The oligomer solution was added to the nucleic acid solution and mixed by rapid pipetting (at least 5 times) to obtain totally 20 µL of polyplex solution. The polyplexes were allowed to form for 40 min under exposure to air oxidation at room temperature in the closed Eppendorf tube.

2.2.4 Fluorescence correlation spectroscopy (FCS)

To estimate the hydrodynamic radii of the polyplexes, fluorescence correlation spectroscopy (FCS) was used. Unlabeled control siRNA (siCtrl) was spiked with 20% of Cy5-labeled siRNA in HBG. Polyplexes containing 10 µg of siRNA for the indicated N/P ratio were prepared in 50 µL of HBG. After incubation at room temperature for 40 min to form polyplexes, the samples were diluted 1:40 in HEPES (20 mM, pH 7.4) and were measured on a home-built confocal microscope by excitation of Cy5 with a pulsed 640 nm laser (LDH-D-C-640, Picoquant, Berlin, Germany). The FCS volume was calibrated using fluorophores with known diffusion coefficients with the calculated probe volume, where the diffusion coefficients could be directly determined by fitting the autocorrelation function. Hydrodynamic radii were calculated from the diffusion coefficients using the Stokes-Einstein relationship assuming a spherical shape of the particles. A detailed description of the method could be found in the supplementary materials in [53].

2.2.5 Size and zeta potential by dynamic light scattering (DLS) measurements

Particle sizes and zeta potentials of siRNA polyplexes were measured using Zetasizer Nano ZS (Malvern Instruments, Worcestershire, U.K.). siRNA polyplexes containing 1.5 µg of nucleic acid in a total volume of 60 µL were further diluted 1:20 with HEPES buffer (20 mM, pH 7.4) before measuring in a folded capillary cell (DTS1060 or DTS1070). For size measurements, each sample was measured three times with 10 subruns at 25 °C. Zeta potential was calculated by the Smoluchowski equation, and each sample was measured 3 times with 10 to 30 subruns at 25 °C.

2.2.6 Gel shift assay

A 2.5% (w/v) agarose gel was prepared by dissolving agarose in TBE buffer (10.8 g of Trizma base, 5.5 g of boric acid, 0.75 g of disodium EDTA, and 1 L of water). After adding GelRed (Biotium, Hayward, CA, USA), the agarose gel was formed in the electrophoresis chamber. siRNA polyplexes containing 500 ng of siRNA were formed and loaded into the wells in the gel after adding 4 µL of loading buffer (6 mL of glycerine, 1.2 mL of 0.5 M EDTA, 2.8 mL of H_2O, 0.02 g of bromophenol blue). Electrophoresis was performed at 120 V for 40 min and the results were recorded by UV transilluminator (Dark Hood DH-40, Biostep, Burkhardtsdorf, Germany).

2.2.7 Particle imaging by transmission electron microscopy (TEM)

A formvar-carbon 300 mesh copper grid (Ted Pella, Redding, CA, USA) was activated by mild plasma cleaning. Afterwards, one drop (10 µL) of the siRNA polyplex solution at N/P 16 (diluted in water) was placed on the grid. Excess liquid was blotted off using filter paper until the grid was almost dry. Subsequently, the copper grid was stained with 10 µL of 1% phosphotungstic acid (PTA) solution (Sigma-Aldrich, Munich, Germany), and analyzed using JEM 1011 transmission electron microscope (JEOL, Tokyo, Japan) at 80 kV.

2.2.8 Atomic force microscopy (AFM)

Polyplexes containing 10 µg of siRNA and the according amount of oligomer for N/P 16 were prepared in 50 µL of HBG. Samples were incubated for 40 min to ensure complete polyplex formation. Samples were diluted 1:50 for AFM measurements in HEPES (20 mM, pH 7.4). The glass slides (diameter of 30 mm, Assistent, Sondheim, Germany) were used as negatively charged flat substrates for particles to be attached onto. After polyplex formation, 500 µL of the diluted polyplexes with positive surface charge were deposited onto the glass slide, which was mounted

to a sample plate (Agilent Technologies, Santa Clara, CA, USA) and incubated for ~3 min, resulting in a surface coated with particles. The solution on the glass slide was subsequently replaced by the pure HEPES (20 mM, pH 7.4). After mounting the sample plate onto the AFM, the cantilever was installed into the device. Samples were imaged with the contact mode on AFM (AFM6000, Agilent Technologies, Santa Clara, CA, USA). Imaging at room temperature was performed with silicon nitride cantilevers (MSCT, nominal spring constant of 10 pN/nm, Bruker, Billerica, MA, USA). Imaging parameters were optimized for best image quality, in combination with the maintenance of the lowest possible set point to minimize damage to the samples.

2.2.9 Cell culture

As FR-expressing cell lines, murine lymphocytic leukemia cells (L1210), murine lung carcinoma cells (M109), human cervix carcinoma cells (KB), and human cervix carcinoma cells stably transfected with the eGFPLuc (enhanced green fluorescent protein/luciferase) gene (KB/eGFPLuc) were cultured in folate-free RPMI 1640 medium (Invitrogen, Karlsruhe, Germany), supplemented with 10% fetal bovine serum (FBS), 4 mM stable glutamine, 100 U/mL penicillin, and 100 µg/mL streptomycin. Human alveolar adenocarcinoma cells (A549), human mammary adenocarcinoma cells (MCF-7), and human mammary adenocarcinoma cells expressing eGFPLuc gene (MCF-7/eGFPLuc) were used as FR-deficient controls. A549 cells were maintained in Dulbecco's modified Eagle's medium (DMEM), supplemented with 10% fetal calf serum, 4 mM stable glutamine, 100 U/mL penicillin, and 100 µg/mL streptomycin. MCF-7 and MCF-7/eGFPLuc cells were grown in DMEM, supplemented with 20 % FBS, 4 mM stable glutamine, 100 U/mL penicillin, and 100 µg/mL streptomycin. The cells were cultured in ventilated flasks inside incubators at 37°C with 5% CO_2 in a humidified atmosphere. Cell lines were grown to 80 - 90% confluent and harvested.

2.2.10 Cellular association and internalization study

For flow cytometric measurements, unlabeled control siRNA (siCtrl) was spiked with 20% of Cy5-labeled siRNA (Cy5-siAHA1) in HBG. L1210 cells were seeded onto 24-well plates at a density of 2×10^5 cells/well in 450 µL of fresh growth medium. KB, M109, A549 and MCF-7 cells were seeded onto 24-well plates at a density of 5×10^4 cells/well, and 24 h later the medium was replaced by 450 µL of fresh growth medium. The cells were treated with 50 µL of siRNA polyplexes containing 2.5 µg of siRNA and corresponding amount of oligomer at N/P 16 (final siRNA concentration: 370 nM). The 24-well plates were incubated on ice for 45 min for cellular

association, or at 37 °C for 4 h for cellular internalization. Then the samples were prepared for flow cytometric measurements.

2.2.11 Ligand competition study

KB cells were seeded onto 24-well plates at a density of 5×10^4 cells/well, and 24 h later the medium was replaced with 450 µL of fresh growth medium, or 450 µL of fresh growth medium containing 100 µM MTX or 100 µM folate, and cells were incubated at 37 °C for 30 min. Then 50 µL of polyplexes containing 2.5 µg of siRNA and indicated amount of oligomer at N/P ratio of 16 (final siRNA concentration: 370 nM) were applied onto the cells. The cells were placed in the incubator at 37 °C for 4 h before flow cytometric measurement.

2.2.12 Fluorescence resonance energy transfer (FRET) intensity in Cy5/TAMRA double-labeled siRNA

KB or L1210 cells were seeded onto 12-well plates at a density of 5×10^4 cells/well, and 24 h later the medium was replaced with 900 µL of fresh growth medium. The cells were treated with 100 µL of polyplexes containing 5 µg of Cy5/TAMRA double-labeled siRNA at N/P 16 (final siRNA concentration: 370 nM) for 45 min. The cells were placed in the incubator at 37 °C for 2 and 4 h before flow cytometric measurement.

2.2.13 Flow cytometry

After transfection, the medium was removed and cells were washed twice with PBS. KB, M109 and MCF-7 cells were trypsinized, and then trypsin was inactivated with 1000 µL of FACS buffer (10% FBS in PBS). The cells were centrifuged (1000 rpm; 5 min) and then resuspended in 600 µL of FACS buffer. For cellular internalization study, the samples were immediately mixed with DAPI at a final concentration of 1 ng/µL before flow cytometry. The amount of Cy5-positive cells was counted through excitation of Cy5 at 635 nm and detection of emission at 665/20 nm by Cyan ADP flow cytometer (Beckman Coulter, Fullerton, CA, USA). The results were recorded by Summit software V4.3.02 (Summit, Jamesville, NY, USA) and evaluated using FlowJo V10.0.6 software (FlowJo, Ashland, OR, USA). For FRET analysis, fluorescence intensity of the cells was measured by BD LSRFortessa X-20 (BD Biosciences, Franklin Lakes, NJ, USA) and evaluated using FACSDiva software (BD Biosciences, Franklin Lakes, NJ, USA) at excitation wavelength of 488 nm and a 660/20 nm filter. All experiments were performed in triplicates.

2.2.14 Intracellular distribution of siRNA polyplexes by time-lapse imaging

5×10^5 KB cells were seeded on 35 mm micro-dishes (ibidi GmbH, Martinsried, Germany) and were incubated with CellLight Late Endosomes-RFP and CellLight Lysosomes-GFP (both from Molecular Probes, Eugene, OR, USA) overnight before measurements. Unlabeled control siRNA (siCtrl) was spiked with 30% of AF 647-labeled siRNA in HBG. Polyplexes containing 5 µg of siRNA for N/P 16 were prepared in 100 µL of HBG. The medium was replaced with 900 µL of fresh medium and 100 µL of polyplexes containing 5 µg of siRNA at N/P 16 (final siRNA concentration: 370 nM). The nuclei were stained with 10 µL/mL of Hoechst 33342 (Dojindo Laboratories, Kumamoto, Japan) for 3 min. The intracellular distribution of siRNA was observed using time-lapse imaging by CLSM (LSM 880, Carl Zeiss, Oberkochen, Germany) for 16 h with a Plan-Apochromate 63×/1.4 oil objective lens, diode laser (405 nm) for Hoechst 33342, Ar laser (458 nm/488 nm/514 nm) for CellLight Late Endosomes-GFP, DPSS laser (561 nm) for CellLight Late Endosomes-RFP and He−Ne laser (633 nm) for AF 647. ZEN 2.1 software (Carl Zeiss, Oberkochen, Germany) was used to process the imaging data.

2.2.15 Endosomal escape of siRNA polyplexes by 3D image reconstruction

5×10^5 KB cells were seeded on 35 mm micro-dishes (ibidi GmbH, Martinsried, Germany) and were incubated with CellLight Late Endosomes-RFP and CellLight Lysosomes-GFP (both from Molecular Probes, Eugene, OR, USA) overnight before measurements. Unlabeled control siRNA (siCtrl) was spiked with 30% of AF 647-labeled siRNA in HBG. Polyplexes containing 5 µg of siRNA for N/P 16 were prepared in 100 µL of HBG. The medium was replaced with 900 µL of fresh medium, and 100 µL of polyplex containing 5 µg of siRNA at N/P 16 was added (final siRNA concentration: 370 nM). After transfection for 45 min, the intracellular distribution of siRNA was observed using 3D reconstruction from serial images from single cell by super-resolution CLSM (LSM 880 combined, Carl Zeiss, Oberkochen, Germany) at 4 h with the abovementioned lens and lasers.

2.2.16 Colocalization analysis of siRNA polyplexes and endolysosomal vesicles.

5×10^4 KB cells were seeded onto 8-well micro-chamber slides (ibidi GmbH, Martinsried, Germany). The medium was replaced by 180 µL of fresh medium 24 h later. Unlabeled control siRNA (siCtrl) was spiked with 30% of AF 647-labeled siRNA in HBG. Late endosomes and lysosomes were labeled with LysoTracker Green (Molecular Probes, Eugene, OR, USA) and the cells were transfected with 20 µL of polyplexes (final concentration: 370 nM at N/P 16) for 45 min. The transfection medium was removed, and then cells were washed with 200 µL of PBS and fixed with 4% paraformaldehyde. Nuclei were stained with DAPI. The intracellular distribution of siRNA was observed by CLSM (LSM 880, Carl Zeiss, Oberkochen, Germany) at 2 and 4 h using a 63×/1.4 oil objective lens, diode laser (405 nm) for DAPI, Ar laser (458 nm/488 nm/514 nm) for LysoTracker Green and He−Ne laser (633 nm) for AF 647.

Colocalization ratios of AF 647-labeled siRNA with late endosomes and lysosomes were calculated using ZEN 2.1 software as follows:

colocalization ratio = AF 647 $pixels_{colocalization}$ /AF 647 $pixels_{total}$

where AF 647 $pixels_{colocalization}$ represents the number of AF 647 pixels overlapping with LysoTracker Green, and AF 647 $pixels_{total}$ represents the total number of AF 647-positive pixels in the cell. For each condition, colocalization ratios were calculated from 5 individual cells.

2.2.17 Fluorescence resonance energy transfer (FRET) imaging in Cy5/TAMRA double-labeled siRNA

5×10^4 KB cells were seeded onto 8-well micro-chamber slides (ibidi GmbH, Martinsried, Germany) and labeled with CellLight Lysosomes-GFP (Molecular Probes, Eugene, OR, USA) overnight before measurements. The medium was replaced by 180 µL of fresh medium, and the cells were transfected with 20 µL of polyplexes containing Cy5/TAMRA double-labeled siRNA (final concentration: 370 nM at N/P 16) for 45 min. The transfection medium was removed, and then cells were washed with 200 µL of PBS and fixed with 4% paraformaldehyde. Nuclei were stained with DAPI. The FRET signal of siRNA was observed by CLSM (LSM 880, Carl Zeiss, Oberkochen, Germany) at 1 and 24 h using a 561nm excitation laser and the lambda stacks were obtained within a range of 565 to 700 nm at a bandwidth of 4.5 nm. The spectral images obtained were linearly unmixed to Cy5 and TAMRA spectra.

2.2.18 Pre-embedding immuno-labeling for TEM

To visualize the siRNA molecules for immuno-electron microscopy, the biotinylated siRNA (740 nM) was first associated with 10 nm neutravidin-gold conjugate (at molecular ratio of 3:1) for 10 min, followed by complexation with the calculated amount of oligomers at N/P 16 in HBG. KB cells were seeded onto round glass coverslips (diameter of 12 mm, Menzel Gläser, Braunschweig, Germany) in 35 mm petri dishes and grown to 80–90% confluence. Thereafter, the coverslips were transferred into wells of 24-well plate and incubated with siRNA polyplexes in culture medium for 15 min, 1 h or 4 h at 37 °C. After incubation, the cells were washed and fixed with PLP fixative according to McLean and Nagane [61] (2% formaldehyde, 0.01 M sodium periodate, 0.075 M lysine in 0.075 M sodium phosphate buffer) at room temperature for 2 h. Cells were slightly permeabilized with 0.01% saponin (Sigma-Aldrich, St. Louis, MO, USA) supplemented with 0.1% BSA in 0.1 M sodium phosphate buffer for 8 min. After permeabilization, the cells were stained with mouse IgG against FR (R&D Systems, Minneapolis, MN, USA) for 1 h and Protein G-6 nm gold conjugate (1:40) (Aurion Immuno Gold Reagents & Accessories, Wageningen, Netherlands) for an additional 1 h. Then the cells were washed, postfixed with 1% osmium tetroxide in the 0.1 M sodium cacodylate buffer (pH 7.4) for 1 h at room temperature, and dehydrated with ethanol. The specimens were embedded in epoxy resin (TAAB Laboratories Equipment Ltd., Reading, UK), cut into ultrathin sections, and contrasted with uranyl acetate and lead citrate. The sections were examined with Tecnai G2 Spirit BioTWIN transmission electron microscope (FEI, Eindhoven, Netherlands) at 120 kV. Electron microphotos were analyzed and processed with Photoshop CS6 (Adobe, San Jose, CA, USA).

2.2.19 Gene silencing mediated by GFP-siRNA *in vitro*

Cells were seeded in 100 µL of medium using 96-well plates at a density of 4×10^3 cells for KB/eGFPLuc and 5×10^3 cells for MCF-7/eGFPLuc per well 24 h prior to the experiment. Before the treatment, medium was replaced with 80 µL of fresh growth medium. siGFP and siGFP-Inf7 were used for silencing of the eGFPLuc protein in comparison with control siRNA (siCtrl and siCtrl-Inf7). Cells were transfected with 20 µL of siRNA polyplexes containing 500 ng of siRNA at certain N/P ratios (final siRNA concentration: 370 nM) at 37 °C for 45 min, then the medium was replaced by 100 µL of fresh growth medium. After incubation for 48 h, the medium was removed and 100 µL of cell culture lysis reagent (Promega, Mannheim, Germany) was added per well. Luciferase activity was measured using the luciferase assay kit (Promega, Mannheim, Germany) and recorded on a Centro LB 960 plate reader luminometer (Berthold, Bad Wildbad, Germany). The relative light units (RLU) are presented as percentage of the luciferase gene

expression obtained with untreated control cells.

2.2.20 Cytotoxicity mediated by EG5 knockdown or MTX conjugates

4×10^3 KB or M109 cells per well were seeded into 96-well plates in 100 µL of growth medium 24 h prior to the treatment. Medium was replaced by 80 µL of fresh medium and 20 µL of polyplexes (at N/P 16 with siEG5, siCtrl, siEG5-Inf7, or siCtrl-Inf7; final concentration of siRNA: 370 nM), plain oligomer, or MTX solution in HBG. After incubation for 24 h (37 °C, 5% CO_2), medium was replaced by 100 µL of fresh growth medium and the cells were maintained for 24 h (37 °C, 5% CO_2). MTT assay (Life Technologies, Darmstadt, Germany) for metabolic activity was performed to evaluate the cell viability and measured by SpectraFluor Plus microplate reader (Tecan, Männedorf, Switzerland). The experiments were performed in triplicates and the cell viability was calculated as percentage compared to untreated control cells.

2.2.21 Evaluation of mitotic aster formation

KB or M109 cells (1×10^4/well) were seeded in 200 µL of fresh growth medium using 8-well Lab-Tek chamber slides (Nunc, Penfield, NY, USA). The medium was replaced by 180 µL of fresh medium 24 h later. The cells were transfected with 50 µL of polyplexes containing 1.15 µg of siRNA (with siEG5, siCtrl, siEG5-Inf7, or siCtrl-Inf7; final concentration: 370 nM at N/P 16) and incubated for 48 h (37 °C, 5% CO_2). The transfection medium was removed, and then cells were washed with 200 µL of PBS and fixed with 4% paraformaldehyde. Nuclei were stained with DAPI (1 µg/mL) and observed under Axiovert 200 fluorescence microscope (Carl Zeiss, Oberkochen, Germany).

2.2.22 Quantitative real-time polymerase chain reaction (qRT-PCR)

qRT-PCR was performed to determine the mRNA level of EG5 gene in transfected cells. KB or L1210 cells (1.5×10^5/well) were seeded in 900 µL of medium onto 6-well plates. The cells were treated with 100 µL of siRNA polyplexes (N/P 16) with a final siRNA concentration of 370 nM and incubated for 24 h. Total RNA was isolated by miRCURY RNA Isolation Kit (Exiqon, Vedbaek, Denmark) followed by reverse transcription using Transcriptor High Fidelity cDNA Synthesis Kit (Roche, Mannheim, Germany) according to the manufacturers' protocols. qPCR was performed in triplicates on a LightCycler 480 system (Roche, Mannheim, Germany) using UPL Probes (Roche, Mannheim, Germany) and Probes Master (Roche, Mannheim, Germany) with GADPH as housekeeping gene. The following probes and primer sequences were used:

human or murine GAPDH (ready-to-use in UPL), human EG5 (UPL Probe #53) (forward: CATCCAGGTGGTGGTGAGAT, reverse: TATTGAATGGGCGCTAGCTT), and murine EG5 (UPL Probe #100) (forward: TTCCCCTGCATCTTTCAATC, reverse: TTCAGGCTTATTCAT TATGTTCTTTG). Results were analyzed by the ΔC_T method. C_T values of GAPDH were subtracted from C_T values of EG5. ΔC_T values of transfected cells were calculated as percentage relative to untreated control cells.

2.2.23 Tumor mouse model

Female 8-week-old nude mice, Rj: NMRI-nu (nu/nu) (Janvier, Le Genest-Saint-Isle, France), were housed in isolated ventilated cages under specific pathogen-free condition with a 12 h light/dark interval, and were acclimated for at least 7 days prior to experiments. Food and water were provided *ad libitum*. Animals were injected with 5×10^6 KB or $0.5\text{-}2 \times 10^6$ L1210 cells subcutaneously (*s.c.*) for biodistribution study, and were injected with 5×10^6 KB or 1×10^6 L1210 cells subcutaneously for EG5 gene silencing assay *in vivo*. The body weight was recorded, and the tumor volume was measured by caliper and calculated as [0.5 × (longest diameter) × (shortest diameter)^2] as stated by Xu *et al.* [62]. All animal experiments were performed according to guidelines of the German law for the protection of animal life and were approved by the local animal ethics committee.

2.2.24 Biodistribution study

For near infrared (NIR) *in vivo* imaging, unlabeled control siRNA (siCtrl) was spiked with 50% of Cy7-labeled siRNA (Cy7-siAHA1) in HBG. When tumors reached the size of 500–800 mm^3, the mice (n = 3-4/per group) were anesthetized with 3% isoflurane in oxygen. siRNA polyplexes containing 50 µg of Cy7-labeled siRNA (N/P 16) in 50 µL of HBG were injected intratumorally (*i.t.*), or in 250 µL of HBG were injected intravenously (*i.v.*), and fluorescence was measured with a CCD camera. Animals were sacrificed for *ex vivo* imaging of tumors and organs at different time intervals after injection. For evaluation of images, efficiency of fluorescence signals was analyzed, after color bar scales were equalized using IVIS Lumina system with Living Image software 3.2 (Caliper Life Sciences, Hopkinton, MA, USA).

2.2.25 Antitumoral potency mediated by EG5 knockdown and MTX conjugates

The animals were randomly divided into 6 groups (n = 6), and 2 days after inoculation of tumor cells, the animals were injected *i.t.* with 50 µL of polyplexes containing 50 µg of siRNA at N/P 16, corresponding amount of plain oligomer or methotrexate. Treatments were applied on day 2, 4, 7, 10, 14 and 17. Tumor sizes of the animals were monitored. Animals were sacrificed after the tumor size reached 1000 mm^3, and Kaplan–Maier survival analysis was performed to compare the lifetime after treatments among different groups.

2.2.26 Gene silencing mediated by EG5-siRNA *in vivo*

When tumors reached 500 mm^3, mice (n = 5/per group) were injected *i.v.* with polyplexes containing 50 µg of siRNA (at N/P 16 with siEG5, siCtrl, siEG5-Inf7, or siCtrl-Inf7) 48 and 24 h before euthanasia. As a part of terminal procedure, blood samples were obtained by cardiac puncture for blood biochemistry examination. After tumors were harvested and homogenized, total RNA was extracted using Trifast (Peqlab, Erlangen, Germany) according to the manufacturer's protocol. The reverse transcription and qRT-PCR was performed as aforementioned.

2.2.27 Blood biochemistry examinations

To isolate plasma, blood samples were collected in EDTA-coated tubes (Multivette 600, Sarstedt, Nümbrecht, Germany) and centrifuged at 3000 rpm for 7 minutes. The supernatant was analyzed for clinical biochemistry parameters: alanine aminotransferase (ALT), aspartate aminotransferase (AST), blood urea nitrogen (BUN) and creatinine in the Clinic of Small Animal Medicine, Faculty of Veterinary Medicine, Ludwig-Maximilians-Universität München.

2.2.28 Statistical analysis

Statistical analysis of the results (mean ± SEM) was evaluated by unpaired *t* test: *$p<0.05$; **$p<0.01$; ***$p<0.001$.

3 Results

3.1 Glutamylated MTX-conjugated nanoplexes

3.1.1 Oligomer structures

This chapter has been partly adapted from:
D.J. Lee, E. Kessel, D. Edinger, D. He, P.M. Klein, L. Voith von Voithenberg, D.C. Lamb, U. Lächelt, T. Lehto, E. Wagner, Dual antitumoral potency of EG5 siRNA nanoplexes armed with cytotoxic bifunctional glutamyl-methotrexate targeting ligand, Biomaterials, 77 (2016) 98-110.

As described previously by Lächelt *et al*. [50], based on solid-phase-supported synthesis method [35, 63] multiple copies of the artificial oligoamino acid succinoyl tetraethylene pentamine (Stp) as a cationic backbone were combined together with α-amino acids, PEG segment and bifunctional MTX ligand to generate sequence-defined monodisperse peptide-like oligomers for siRNA delivery [50] (Figure 3.1.1A). A two-armed structure was linked by lysine, in which each arm was composed of 4 Stp and a terminal cysteine. In the center of the two-armed core, PEG comprising 24 ethylene oxide units was coupled. MTX was attached *via* the γ- (**638**-**641**), or α-carboxy group (**642**) of glutamic acid to the exposed part of the PEG segment. For assessment of polyglutamylation-related activity of MTX conjugates, 2 (**639**), 4 (**640**) or 6 (**641**) glutamic acid units between the γ-carboxy group of MTX and the PEG segment had been introduced. Structures are illustrated in Figure 3.1.1B and listed in Table 3.1.1. For control structures, folate was used as non-toxic monofunctional targeting ligand (**356**) and alanine as a non-functional ligand substitute (**188**).

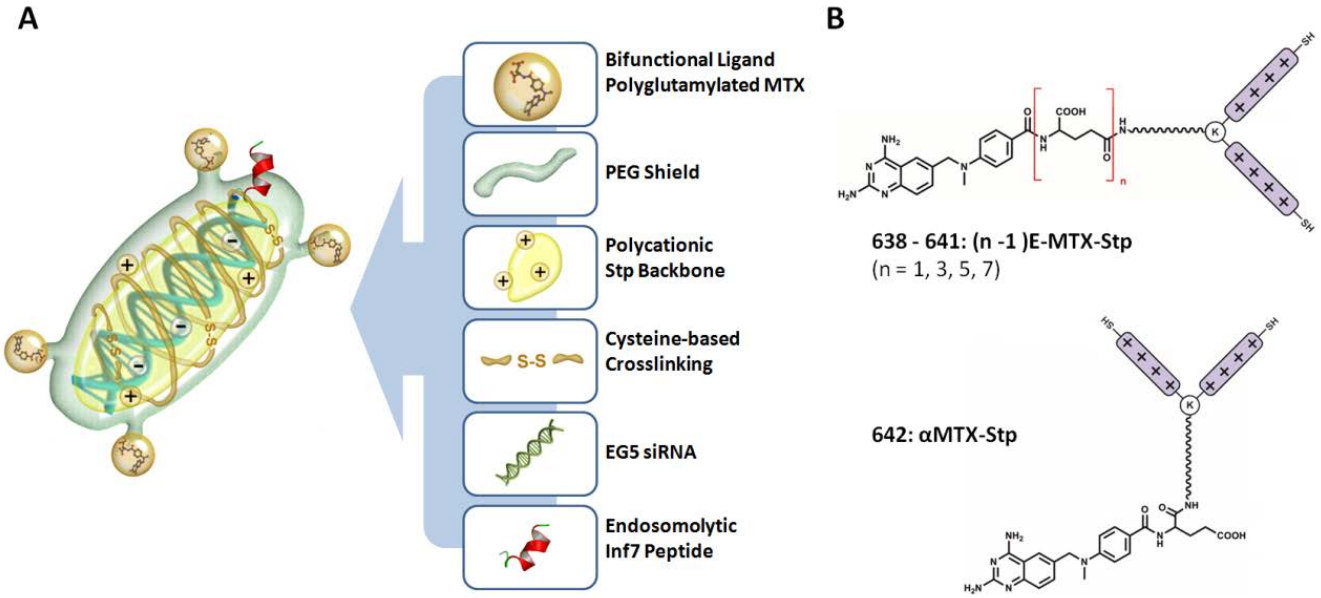

Figure 3.1.1. Polyplexes with bifunctional polyglutamylated MTX ligand for siRNA delivery. (A) Schematic diagram of the siRNA polyplex formulation. (B) Overview of the oligomers with MTX polyglutamates. The synthetic procedures were described in Lächelt *et al.* [50]. A two-armed structure was linked by lysine, in which each arm composed of 4 Stp and a terminal cysteine. MTX was attached *via* γ- (**638**-**641**), or α-carboxy group (**642**) to the exposed part of the PEG segment. "K" represents lysine. "+" in gray represents a cationic oligoamino acid building block (Stp). "~" represents $dPEG_{24}$ motifs.

Table 3.1.1. The sequences of oligomers.[a]

Oligomer	Sequence (C→N)	Abbreviation
188	A-$dPEG_{24}$-K(Stp_4-C)$_2$	A-Stp
356	C-Stp_4-K(Stp_4-C)-$dPEG_{24}$-FolA	FolA-Stp
638	K($dPEG_{24}$-MTX)-K(Stp_4-C)$_2$	MTX-Stp
639	K($dPEG_{24}$-E_2-MTX)-K(Stp_4-C)$_2$	2E-MTX-Stp
640	K($dPEG_{24}$-E_4-MTX)-K(Stp_4-C)$_2$	4E-MTX-Stp
641	K($dPEG_{24}$-E_6-MTX)-K(Stp_4-C)$_2$	6E-MTX-Stp
642	K($dPEG_{24}$-αMTX)-K(Stp_4-C)$_2$	αMTX-Stp

[a] A, alanine; C, cysteine; E, glutamic acid; K, lysine; Stp, succinoyl tetraethylene pentamine; $dPEG_{24}$, poly(ethylene glycol); FolA, folic acid; MTX, methotrexate. Details can be found in [50].

3.1.2 Physicochemical characteristics of MTX-conjugated siRNA polyplexes

siRNA was formulated with MTX conjugates at different N/P ratios and measured the particle sizes by fluorescence correlation spectroscopy (FCS). As shown in Table 3.1.2 and Figure 3.1.2, the hydrodynamic diameter for different oligomers at N/P 16 was ranging between 5.2 to 6.6 nm. Similarly, polyplexes formed at different N/P ratios did not affect the size significantly, for example, MTX conjugate **640** formed polyplexes with the size between 5.6 to 6.4 nm at different N/P ratios (Figure 3.1.3).

Table 3.1.2. Hydrodynamic diameter (d_h) of polyplexes loaded with Cy5-labeled siRNA at different N/P ratios determined by fluorescence correlation spectroscopy (FCS).

Oligomer	N/P	d_h (nm)[c]	Diffusion Coefficient (μm²/s)
Cy5-siRNA	-	4.6 (± 0.2)	96 (± 2) [b]
356	16	6.6 (± 0.3)	66 (± 1) [a]
638		5.6 (± 0.3)	79 (± 1) [a]
639		5.6 (± 0.3)	78 (± 1) [a]
641		5.2 (± 0.2)	86 (± 2) [a]
640	3	5.6 (± 0.3)	79 (± 1) [a]
	10	6.2 (± 0.3)	70 (± 2) [a]
	16	6.4 (± 0.3)	68 (± 1) [a]
	20	5.8 (± 0.3)	75 (± 2) [a]
	28	5.8 (± 0.3)	75 (± 2) [a]

[a] Errors for the diffusion coefficients are given as Jacobians of the fit. They do not contain any information about systematic deviations.
[b] The error for Cy5-siRNA was determined from six independent measurements of the siRNA.
[c] The absolute errors of the hydrodynamic diameters of the polyplexes were calculated as described in supplementary methods in [53]. The experiments were performed in collaboration with Dr. Lena Voith von Voithenberg (Department of Chemistry, Ludwig-Maximilians-Universität München).

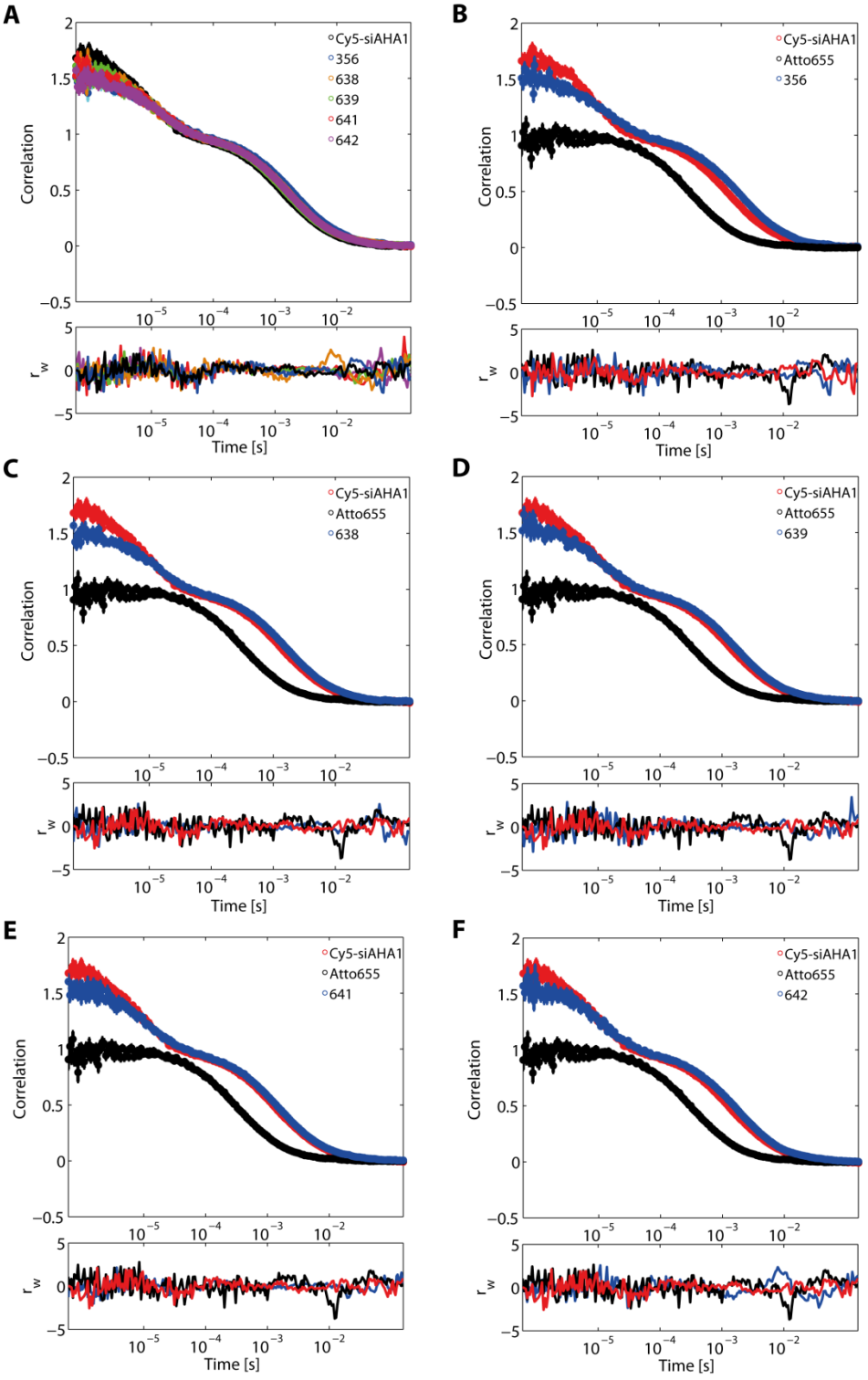

Figure 3.1.2. FCS measurements of Cy5-labeled polyplexes at N/P 16 in comparison to free Atto655 and Cy5-siRNA (Cy5-siAHA1). (A) As an overview, the normalized autocorrelation functions and weighted residuals for the fitted data for free Cy5-siRNA, and **356**, **638**, **639**, **641**, and **642** polyplexes. (B-F) Comparison of normalized autocorrelation functions of Atto655, Cy5-siRNA, and (B) **356**, (C) **638**, (D) **639**, (E) **641**, (F) **642** polyplexes. The experiments were performed in collaboration with Dr. Lena Voith von Voithenberg (Department of Chemistry, Ludwig-Maximilians-Universität München).

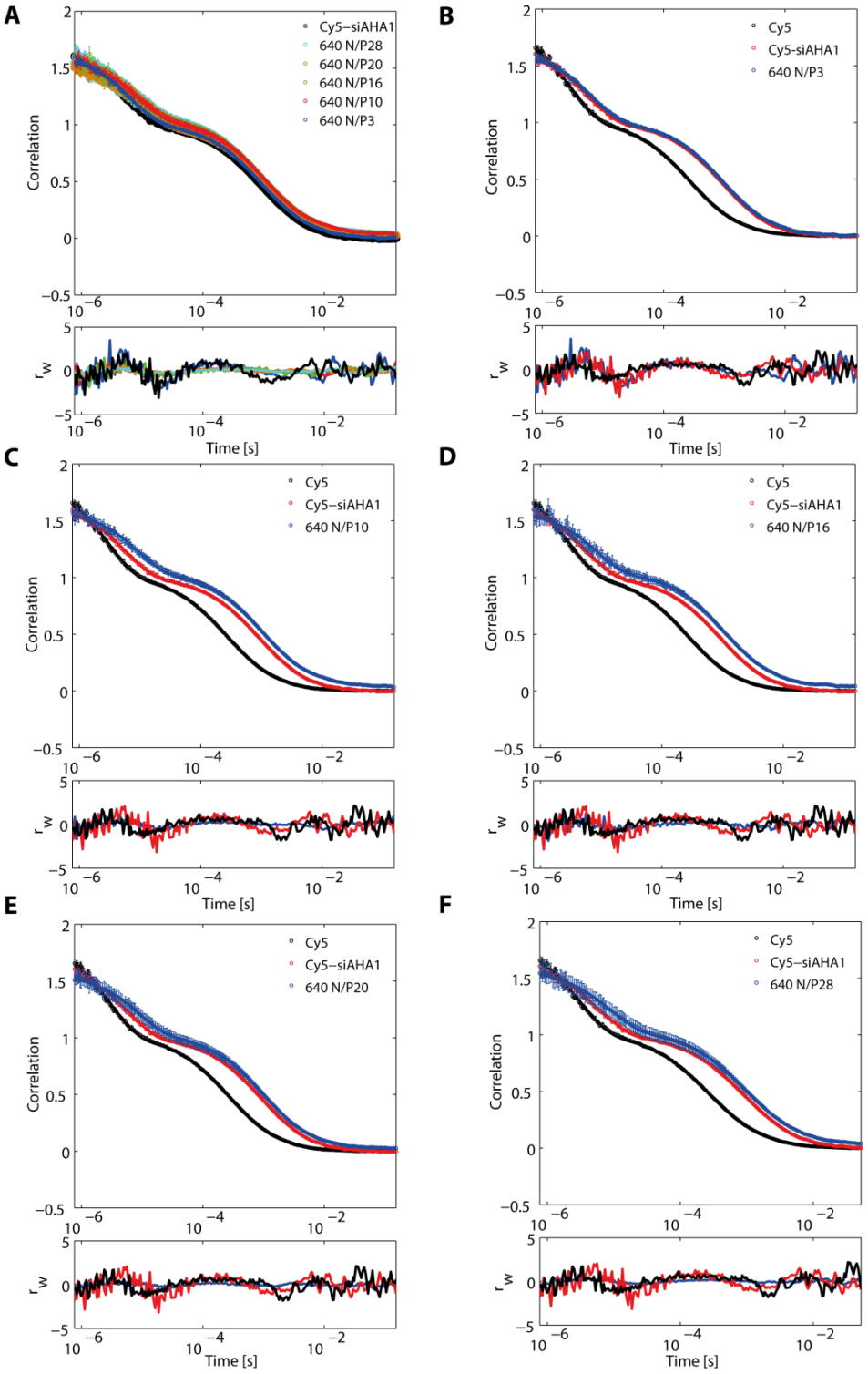

Figure 3.1.3. FCS measurement of Cy5-labeled **640** polyplexes at different N/P ratios in comparison to free Cy5 and Cy5-siRNA (Cy5-siAHA1). (A) As an overview, the normalized autocorrelation functions and weighted residuals for the fitted data of free Cy5-siRNA, and **640** polyplexes at different N/P ratios. (B-F) Comparison of normalized autocorrelation functions of Cy5, Cy5-siRNA, and the polyplexes at (B) N/P 3, (C) N/P 10, (D) N/P 16, (E) N/P 20, and (F) N/P 28. The experiments were performed in collaboration with Dr. Lena Voith von Voithenberg (Department of Chemistry, Ludwig-Maximilians-Universität München).

Previous findings indicated that such very small oligomer/siRNA nanoplexes are not suitable for standard analysis by dynamic laser light scattering (DLS) [64-66]. Therefore, to further study the morphology of **640** siRNA polyplexes, we carried out atomic force microscopy (AFM) and transmission electron microscopy (TEM) measurements. As shown in Figure 3.1.4 and 3.1.5, these images indicated the formation of homogeneous spherical nanoparticles with size (7.7 ± 0.8 nm by AFM; 6.8 ± 0.2 nm by TEM) in a range similar to the FCS measurements. Also in the FCS experiments, no aggregation was observed for these polyplexes. Hence, all evidence indicates that the siRNA polyplexes were shielded and stable.

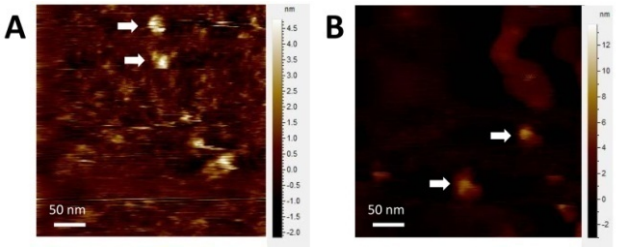

Figure 3.1.4. AFM images of siRNA polyplexes at N/P 16: (A) **356** polyplexes (arrows): d = 5.3 ± 0.6 nm; (B) **640** polyplexes (arrows): d = 7.7 ± 0.8 nm. The light intensity reflects the height of nanoparticles. The scale bars represent 50 nm. The experiments were performed in collaboration with Dr. Rong Zhu (Institute of Biophysics, Johannes-Kepler-Universität Linz).

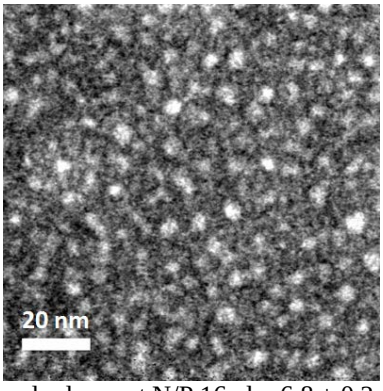

Figure 3.1.5. TEM image of **640** siRNA polyplexes at N/P 16. d = 6.8 ± 0.2 nm. The scale bar represents 20 nm. The experiment was performed in collaboration with Susanne Kempter (Faculty of Physics, Ludwig-Maximilians-Universität München).

To examine the effect of PEGylation on the surface charge of polyplexes, zeta potential of polyplexes at various N/P ratios was measured (Table 3.1.3). At N/P 16, zeta potential values of the ligand-equipped polyplexes remained close to neutrality, with a distribution between 0.2 to 2.5 mV. In the case of **640**, at N/P 3, the zeta potential was 0.03 mV, and remained close to neutral with increasing N/P ratio. Finally, even at very high ratio of oligomer over siRNA (N/P 28), the zeta potential was neutral, suggesting that PEGylation successfully shielded the surface charge of siRNA polyplexes.

Table 3.1.3. Zeta potential values of siRNA polyplexes at different N/P ratios determined by dynamic light scattering (DLS) measurements.

Oligomer	N/P	Zeta Potential (mV)
638	16	0.9 (± 0.3)
639		0.2 (± 0.2)
641		0.6 (± 0.1)
642		2.5 (± 1.2)
640	3	0.03 (± 0.04)
	10	-3.5 (± 0.6)
	16	1.3 (± 0.8)
	20	3.1 (± 0.4)
	28	-1.6 (± 0.9)

3.1.3 MTX as targeting ligand for receptor-mediated uptake

It is recognized that folates and antifolates are mainly internalized into the cells either through folate receptor (FR) or reduced folate carrier (RFC). To validate targeting capacity of the MTX-conjugated siRNA polyplexes, we used fluorescent Cy5-labeled siRNA, and studied the binding profile with flow cytometry. To investigate selective targeting ability of MTX conjugates against FR, we sought to take advantage of the two cancer cell lines, FR-α-rich KB cells [67] and FR-deficient A549 cells [68-70]. Comparison of relative binding efficiency of fluorescently labeled folate in both cell lines is shown in Figure 3.1.6.

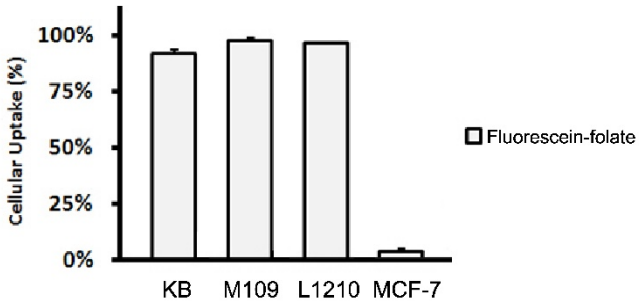

Figure 3.1.6. Binding activity of fluorescein-labeled folate ligand in different cell lines measured by flow cytometry.

KB and A549 cells were treated with MTX-based **640** siRNA polyplexes, folate-based **356** siRNA polyplexes and non-targeted alanine control **188** siRNA polyplexes formed at N/P 16 for 45 min on ice, and then binding of the polyplexes was analyzed by flow cytometry (Figure 3.1.7). For the alanine-substituted control **188**, siRNA polyplexes barely bound to both cell lines (< 1 % positive cells). Generally, the folate-substituted control conjugate **356** and MTX oligomer conjugates (**638**-**642**) exhibited strong cellular association in FR-rich KB cells. The binding rate of tetraglutamyl-MTX conjugate **640** (67%) was comparable to that of folate substituted control conjugate **356** (71%). The binding levels for the rest of MTX conjugates in KB cells were similar, which were lower than the level for **356**. On the other hand, in FR-deficient A549 cells, the uptake capacity of **356** was significantly reduced (18% positive cells), and MTX conjugates (**638**-**642**) all failed to bind to the A549 cells (< 3% positive cells), supporting the FR-specific cellular association with MTX conjugates.

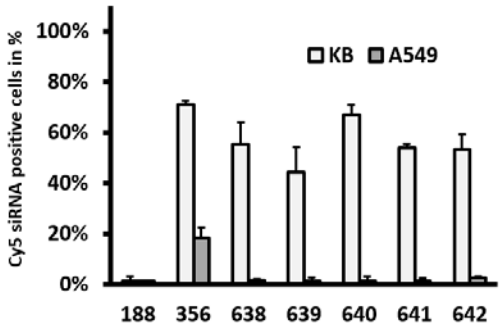

Figure 3.1.7. The receptor association capacity of MTX conjugates (**638**-**642**) was evaluated by comparing the binding of siRNA polyplexes by FR-overexpressing KB vs. FR-deficient A549 cells. The amount of Cy5-positive cells was analyzed through excitation of the dye at 635 nm and detection of emission at 665/20 nm by flow cytometry. **188** as a negative alanine substituted control, and **356** as folate-conjugated control were used for comparison with MTX conjugates.

To prove that the binding of the polyplexes to the cells is ligand-dependent, the competition assay with free ligands was carried out. For this, KB cells were pretreated with folate or MTX, and then treated the cells with **640** siRNA polyplexes or **356** siRNA polyplexes. As implicated by flow cytometry analysis (Figure 3.1.8), if KB cells were pre-incubated with excess of free MTX (100 μM), uptake level of MTX conjugate **640** was reduced by 53%, as MTX ligands of **640** competed with free MTX for limited receptors. Since FR has several-hundred-fold higher binding affinity for folate than for MTX [71], cellular uptake of folate conjugate **356** was not influenced by free MTX. Nevertheless, in the presence of free folate (100 μM), cellular binding of **356** and **640** was almost completely inhibited by 90% and 99%, respectively. In comparison, the binding capacity of alanine control **188** was extremely low under either condition. Based on the observations that the MTX conjugates bind to the FR-expressing KB cells in a receptor-specific fashion, and the binding was reversed by pre-incubation with excess free folate or MTX, these cellular association studies demonstrated that MTX oligomer conjugates target the KB cells mainly through the FR.

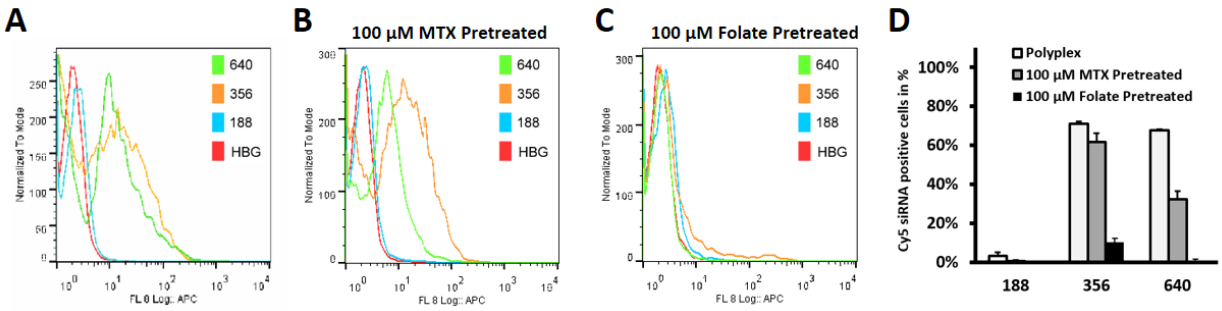

Figure 3.1.8. The ligand competition study of MTX conjugate (**640**), folate conjugate (**356**) and untargeted conjugate (**188**) in the presence of excess free MTX or folate evaluated by flow cytometry. KB cells were treated with (A) siRNA polyplexes for 4 h, or (B) pre-incubated with 100 µM of MTX or (C) 100 µM of folic acid for 30 min before incubation with siRNA polyplexes for 4 h. siRNA polyplexes were formed at N/P 16 using Cy5-labeled siRNA. (D) The internalization profile for the ligand competition study. The amount of Cy5-positive cells was analyzed through excitation of the dye at 635 nm and detection of emission at 665/20 nm.

3.1.4 Gene silencing efficiency

After showing that the MTX-modified oligomer/siRNA polyplexes utilized FR for cellular association, next their ability to be taken up by the cells and induce target gene silencing was measured. To validate this, siRNA targeting eGFP (siGFP) or control siRNA (siCtrl) to transfect the cells stably expressing eGFP-Luciferase (eGFPLuc) fusion protein was used, and gene silencing of siRNA polyplexes *via* luciferase activity was evaluated by luminometric analysis. Previous studies with similar oligomers indicated that these siRNA polyplexes faced the problem of endosomal degradation—they are too small to effectively release into the cytosol [33]. Hence, to improve endosomal escape of siRNA polyplexes, the influenza virus haemagglutinin subunit 2 (HA2) variant Inf7 as pH-specific endosome fusion peptide was coupled to the 5' end of siRNA sense strand [33, 72]. As shown in Figure 3.1.9, glutamyl-MTX conjugates (**638**-**642**) containing Inf7-modified siGFP (siGFP-Inf7) at N/P 16 exhibited significant gene silencing efficiency in KB/eGFPLuc cells, as 84-93% of luciferase activity was suppressed. Among MTX conjugates, **640** (4E-MTX-Stp) polyplexes provided the most potent gene silencing activity (93%). In contrast, there was no silencing effect for siRNA polyplexes of alanine control **188**, furthermore highlighting the specificity provided by the MTX targeting ligand. The luciferase activity in KB/eGFPLuc cells treated with controls, including siCtrl-Inf7 polyplexes, siGFP without Inf7 or plain MTX oligomers were similar, 49-67% compared to untreated cells (Figure 3.1.9 and 3.1.10).

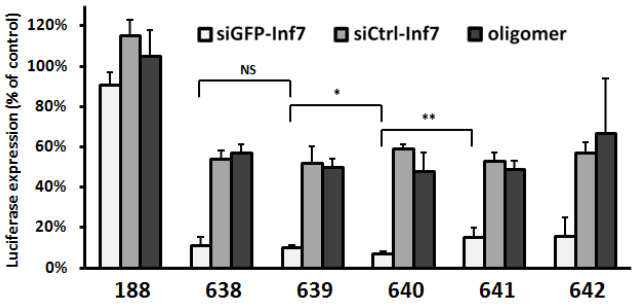

Figure 3.1.9. Gene silencing efficiency of MTX conjugates containing eGFP-targeted siRNA (siGFP) or control siRNA (siCtrl) in KB cells expressing eGFPLuc protein (KB/eGFPLuc cells). MTX conjugates were incorporated with different glutamic acid units (**638**-**642**) at N/P 16. Plain oligomers were added in concentrations corresponding to the concentrations of the respective polyplexes at the indicated N/P values. siRNA was modified with the endosomolytic peptide Inf7.

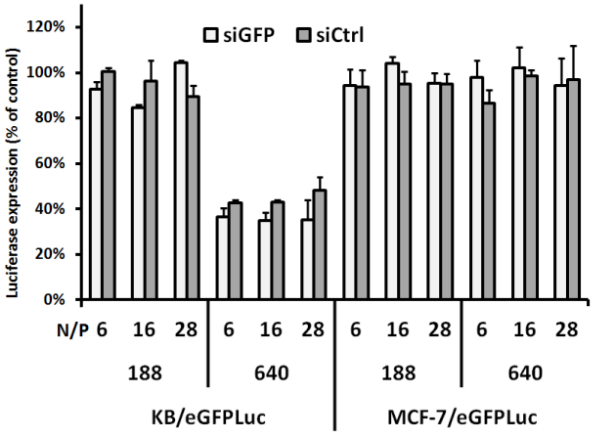

Figure 3.1.10. Gene silencing efficiency with siGFP or siCtrl (both without Inf7 peptide) in FR-overexpressing KB/eGFPLuc cells or FR-deficient MCF-7/eGFPLuc cells using MTX conjugate (**640**) or alanine substituted control (**188**) at different N/P ratios.

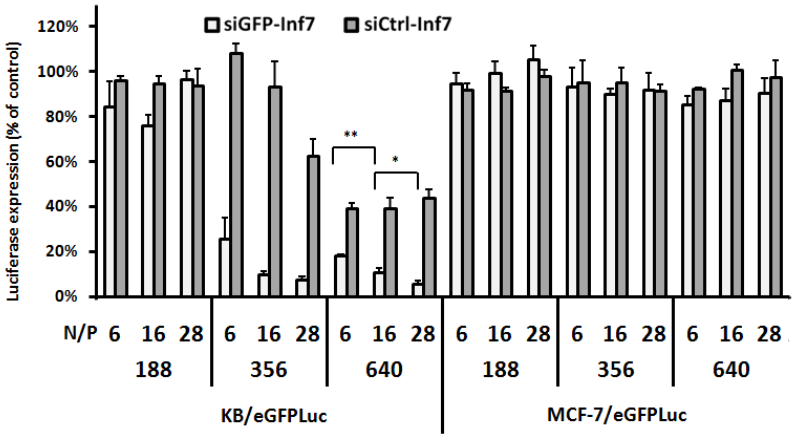

Figure 3.1.11. Gene silencing efficiency in FR-overexpressing KB/eGFPLuc cells (left) or FR-deficient MCF-7/eGFPLuc cells (right) using MTX conjugate (**640**) at different N/P ratios. siRNA was modified with the endosomolytic peptide Inf7.

Instead of displaying a RNAi effect, the reduced luciferase activity here demonstrated the intrinsic cytotoxicity of MTX ligands by inhibiting DHFR. Looking at Figure 3.1.11, in KB/eGFPLuc cells, silencing activity of tetraglutamylated MTX analogue **640** was increased while N/P ratio was higher; however, the luciferase expression level in cells treated with siCtrl-Inf7 was not altered at various N/P ratios. More importantly, in comparison with FR-positive KB/eGFPLuc cells, transfections with folate conjugate (**356**) or MTX conjugate (**640**) containing siGFP-Inf7 in FR-negative MCF-7/eGFPLuc cells did not have any impact on luciferase expression or possible cytotoxicity. Taken together, the gene silencing assay further indicated that MTX targeting allows the siRNA polyplexes to access the cytoplasm of the cells *via* specific FR-mediated endocytosis. MTX-conjugated oligomers complexed with Inf7-modifed siRNA, especially **640**, showed not only striking targeted gene-specific silencing ability, but also tissue-specific cytotoxic potential mediated by glutamylated MTX.

3.1.5 Augmented cytotoxicity by MTX conjugates and EG5 gene knockdown

As mentioned above, MTX conjugates facilitate their cytotoxic effects by inhibiting DHFR, and the inhibition potency is attributed to the glutamylation degree of MTX conjugates [50]. The next question is, whether the cytotoxicity could be enhanced by using MTX-conjugated oligomers in combination with antitumoral siRNA. For this purpose, MTX-conjugated oligomers were exploited to carry siRNA against EG5 (siEG5-Inf7), which is able to block mitosis. As shown in Figure 3.1.12A, MTT assay reflected that all glutamyl-MTX conjugates were cytotoxic in FR-expressing KB cells compared to alanine (**188**) or folate-substituted control (**356**). The cytotoxicity of the conjugates was elevated with an increasing degree of polyglutamylation, and notably, **639** (2E-MTX-Stp), **640** (4E-MTX-Stp) and **641** (6E-MTX-Stp) were more toxic compared to free MTX. Meanwhile, in FR-negative MCF-7 cells, no similar cytotoxic effects induced by MTX-conjugated or folate-substituted oligomers were found (Figure 3.1.13 and 3.1.14).

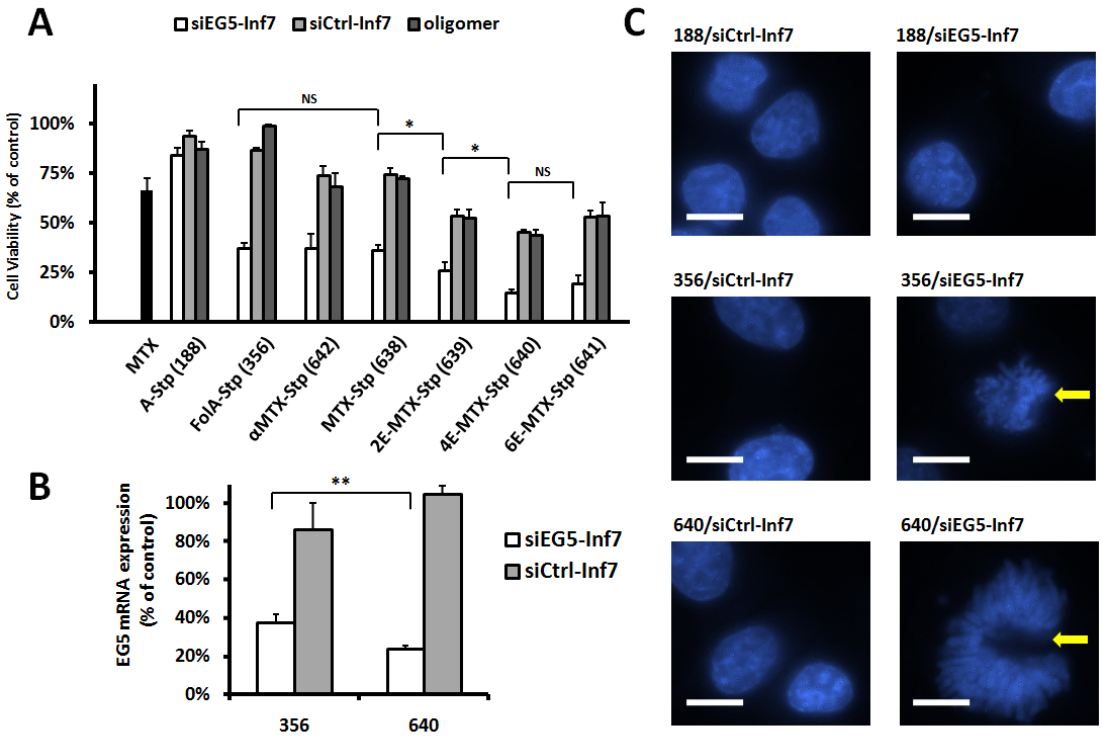

Figure 3.1.12. Transfection with Inf7 peptide-modified EG5-targeted siRNA (siEG5-Inf7) or control siRNA (siCtrl-Inf7) polyplexes at N/P 16 in KB cells. (A) MTT assay in KB cells after transfection with MTX conjugates (**638**-**642**), alanine conjugate (**188**) or folate conjugate (**356**). Free MTX or plain oligomer was applied in concentration corresponding to that of siRNA polyplexes. (B) mRNA level of EG5 gene measured by qRT-PR after transfection with MTX conjugate (**640**) or folate control (**356**). GAPDH was used as housekeeping gene. (C) KB cells treated with MTX conjugate (**640**), alanine conjugate (**188**) or folate conjugate (**356**) polyplexes observed under the fluorescent microscope. The mitotic blockade that was induced by EG5 knockdown caused "aster formation" of nuclear DNA (arrows). DAPI stain. The scale bars represent 10 μm.

It was further examined whether co-delivery of MTX conjugates and siEG5-Inf7 could potentiate the cytotoxic effect. As seen in Figure 3.1.12A, similar correlation between glutamylation degree and siEG5-induced cytotoxicity was found. Among the MTX conjugates, **640** (4E-MTX-Stp) and **641** (6E-MTX-Stp) polyplexes provided the highest potency to reduce cell viability of KB cells. As compared to free MTX or **356** siEG5-Inf7 polyplexes, MTX-conjugate siEG5-Inf7 polyplexes induced significantly superior cytotoxicity. Next, EG5-specific gene silencing was confirmed at mRNA level by qRT-PCR in KB cells (Figure 3.1.12B), where the tetraglutamyl variant **640** triggered very efficient downregulation of EG5 mRNA level, while it was significantly more potent than the folate-substituted control **356** ($p < 0.01$). Finally, functional EG5 gene silencing was confirmed *via* aster formation of nuclear DNA, where downregulation of EG5 induced a mitotic arrest in KB cells which had been transfected with **640** siEG5-Inf7 polyplexes or **356** siEG5-Inf7 polyplexes (Figure 3.1.12C). These results clearly indicated efficient silencing of EG5 expression at mRNA level, followed by mitotic blockade and finally cell death in KB cells. Moreover, it suggested that augmented tumor cell killing ability was mediated by a dual mechanism combining glutamyl-MTX oligomer with antitumoral siRNA.

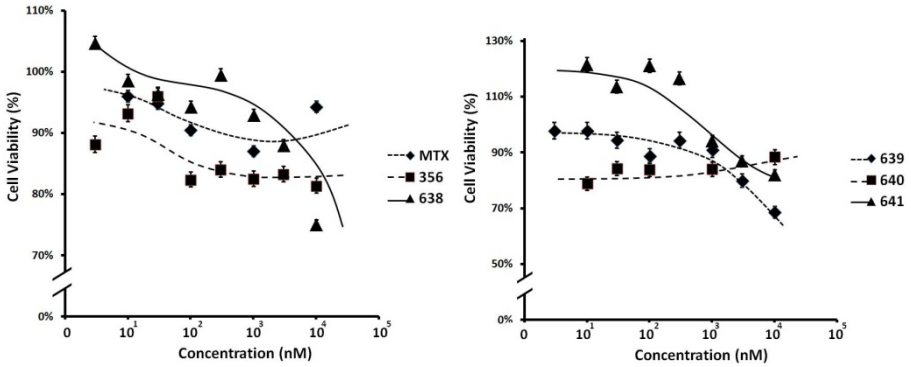

Figure 3.1.13. MTT assay in MCF-7 cells treated with MTX or oligomers **356**, **638**, **639**, **640**, **641** at concentration between 1 - 10^4 nM for 48 h.

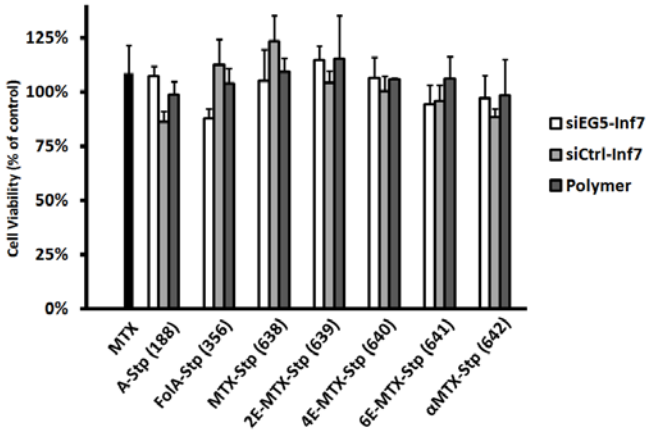

Figure 3.1.14. MTT assay in MCF-7 cells treated with MTX, oligomer or polyplexes (at 370 nM of siEG5-Inf7 or siCtrl-Inf7) for 24 h.

3.1.6 Prolonged intratumoral retention

The half-life of siRNA *in vivo* is short, predominantly due to rapid elimination by renal filtration and biodegradation by RNases [73]. For example, our group previously reported that intratumoral retention of free siRNA lasts merely for 4 h [33]. From the previous work with analogous folate-PEG siRNA polyplexes, we know that these small (<10 nm) nanoparticles are stable in the blood upon systemic *i.v.* injections, but rapidly eliminated *via* kidneys, with recovery of intact polyplexes from urine (Figure S16 and S17 in Dohmen *et al*. [23]). For this reason, both in the previous and the current study intratumoral injection (*i.t.*) was the selected route of administration.

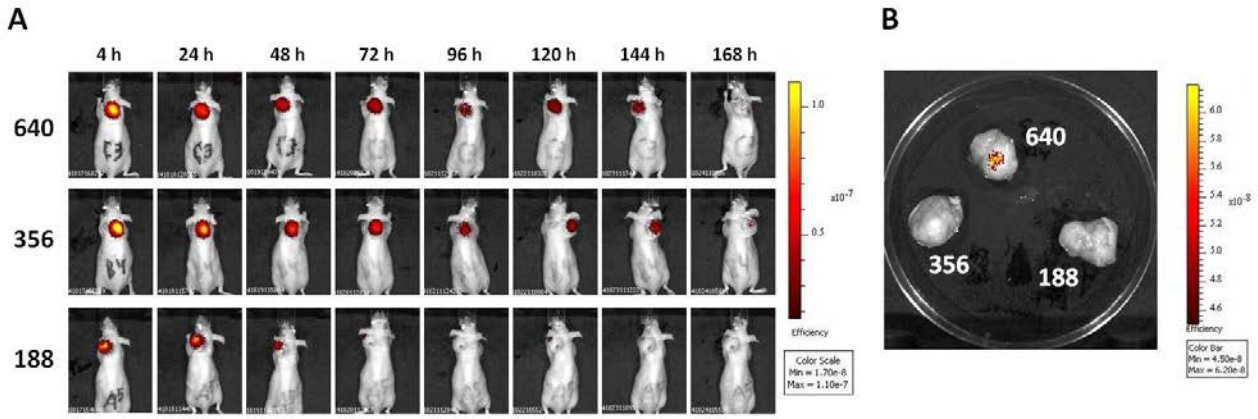

Figure 3.1.15. Intratumoral distribution of siRNA polyplexes at N/P 16 in NMRI-nude mice bearing KB xenograft tumors determined by NIR fluorescence bioimaging. (A) Time-dependent retention of 50 µg of Cy7-labeled siRNA after intratumoral injection using MTX-conjugated oligomer **640** (upper panel), folate-conjugated control **356** (middle panel) or alanine substituted control **188** (lower panel) as carrier. (B) Harvested tumor samples at 168 h after injection of siRNA polyplexes. Experiments were performed in triplicates; a representative animal of each group is shown. The experiments were performed in collaboration with Eva Kessel (Dr. med. vet. study, Department of Pharmacy, Ludwig-Maximilians-Universität München).

To further examine whether MTX-conjugated oligomers could enhance the retention of siRNA within the tumor, Cy7-labeled siRNA formulated with **640** at N/P 16 was administered *i.t.* to KB tumor-bearing mice. The biodistribution study with Cy7-labeled siRNA measured by near infrared (NIR) fluorescence imaging (Figure 3.1.15A) showed that the conjugation of MTX as targeting ligand significantly increased the tumoral retention of siRNA. Both targeted siRNA polyplexes (**640** and **356**) carried out remarkably longer retention (5 days) than that of untargeted **188** siRNA polyplexes by ~120 h. The MTX-based **640** siRNA polyplexes showed comparable retention as folate-based **356** siRNA polyplexes, and Cy7-labeled siRNA was still detectable 168 h after injection (Figure 3.1.15B). The biodistribution study provided evidence that these siRNA polyplexes were eliminated through renal clearance (Figure 3.1.16).

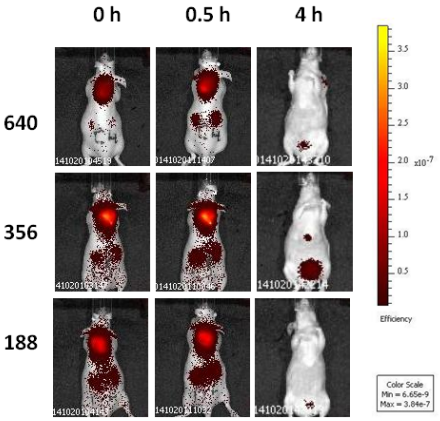

Figure 3.1.16. Renal clearance of siRNA polyplexes in tumor-bearing NMRI-nude mice determined by NIR fluorescence bioimaging. After intratumoral injection using MTX-conjugated oligomer **640** (upper panel), folate-conjugated control **356** (middle panel) or alanine-substituted control **188** (lower panel) as carrier, Cy7-labeled siRNA was detected in the kidneys and the bladder. Experiments were performed in triplicates; a representative animal of each group is shown. The experiments were performed in collaboration with Eva Kessel (Dr. med. vet. study, Department of Pharmacy, Ludwig-Maximilians-Universität München).

3.1.7 Dual *in vivo* therapeutic effects by MTX-conjugated siRNA polyplexes

After confirming that FR-targeted siRNA polyplexes were well-retained in the tumor tissue, we further investigated the therapeutic potential of these polyplexes. For this, we formulated polyplexes of the tetraglutamyl-MTX conjugate **640** with siEG5-Inf7 or siCtrl-Inf7, free **640** (without siRNA), or polyplexes of the folate conjugate **356** with siEG5-Inf7, and administered these formulations *i.t.* in the KB tumor-bearing nude mice. In line with previous intratumoral administration studies, 50 µg of siRNA (diluted in 50 µL of HBG) was applied [33, 36]. To avoid unspecific immune reactions, we used 2' OMe-modified siRNA that is designed not to trigger toll-like receptor (TLR)-mediated immune responses [29, 30]. The post-treatment survival was recorded to provide Kaplan–Maier survival analysis. All animals treated with siRNA polyplexes showed significantly reduced tumor growth compared to untreated controls (Figure 3.1.17A). Importantly, combination treatment with **640** siEG5-Inf7 polyplexes nearly completely inhibited tumor growth 8 days after the treatment (Figure 3.1.17B), and all of these animals still showed no palpable or measurable tumor 17 days after the treatment (Figure 3.1.18). Encouragingly, three animals receiving **640** siEG5-Inf7 polyplexes have survived without recurrence until the study was ended (day 70) (Figure 3.1.17C). In addition, **640** siCtrl-Inf7 polyplexes induced superior effect over free **640** to inhibit tumor growth. With regard to antitumoral efficacy, the big difference between the EG5 and the control siRNA group **640** siCtrl-Inf7 polyplexes ruled out a significant contribution of immune reactions to the therapeutic effect. Nevertheless, **640** siCtrl-Inf7 polyplexes mediated higher antitumoral effect than that of free **640** (*i.e.* without siRNA complexation) to inhibit tumor growth. Possible explanations could be better intratumoral

retention of multiple conjugated MTX ligands by **640** siRNA-Inf7 nanoparticle formation, or improved cytosolic delivery of the MTX molecules facilitated by the endosomolytic Inf7 peptide. Interestingly, **356** siEG5-Inf7 polyplexes resulted in comparable effect in terms of tumor suppression and survival time as free **640** (30.8 ± 2.3 days vs. 29.7 ± 2.4 days).

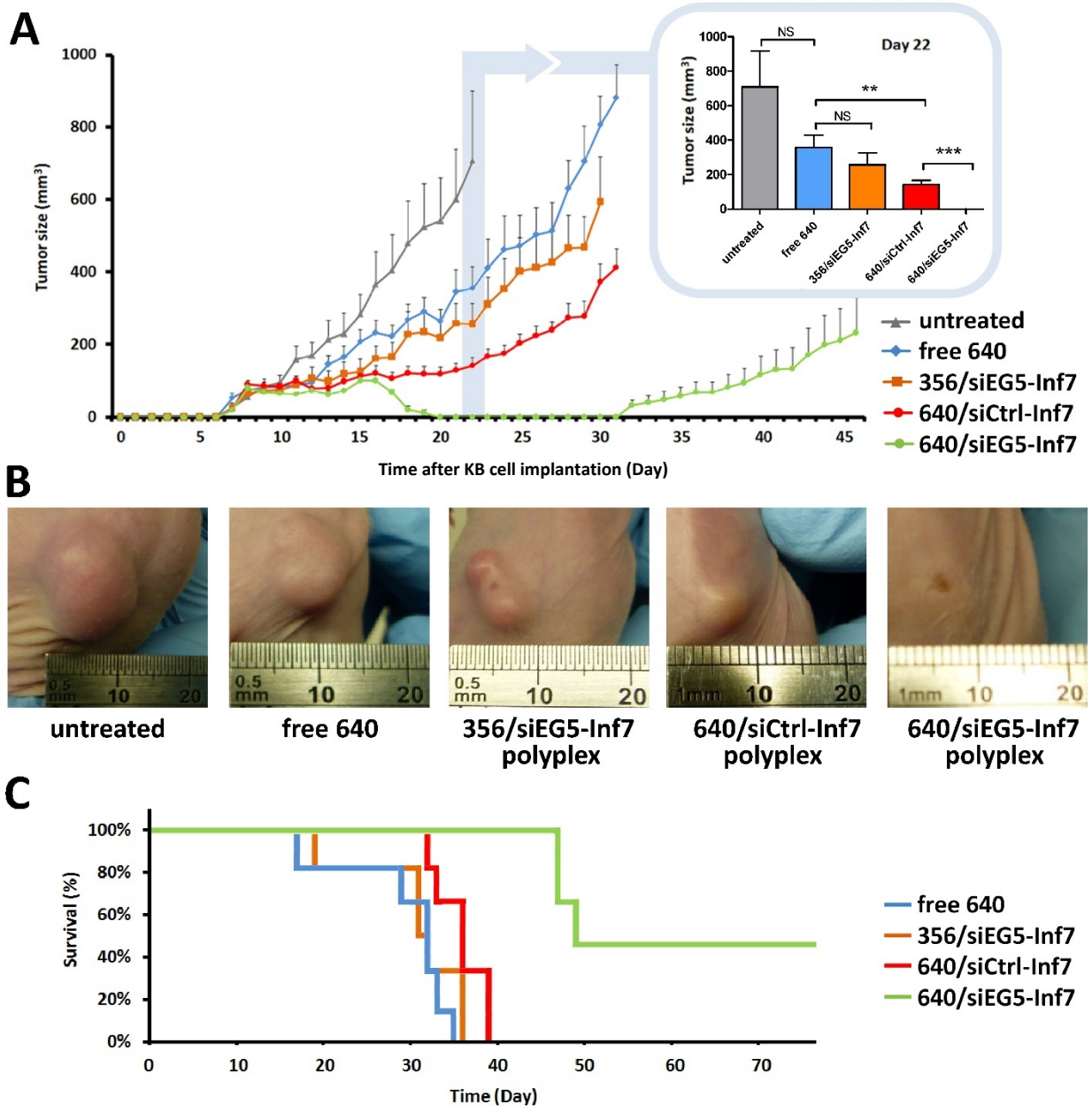

Figure 3.1.17. *In vivo* validation of augmented antitumoral effect by MTX-conjugated siRNA polyplexes. (A) Therapeutic efficacy of MTX-conjugated **640** polyplexes (with siEG5-Inf7 or siCtrl-Inf7), free oligomer **640** (without siRNA), or folate-conjugated **356** siEG5-Inf7 polyplexes in KB xenograft (n = 6 per group). The insert shows a comparison of the tumor volume in different groups 5 days after the last treatment (day 22). (B) Representative KB tumor lesions from the cohorts in (A) on day 25. (C) The Kaplan–Maier survival curve of the animals treated with indicated formulations. In the animals receiving **640** siEG5-Inf7 polyplexes, tumors largely disappeared by day 22, and in 3 animals no recurrence was observed until the end of the study (day 70). The experiments were performed in collaboration with Eva Kessel (Dr. med. vet. study, Department of Pharmacy, Ludwig-Maximilians-Universität München).

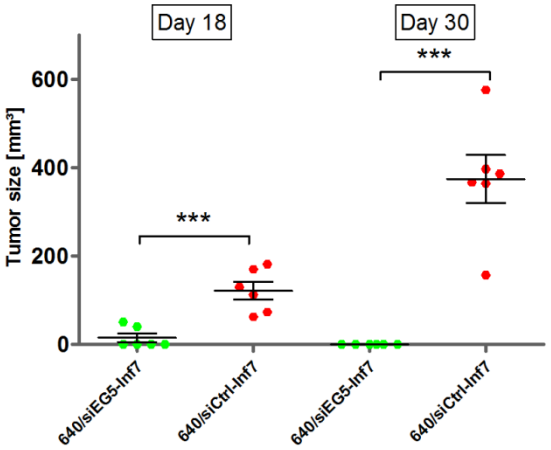

Figure 3.1.18. KB tumor-bearing animals were administered *i.t.* with **640** siRNA polyplexes (with siEG5-Inf7 or siCtrl-Inf7, and the tumor sizes were measured 1 day (day 18) or 17 days (day 30) after the last treatment. No palpable or measurable tumor was found on day 30 in the animals treated with **640** siEG5-Inf7. The experiments were performed in collaboration with Eva Kessel (Dr. med. vet., Department of Pharmacy, Ludwig-Maximilians-Universität München).

In the tumors treated with **640** siEG5-Inf7 polyplexes or **356** siEG5-Inf7 polyplexes, necrotic tumor tissue accompanied by an active healing process was observed. In general, scars started to fade and thin out gradually after the treatments (Figure 3.1.19). At the same time, equivalent intratumoral dosages of free MTX did not reduce tumor growth (Figure 3.1.20). Moreover, monitoring of body weights demonstrated that the treatment was well tolerated (Figure 3.1.21). Temporary stagnation of body weight (days 11–18) in the treated animals was possibly due to tumor necrosis-associated discomfort, and a rapid gain of weight after the treatments was noted. These results suggest that the tetraglutamyl-MTX ligand provides tumor-suppressive potential, and effective EG5 silencing by FR-targeted polyplexes represents a potential strategy for tumor treatment, which can be further combined with MTX-conjugated **640** for improved therapeutic efficacy.

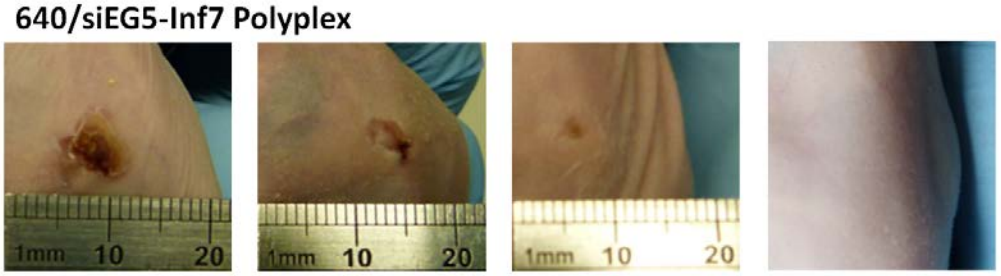

Figure 3.1.19. The necrotic tumor tissue followed by an active healing process was found in the KB tumor-bearing animals treated with **640** siEG5-Inf7 polyplexes or **356** siEG5-Inf7 polyplexes. The healing process could be different for different individuals, while the wounds were eventually repaired as shown in the representative pictures from the animals treated with **640** siEG5-Inf7 polyplexes.

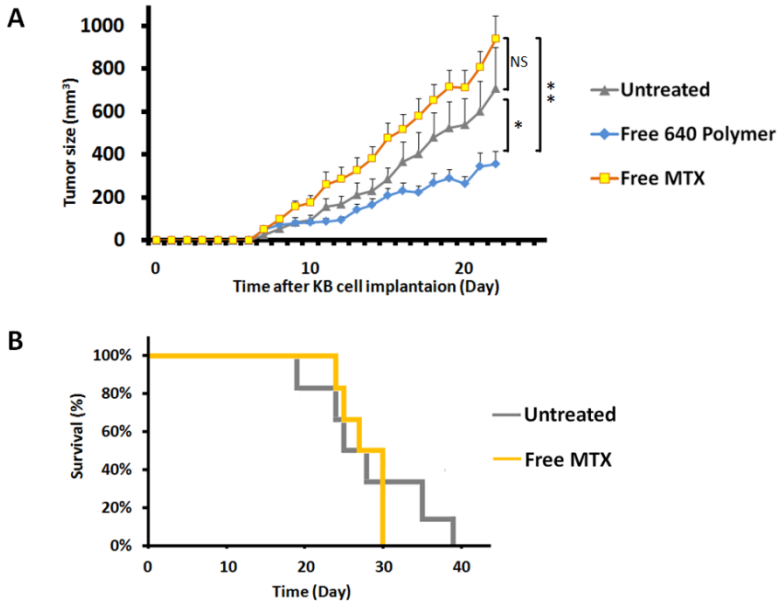

Figure 3.1.20. Tumor growth curve after the intratumoral injection of free MTX or glutamyl-MTX conjugate **640** in KB xenografts (n = 6 per group). (A) Therapeutic efficacy of free MTX or free oligomer **640**. (B) The Kaplan–Maier survival curve of the animals receiving indicated formulations. The experiments were performed in collaboration with Eva Kessel (Dr. med. vet. study, Department of Pharmacy, Ludwig-Maximilians-Universität München).

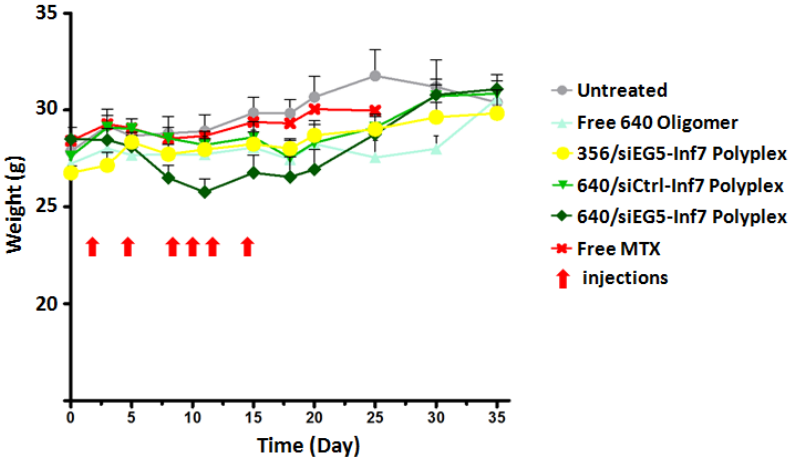

Figure 3.1.21. The body weights of the animals receiving different formulations were monitored on a daily basis until the animals were sacrificed. The experiments were performed in collaboration with Eva Kessel (Dr. med. vet. study, Department of Pharmacy, Ludwig-Maximilians-Universität München).

3.2 Targeted combinatorial polyplexes (TCPs)

3.2.1 Formation of TCPs

This chapter has been partly adapted from:
D.J. Lee, D. He*, E. Kessel, K. Padari, S. Kempter, U. Lächelt, J.O. Rädler, M. Pooga, E. Wagner, Tumoral gene silencing by receptor-targeted combinatorial siRNA polyplexes, J Control Release, 244 (2016) 280–291 (shared first authorship).*

Based on previous studies, four oligomers were selected from the library to generate novel combinatorial formulations for targeted siRNA delivery (Scheme 3.2). This work was performed in collaboration with Dr. Dongsheng He (PhD study, Department of Pharmacy, Ludwig-Maximilians-Universität München). Three-arm Stp oligomers **386** and **689**, were chosen for their strong siRNA binding ability, which provide a highly stable cationic core to compact siRNA [35, 36, 74]. Moreover, PEG-folate-conjugated Sph oligomers (4-arm) **709** and (2-arm) **717**, were used for FR targeting and surface shielding [75]. Here we combined these two types of oligomers, in order to optimize the siRNA polyplexes by co-formulation. All oligomers contain terminal cysteines with free thiol groups for subsequent disulfide formation within siRNA polyplexes. As standard disulfide formation by air oxidation has been found to be a rather slow and incomplete process, we intended to make this step faster and more specific. Therefore, we activated the thiol groups of oligomer #1 with 5,5'-dithio-bis(2-nitrobenzoic acid) (DTNB) to produce TNB-modified oligomer (Figure 3.2.1A). The TNB-modified oligomer formed a binary siRNA polyplex with siRNA, and in the following incubation with the unmodified thiol-oligomer #2 it would undergo a fast uni-directional coupling through disulfide formation with the free thiol groups of thiol-oligomer #2 in three dimensions, resulting in hypothetic nanogel structures (Scheme 3.2). The combination of siRNA with both oligomers thus generated targeted combinatorial polyplexes (TCPs), which were composed of compact cationic core for siRNA binding, well-shielded PEG layer and folates as targeting ligands (Figure 3.2.1B). TCPs were optimized by testing different TNB-modified oligomers #1 / unmodified thiol oligomers #2 at various molar ratios, and by evaluating three different siRNA / oligomer #1 / oligomer #2 mixing sequences. Preliminary gene silencing experiments (Figure 3.2.2) demonstrated that tested mixing sequences presented similar efficiencies as the first alternative (pre-incubated siRNA with the TNB-modified oligomer #1, followed by disulfide exchange reaction with thiol oligomer #2). For practical reasons, all further testing was performed with this mixing sequence.

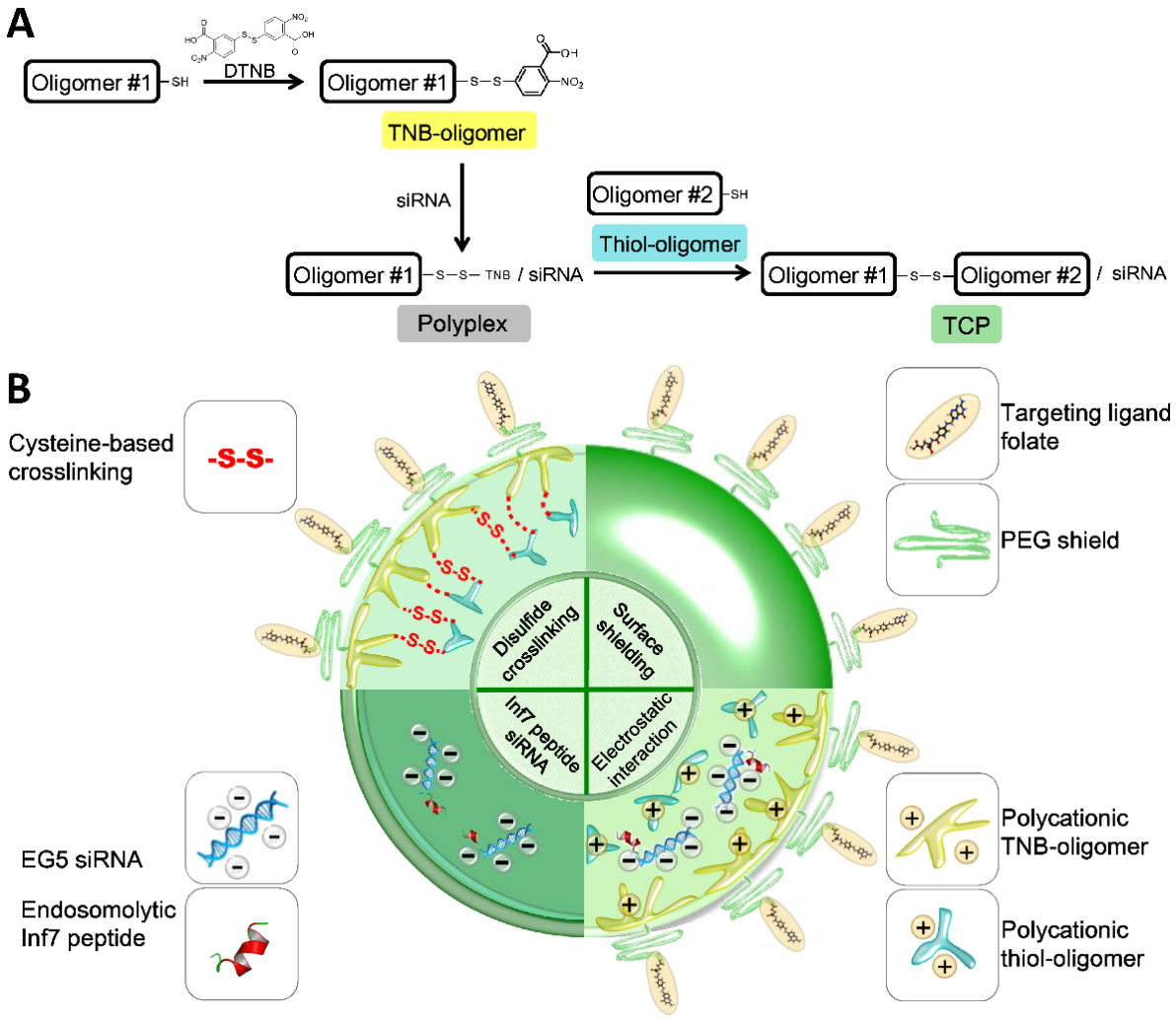

Figure 3.2.1. Targeted combinatorial polyplexes (TCPs) with folate ligand for siRNA delivery. (A) TNB-modified oligomer #1 was obtained by reacting the solid-phase derived thiol precursor oligomer #1 with 10 eq of DTNB for 2 h at room temperature. The incubation of TNB-modified oligomer #1 with siRNA formed a binary polyplex. Addition of thiol-oligomer #2 resulted in fast uni-directional coupling of TNB-modified oligomer #1 through disulfide formation with the free thiol groups of #2. In this way siRNA, TNB-modified oligomer and unmodified thiol-oligomer were formulated to produce a TCP. (B) Schematic presentation of key elements of a TCP. Endosomolytic Inf7 peptide was conjugated to siRNA for enhanced endosomal escape [33].

As a result, four combinatorial formulations, TCP1, TCP2, TCP3 and TCP4, were developed (Scheme 3.2). TCP1 and TCP3 shared the similar combined structure of **386** + **709** (Scheme 3.2 top); TCP2 and TCP4 shared the similar combined structure of **689** + **717** (Scheme 3.2 bottom). Differences rose from the alterative TNB-activations of oligomers. After systematic screening and evaluating different molar ratios of oligomers (Tables S1-S4 in [76]), equal molar (1:1) oligomer ratios at N/P 16 was determined as most useful for the subsequent experiments.

	TCP1	TCP3
TNB-Oligomer #1	(4-arm **873**) K-(PEG$_{24}$-Folate)-K-[K-(Sph$_4$-C-TNB)$_2$]$_2$ (N/P 11.2)	(3-arm **769**) TNB-C-Stp$_3$-K-(Stp$_3$-C-TNB)$_2$ (N/P 4.8)
Thiol-Oligomer #2	(3-arm **386**) C-Stp$_3$-K-(Stp$_3$-C)$_2$ (N/P 4.8)	(4-arm **709**) K-(PEG$_{24}$-Folate)-K-[K-(Sph$_4$-C)$_2$]$_2$ (N/P 11.2)
Combined Structure	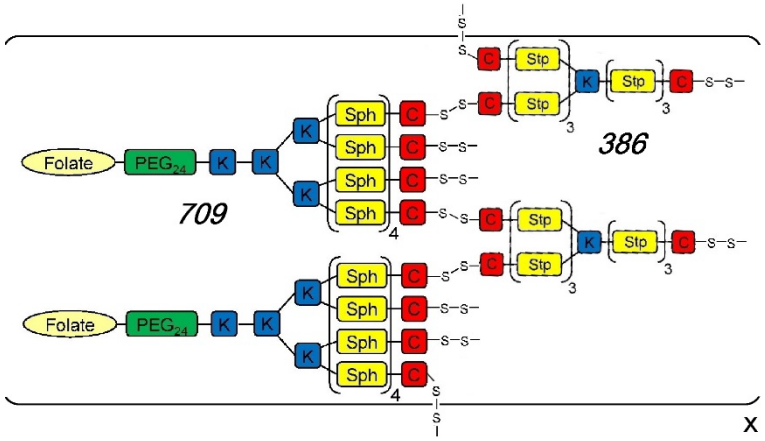 (709-S-S-386-S-S)$_x$	

	TCP2	TCP4
TNB-Oligomer #1	(3-arm **770**) TNB-C-H-(Stp-H)$_3$-K-[(H-Stp)$_3$-H-C-TNB]$_2$ (N/P 7.4)	(2-arm **874**) K-(PEG$_{24}$-Folate)-K-(Sph$_4$-Y$_3$-C-TNB)$_2$ (N/P 8.6)
Thiol-Oligomer #2	(2-arm **717**) K-(PEG$_{24}$-Folate)-K-(Sph$_4$-Y$_3$-C)$_2$ (N/P 8.6)	(3-arm **689**) C-H-(Stp-H)$_3$-K-[(H-Stp)$_3$-H-C]$_2$ (N/P 7.4)
Combined Structure	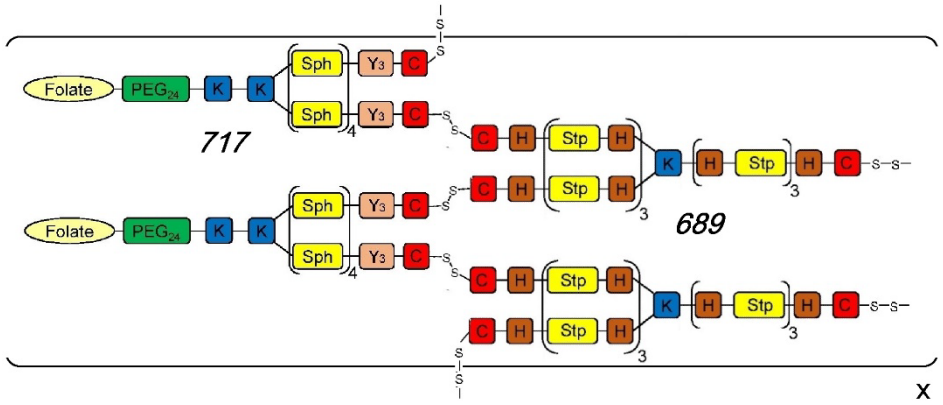 (717-S-S-689-S-S)$_x$	

Scheme 3.2. Targeted combinatorial polyplex (TCP) formulations. siRNA was co-formulated with TNB-modified oligomers and unmodified thiol-oligomers at various molar ratios to form the TCP carriers. In most experiments polyplexes were formed at N/P 16 using an equal molar oligomer ratio of 1:1; for these conditions the individual N/P ratio of each oligomer is presented. The oligomer sequences are indicated (left to right) from C- to N- terminus. C: cysteine; H: histidine; K: lysine; Y: tyrosine; S-S: disulfide crosslinking; PEG$_{24}$: polyethylene glycol; TNB: 5-thio-2-nitrobenzoic acid; Stp: succinoyl-tetraethylene pentamine; Sph: succinoyl-pentaethylene hexamine. K-(and K-[refer to branchings by α- and ε-amino modification of lysines. x: hypothetic nanogel structures resulting from disulfide crosslinking in three dimensions within the TCP.

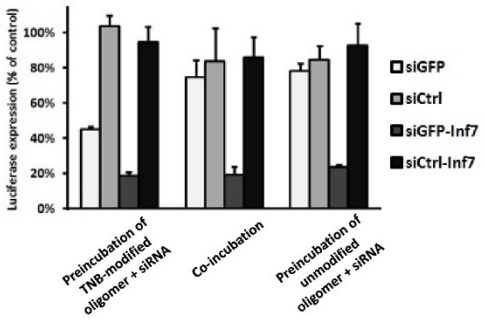

Figure 3.2.2. Gene silencing efficiency of TCP1 in KB/eGFPLuc cells using different alternative mixing sequences. The siRNA polyplexes were prepared at N/P 16 with 370 nM siRNA: siGFP, siCtrl, siGFP-Inf7 or siCtrl-Inf7. The different mixing sequences were compared: Alternative (1), also used for the majority of experiments; the TNB-modified oligomer solution was pre-incubated with siRNA solution for 30 min, then was incubated with unmodified oligomer solution for 40 min. Alternative (2), the TNB-modified oligomer solution and unmodified oligomer solution were incubated all together with siRNA solution for 40 min. Alternative (3), unmodified oligomer solution was pre-incubated with siRNA solution for 30 min, then further incubated with TNB-modified oligomer solution for 40 min.

3.2.2 Physicochemical characterizations

Formulating TCPs (Scheme 3.2) at N/P 16, we measured the particle sizes by dynamic laser-light scattering (DLS) based on different molar ratios of [TNB-modified oligomer #1 / unmodified thiol-oligomer #2]. At the ratio of 1:1, the sizes of the two **386 + 709** formulations, TCP1 and TCP3, are 104 nm and 209 nm, respectively, whereas the two **689 + 717** formulations, TCP2 and TCP4, have a larger size of ~ 400 nm (Table 3.2.1). To examine the effect of PEG shielding on the surface charge of TCPs, zeta potentials of siRNA polyplexes at N/P 16 were measured (Table 3.2.1). For TCP1, TCP2 and TCP4, the zeta potential values were reduced from approximately ≥ +20 mV [35] to values around + 8-9 mV. It is interesting that TCP3, comprising the same oligomers by a different activation scheme, displayed a highly positive zeta potential of +24 mV.

Formulation	Size (nm)	PdI	Zeta potential (mV)
TCP1	103.5 ± 0.8	0.239 ± 0.026	9.1 ± 0.2
TCP2	429.4 ± 53	0.213 ± 0.017	7.93 ± 0.21
TCP3	208.8 ± 3.4	0.267 ± 0.011	24.3 ± 0.3
TCP4	398.3 ± 63.5	0.229 ± 0.017	8.1 ± 0.05

Table 3.2.1. Size and zeta potential of TCPs at N/P 16 measured by DLS measurements. [TNB-modified oligomer / unmodified thiol-oligomer] molar ratio = 1:1. The experiments were performed by Dr. Dongsheng He (PhD study, Department of Pharmacy, Ludwig-Maximilians-Universität München).

To study the morphology of these formulations, we carried out transmission electron microscopy (TEM) measurements. As shown in Figure 3.2.3A, these images indicated the formation of homogeneous spherical nanoparticles with sizes in a range consistent with the DLS measurements. No aggregates were observed for these siRNA polyplexes. Moreover, to validate the siRNA binding activity of TCPs, we analyzed the siRNA polyplex formation by agarose gel shift assay (Figure S2-5 in [76]). In general, when increasing the fraction of 3-arm Stp oligomers in TCP formulations, the siRNA binding was significantly increased. Apparently the 3-arm Stp oligomers

were essential for compaction and stability of siRNA polyplexes. At the molar ratio of 1:1, all TCP formulations exhibited complete siRNA binding at N/P 16 (Figure 3.2.32B).

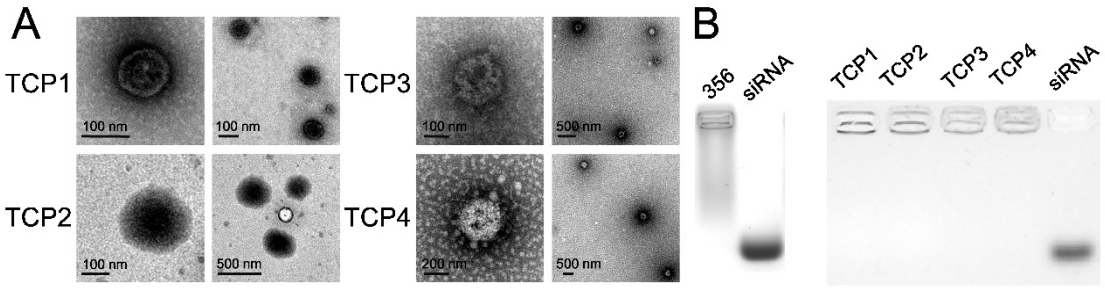

Figure 3.2.3. Physicochemical assessments of TCPs. (A) TEM images of TCPs at N/P 16. (B) siRNA binding of TCPs at N/P 16 determined by agarose gel shift assay. Free siRNA and folate-linked PEGylated oligomer **356** [33] were used as controls.

3.2.3 Receptor-mediated uptake of TCPs

As folate retains high affinity for FR following derivatization *via* one of its two carboxylate groups [77], folate conjugation presents an advantageous strategy for FR-targeted drug delivery. To validate targeting capacity of the folate-linked TCPs, fluorescent Cy5-labeled siRNA was used to study the cellular internalization profile by flow cytometry. To investigate selective targeting ability of TCPs against FR, FR-rich cancer cell lines (murine lymphocytic leukemia L1210 cells, murine lung carcinoma M109 cells and human cervix carcinoma KB cells) and FR-deficient human mammary adenocarcinoma MCF-7 cells [45, 67, 78-80] were applied for the following experiments.

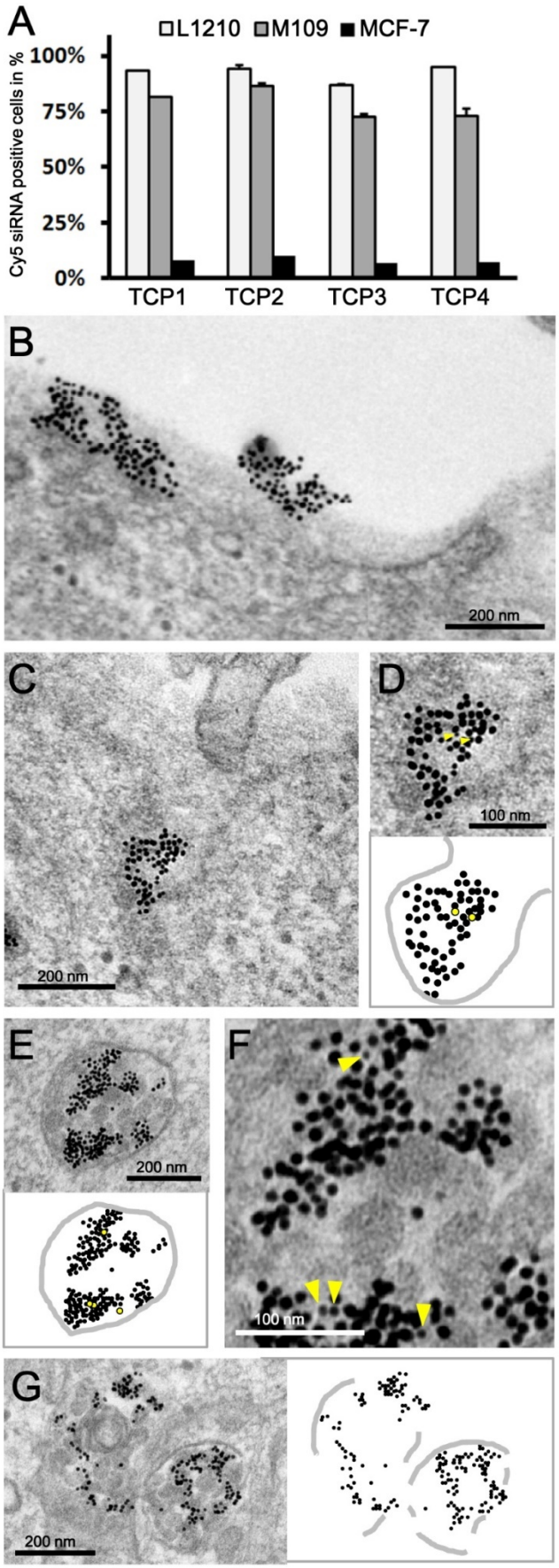

Figure 3.2.4. Folate receptor (FR)-mediated uptake and intracellular distribution of TCPs. (A) The cellular internalization capacity of TCPs was evaluated by comparing the cellular internalization of siRNA polyplexes into FR-overexpressing M109 and L1210 vs. FR-deficient MCF-7 cells. siRNA polyplexes were prepared at N/P 16 with Cy5-labeled siRNA. The cells were incubated with siRNA polyplexes at 37 °C for 4 h before flow cytometric measurements. The amount of Cy5-positive cells was analyzed through excitation of the dye at 635 nm and detection of emission at 665/20 nm. (B-G) Immuno-TEM of FR-mediated endocytic pathway of TCP1 in FR-overexpressing KB cells. TCP1 was formed at N/P 16 with biotinylated-siRNA tagged with 10 nm neutravidin-gold particles. FR was visualized with anti-FR-α antibodies and Protein-G coupled to 6 nm gold particles. (B) Association of siRNA polyplexes with the cell surface after incubation of cells with siRNA polyplexes for 15 min. (C) The colocalization of siRNA polyplexes with FR in membrane invagination after incubation for 15 min. (D) The FR localizing in close proximity to siRNA polyplexes in membrane invagination indicated by yellow arrowheads or dots in higher-magnification image and the scheme of (C), respectively. (E) Colocalization of FR (yellow dots) with siRNA polyplexes inside endosomal vesicles after incubation for 1 h. (F) The higher-magnification image of (E) indicating FR by yellow arrowheads. (G) Endosomal structures with disrupted membrane, indicating endosomal escape of siRNA molecules after incubation for 4 h. The experiments were performed in collaboration with Dr. Kärt Padari (Institute of Molecular and Cell Biology, University of Tartu).

The cells were treated with TCPs at N/P 16 for 4 h at 37 °C, and then uptake of siRNA polyplexes was analyzed by flow cytometry (Figure 3.2.4A). Generally, all the TCP formulations exhibited strong cellular internalization in FR-rich cells. The uptake levels for TCPs in L1210 cells were similar (87-95% positive cells), which were higher than the levels in M109 cells (73-86% positive cells). In contrast, after transfecting FR-deficient MCF-7 cells with TCPs, the uptake levels were very low (5-9%). Hence, the cellular uptake studies demonstrated that folate-conjugated TCP formulations were taken up into cells in a receptor-specific fashion, based on the observations that siRNA polyplexes efficiently bound to FR-expressing L1210 and M109 cells, and the uptake of TCPs diminished in FR-negative MCF-7 cells. To further confirm the involvement of FR in the cellular uptake of TCPs, and to gain more detailed insight into how these polyplexes associate with receptors and how they are endocytosed by cells, immuno-TEM was used [81]. These studies were performed during a research visit at Institute of Molecular and Cell Biology, University of Tartu. For detecting the colocalization of TCPs and FR, we used different sizes of gold particles for immuno-labeling. The primary antibodies against FR were visualized with Protein G-gold conjugates (6 nm in diameter), whereas biotinylated siRNA was labeled with neutravidin-gold conjugates (10 nm in diameter). Namely, 6 nm-gold probe for detecting FR and 10 nm gold tag for detecting siRNA polyplexes should be distinguishable in cells by TEM at ultrastructural scale. To examine the internalization process of TCPs starting from their initial binding to the cell surface and subsequent intracellular pathway, FR-positive KB cells were incubated with 10 nm gold label-containing TCP1 for 15 min, 1 h and 4 h. After incubation for 15 min, siRNA polyplexes were detected as electron dense particles associated with the cell surface (Figure 3.2.4B) and induced invaginations in the plasma membrane of KB cells (Figure 3.2.4C). As illustrated in the higher-magnification image we observed the receptors (indicated by arrowheads in Figure 3.2.4D) were in close proximity to siRNA polyplexes in endosomal invaginations. At 1 h, inside cells, most of siRNA polyplexes were entrapped in endosomal structures, where they formed large dense TCP1 clusters and some retained association with the membrane of endosomal vesicles (Figure 3.2.4E). Although the polyplexes localized in densely packed clusters in the endosomal structures, we were able to distinguish some smaller gold particles representing the FR that had associated with TCPs (arrowheads in Figure 3.2.4F). In addition, a small fraction of the endosomal structures had lost the intactness of its limiting membrane (Figure 3.2.4G) already within 4 h and siRNA molecules had escaped from the ruptured vesicles, and infrequently, single 10 nm gold particles denoting TCPs were detected diffusely in cytosol. In contrast, non-targeted siRNA polyplexes were very rarely detected in KB cells or associated with their surface.

3.2.4 Gene silencing efficiency of TCPs

After showing that the folate-conjugated TCPs utilized FR for cellular association and intracellular delivery of siRNA, next their ability to induce target gene silencing was evaluated. In order to validate this, siGFP or siCtrl was used to transfect the KB/eGFPLuc cells, and gene silencing efficiency of siRNA polyplexes was evaluated *via* luciferase activity by luminometric analysis. Former studies of our group indicated that PEGylated siRNA polyplexes, similar as several other PEG-shielded polyplexes [82], face the problem of endosomal entrapment into the cytosol [33]. For this reason, the synthetic peptide Inf7, previously designed as pH-specific analog of the influenza virus hemagglutinin subunit 2 (HA2) N-terminal fusion sequence [72, 83, 84], was covalently coupled to siRNA as endosomolytic agent [33, 53, 85]. In this assay, we sought to compare the transfection efficiency of TCPs with the previously published **356** [33]. As shown in Figure 3.2.5, all the TCP formulations containing Inf7-modified siGFP (siGFP-Inf7) at N/P 16 mediated significant gene silencing efficiency in KB/eGFPLuc cells, as 75-94% of luciferase activity was suppressed. Among these TCP formulations, TCP1 exhibited the most potent gene silencing activity (94%), which is comparable to **356** nanoplexes (90%) and superior to the rest of TCPs. In contrast, in the cells treated with unmodified siGFP polyplexes, the silencing effect was significantly decreased (45-63% for TCPs and 35% for **356**), further highlighting that Inf7 peptide is necessary for sufficient release of siRNA into cytosol, as reported earlier [33, 53, 85].

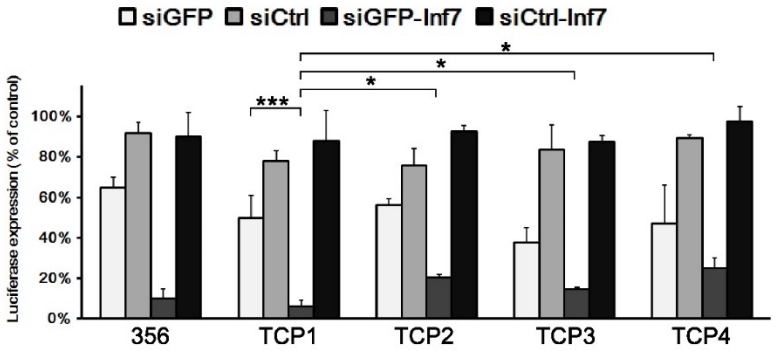

Figure 3.2.5. Gene silencing efficiency of TCPs in KB cells expressing eGFPLuc fusion protein (KB/eGFPLuc cells). The siRNA polyplexes were prepared at N/P 16 with different siRNA sequences: eGFP-targeted siRNA (siGFP), control siRNA (siCtrl), or siRNA chemically linked with the endosomolytic peptide Inf7 (siGFP-Inf7 or siCtrl-Inf7).

3.2.5 Tumor-specific toxicity mediated by EG5 gene silencing

As aforementioned, TCPs facilitated functional gene silencing with Inf7-modified siRNA *in vitro*, we next sought to investigate, whether we could mediate tumor-specific cytotoxicity by using antitumoral siRNA. For this purpose, we exploited siRNA against EG5 (siEG5-Inf7) that corresponds to a sequence of the EG5 coding region conserved between human and mouse, which is able to block the formation of bipolar mitotic spindles, causing cell-cycle arrest and induction of apoptosis [27]. After incubating the cells with siEG5-Inf7 TCPs, MTT assay revealed that all the TCP formulations were cytotoxic to the FR-expressing M109 cells (Figure 3.2.6A). TCP1 and TCP2 mediated the higher cell killing (90%; 85%) than TCP3, TCP4 or the folate-conjugated ***356***. Besides, siCtrl-Inf7 TCPs did not affect cell viability of M109 cells. Meanwhile, in FR-negative MCF-7 cells, there's no similar cytotoxic effect induced by TCPs (Figure 3.2.6B). Moreover, functional EG5 gene silencing was confirmed *via* aster formation of nuclear DNA, where downregulation of EG5 induced a mitotic arrest in siEG5-Inf7-treated M109 cells. After incubation with siEG5-Inf7 polyplexes, Figure 3.2.6C showed the typical mitotic figures in dividing cells by DAPI staining. No aster formation could be observed after application of control siRNA polyplexes. Further examination of EG5-specific gene silencing at mRNA level was performed by qRT-PCR in FR-expressing L1210 cells. Figure 3.2.6D revealed that all the siEG5-Inf7 TCPs triggered very efficient downregulation of EG5 Mrna levels, while TCP1 was significantly more potent than the rest of formulations. In the siCtrl-Inf7-treated cells, the mRNA expression levels were similar to untreated cells, which also reflected that there was no off-target effect by TCPs. Therefore, these results clearly supported that folate-conjugated TCPs enabled efficient silencing of EG5 gene expression at mRNA level, followed by mitotic blockade and finally cell death in FR-positive cells.

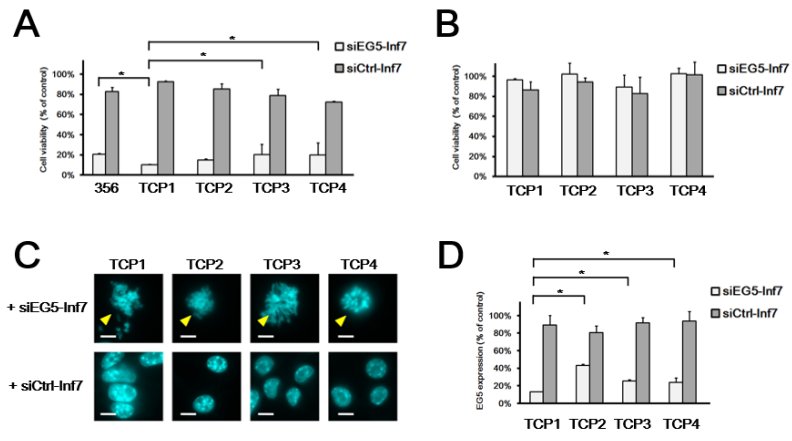

Figure 3.2.6. Cell transfections with TCPs containing Inf7 peptide-modified EG5-targeted siRNA (siEG5-Inf7) or control siRNA (siCtrl-Inf7) at N/P 16. MTT assay in (A) FR-positive M109 cells and (B) FR-negative MCF-7 cells after transfection with TCPs. (C) M109 cells treated with TCPs visualized by fluorescence microscopy after DAPI staining of DNA. The mitotic blockade that was induced by EG5 knockdown caused "aster formation" of nuclear DNA (arrowheads). The scale bars represent 10 μm. (D) mRNA level of EG5 gene measured by qRT-PCR after transfection of TCPs in FR-positive L1210 cells. GAPDH was used as housekeeping gene.

3.2.6 Distribution of TCPs in tumor-bearing mice upon systemic administration

Upon systemic administration, unmodified siRNA is easily eliminated *via* renal clearance because of the small size, thus the half-life of siRNA *in vivo* is very short (few minutes) [86]. Moreover, it can also be enzymatically degraded by endogenous RNases with a serum half-time ranges from several minutes to 1 h [87]. To investigate whether TCPs could improve the distribution profile of siRNA, TCP1, the most potent formulation *in vitro* with favorable size and surface charge, was selected for the further *in vivo* studies. The two single oligomer components of TCP1, *i.e.* 3-arm Stp-based oligomer **386** and DTNB-modified 4-arm PEGylated folate-equipped Sph oligomer **873**, were used for comparison. FR-expressing L1210 tumor cells were implanted subcutaneously in nude mice. We formulated different Cy7-labeled siRNA (50 µg of siRNA) polyplexes at N/P 16, and administered these siRNA polyplexes intravenously (*i.v.*). The biodistribution of Cy7-labeled siRNA measured by near infrared (NIR) fluorescence imaging (Figure 3.2.7A) showed that for TCP1 the systemic distribution of Cy7 signal lasted more than 1 h, and in the meanwhile the tumoral retention of siRNA was observed. In case of the non-targeted 3-arm Stp-based oligomer, Cy7 signal disappeared after ~30 min, and siRNA barely reached the tumor site.

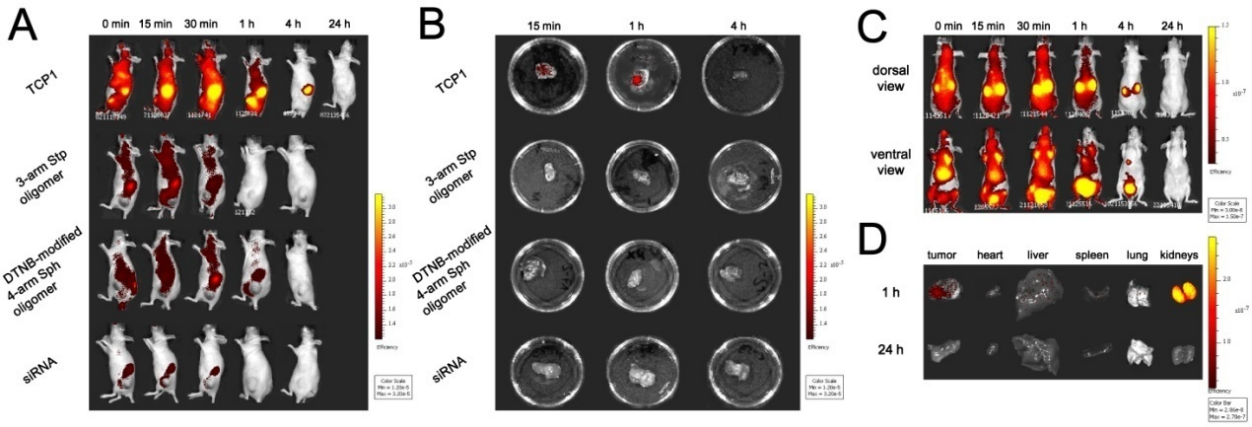

Figure 3.2.7. Biodistribution of siRNA polyplexes at N/P 16 in NMRI-nude mice bearing L1210 tumors determined by NIR fluorescence bioimaging. (A) Time-dependent retention of 50 µg of Cy7-labeled siRNA after *i.v.* injection using TCP1, 3-arm Stp oligomer **386**, DTNB-modified PEGylated folate-conjugated 4-arm Sph oligomer **873** as carriers. Lateral views of animals were shown to present the tumor sites. (B) Tumors harvested 15 min, 1 h or 4 h after injection of siRNA polyplexes. (C) Distribution and elimination of TCP1 over 24 h. (D) Tumors and organs of TCP1-treated animals harvested 1 h or 24 h after injection of siRNA polyplexes. Experiments were performed with 3-4 animals per group; a representative animal of each group is shown. The experiments were in collaboration with Eva Kessel (Dr. med. vet. study, Department of Pharmacy, Ludwig-Maximilians-Universität München).

Additionally, DTNB-modified 4-arm folate conjugate exhibited the first evidence for the tumoral retention of siRNA within 15 min, and the systemic distribution was longer than 3-arm Stp-based oligomer. As control, free siRNA was rapidly filtered by kidneys within 30 min. Notably, Cy7 siRNA was detectable in harvested tumors only from TCP1-treated animals at 1 h, while there was no Cy7 signal in the rest of groups (Figure 3.2.7B). In TCP1-treated animals, the tumor presented the second highest remaining Cy7 signal after the kidneys at 1 h, and both *in vivo* and

ex vivo imaging reflected that siRNA was eliminated through renal clearance within 24 h (Figure 3.2.7C and D).

3.2.7 Tumor-targeted EG5 gene silencing *in vivo*

After confirming that FR-specific TCP1 successfully delivered siRNA in the tumor tissue *via* systemic administration, we sought to validate the functional gene silencing of TCP1 *in vivo*. For this purpose, we formulated TCP1 with siEG5-Inf7 or siCtrl-Inf7 (50 µg of siRNA) at N/P 16, and administered these siRNA polyplexes *i.v.* in the L1210 tumor-bearing mice twice. 24 h after the last treatment, the tumors were harvested. RNA was isolated from tumor tissues, and mRNA expression levels of EG5 gene were evaluated by qRT-PCR. Compared to untreated controls, the siEG5-Inf7 TCP1 reduced the EG5 gene expression by 46%. Importantly, the siCtrl-Inf7 TCP1 showed negligible effects on EG5 mRNA level as compared with untreated tumors (Figure 3.2.8 A).

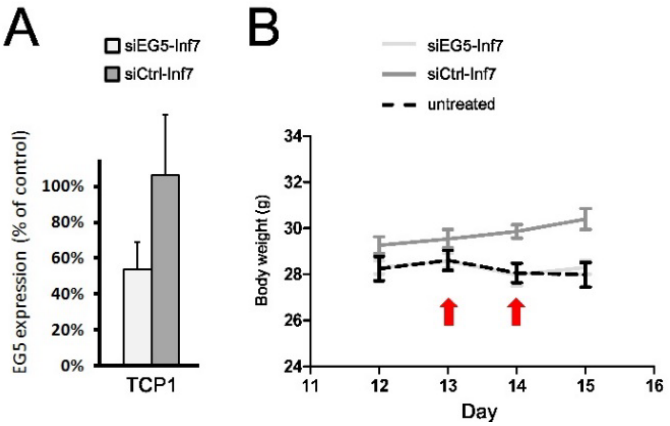

Figure 3.2.8. Tumor-targeted gene silencing efficiency of TCP1 in L1210 tumor-bearing mice. (A) mRNA level of EG5 gene after two-fold *i.v.* injection of TCP1 with 50 µg of siEG5-Inf7 or siCtrl-Inf7 at N/P 16. (B) Body weight development over treatment period. The *i.v.* injections were performed at day 13 and 14 as indicated by arrows. The body weight curves of TCP1-treated animals were compared to that of untreated animals over the same time after tumor inoculation. Experiments were performed with 5 animals per group. The experiments were in collaboration with Eva Kessel (Dr. med. vet. study, Department of Pharmacy, Ludwig-Maximilians-Universität München).

Systemic circulation of siRNA polyplexes might also lead to enhanced exposure to non-target tissues which might cause side effects; we thus monitored the body weights and carried out blood biochemistry examination as preliminary evaluation of potential side effects. As seen in Figure 3.2.8B, the body weight curves indicate that the treatments were well-tolerated compared to untreated controls. We took blood samples 24 h after the treatments to determine the four clinical biochemistry parameters (ALT, AST, BUN and creatinine). Elevated liver enzymes (ALT and AST) would indicate formulation-related liver damage or acute hepatitis, while increased BUN or creatinine would be related to renal malfunctions. As presented in Table 3.2.2, in the treatment groups, liver enzymes were almost equivalent to the untreated control group. In terms of BUN, there was no significant elevation, either. Creatinine showed an elevation for TCP1 with siEG5-

Inf7 treated animals compared to untreated controls, but still these serum values were lower than the reference range of female NMRI-nu/nu mice at the same age (data sheet of NMRI-nu/nu, Janvier Labs). Therefore, TCP1 exhibited siRNA delivery into the tumor and resulted in EG5 gene silencing at mRNA level in the absence of detectable adverse effects.

Table 3.2.2. Clinical biochemistry parameters (ALT, AST, BUN and creatinine). Plasma was obtained from the treated animals 24 h after the second injection (n = 5) compared to untreated tumor-bearing mice (n = 3) that were euthanized on the same day.

	ALT (U/L)	AST (U/L)	Creatinine (mg/dL)	BUN (mg/dL)
TCP1 + siEG5-Inf7	34 ± 15	80 ± 28	0.1 ± 0.01*	43 ± 13
TCP1 + siCtrl-Inf7	39 ± 2	115 ± 36	0.08 ± 0.02	39 ± 6
Untreated	46 ± 15	113 ± 23	0.07 ± 0.01	38 ± 7

* significant difference between untreated control and TCP1 + siEG5-Inf7 treated group.

3.3 Targeted lipopolyplexes (TLPs)

3.3.1 Formation of TLPs

To prepare targeted lipopolyplexes (TLPs) for siRNA delivery, four oligomers from a recently established library of sequence-defined oligomers were chosen (Figure 3.3.1A) [33, 35-37]. Among these, the PEG-folate-conjugated Stp oligomer (**356**) formed neutralized siRNA nanoplexes (TEM images shown in Figure 3.3.1B) but with moderate siRNA binding ability (Figure 3.3.2) [33]. At the same time, fatty acid-modified **454** siRNA polyplexes formed positively charged particles with diameter of 100-130 nm (TEM images were shown in Figure 3.3.1B) with very prominent siRNA binding ability (Figure 3.3.3) [37, 59]. Thus, to optimize the physicochemical properties of siRNA polyplexes, **356** was combined with **454** by different [targeted PEG oligomer / lipo-oligomer] molar ratios to formulate siRNA as TLP1 formulation. For that both oligomers contain terminal cysteines, crosslinkage through disulfide formation is assumed to glue together all three components.

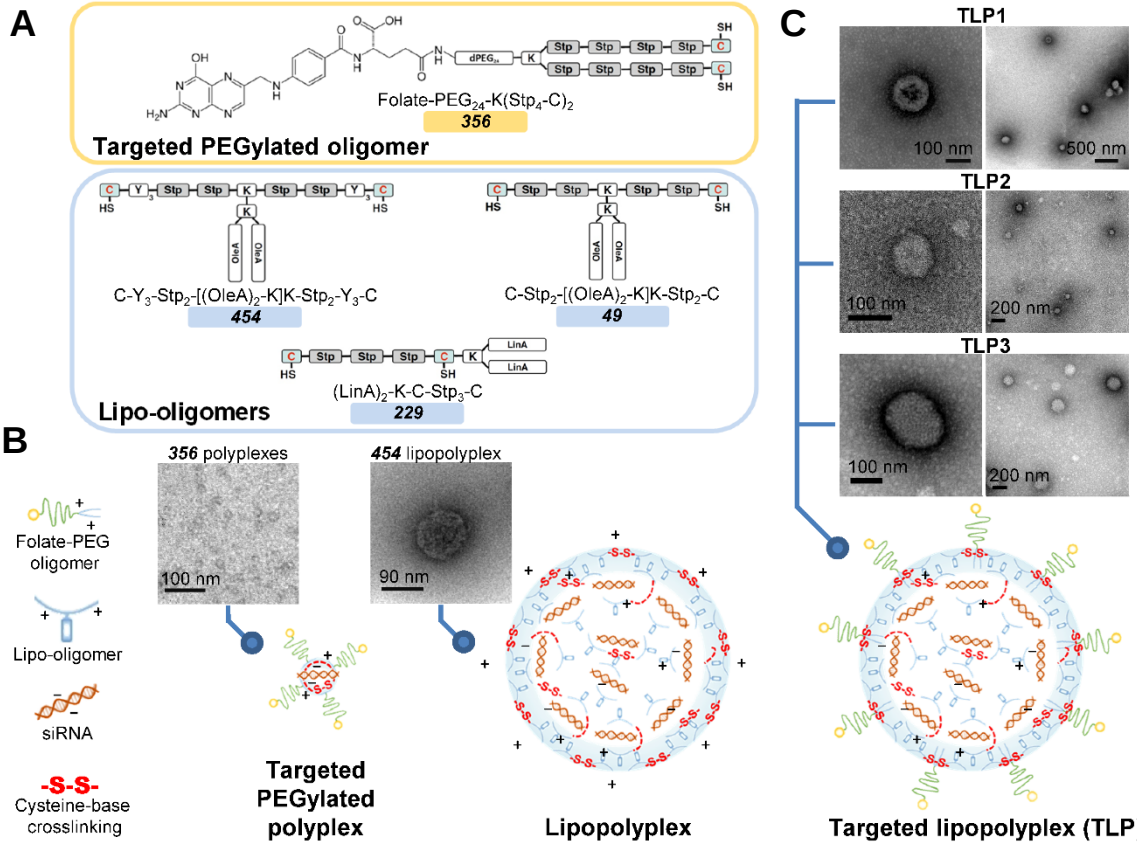

Figure 3.3.1. Targeted lipopolyplexes (TLPs) for siRNA delivery. (A) Structures of targeted PEGylated oligomer (**356**) and lipo-oligomers (**454**, **49** and **229**). C: cysteine; K: lysine; Y: tyrosine; PEG: polyethylene glycol; Stp: succinoyl-tetraethylene pentamine; OleA: oleic acid; LinA: linolic acid; K(and K[refer to branchings by α- and ε-amino modification of lysines. Illustrations and TEM micrographs of (B) targeted PEGylated polyplexes (by folate-conjugated **356** and siRNA), lipopolyplexes (by oleic acid-modified **454** and siRNA) and (C) TLPs (by co-formuations of targeted PEGylated oligomer, lipo-oligomer and siRNA). TLP1: **356** + **454**; TLP2: **356** + **49**; TLP3: **356** + **229**). The TEM imaging was performed in collaboration with Susanne Kempter (Faculty of Physics, Ludwig-Maximilians-Universität München).

Figure 3.3.2. siRNA binding of targeted PEG oligomer (**356**) at N/P 16 determined by agarose gel shift assay. Free siRNA was used as control.

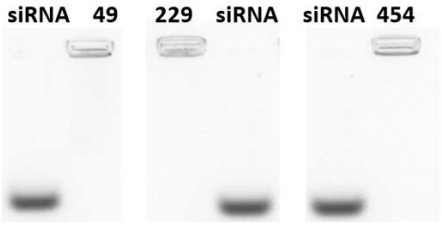

Figure 3.3.3. siRNA binding of lipo-oligomers (**49**, **229**, **454**) at N/P 16 determined by agarose gel shift assay. Free siRNA was used as control.

Table 3.3.1. TLP Formulations[a]

Formulation	Targeted PEG Oligomer	Lipo-Oligomer
TLP1	Folate-PEG$_{24}$-K(Stp$_4$-C)$_2$ (**356**)	C-Y$_3$-Stp$_2$-[(OleA)$_2$-K]K-Stp$_2$-Y$_3$-C (**454**)
TLP2		C-Stp$_2$-[(OleA)$_2$-K]K-Stp$_2$-C (**49**)
TLP3		(LinA)$_2$-K-C-Stp$_3$-C (**229**)

[a] The sequence implies from C- terminal to N- terminal. C: cysteine; K: lysine; Y: tyrosine; PEG: polyethylene glycol; Stp: succinoyl-tetraethylene pentamine; OleA: oleic acid; LinA: linolic acid; K(and K[refer to branchings by α- and ε-amino modification of lysines.

Moreover, based on this strategy, as shown in Table 3.3.1 and Figure 3.3.1C, lipo-oligomer with different motifs such as oleic acid lipo-oligomer (**49**) or linolic acid lipo-oligomer (**229**) was combined with targeted PEGylated oligomer (**356**) to prepare TLP2 and TLP3, respectively.

As measured by dynamic light scattering (DLS) (Table 3.3.2), the surface charge of TLP1 at N/P 16 was dramatically shifted from +16.4 mV (at the ratio of 0%:100% lipo-oligomer) to +2.5 mV (at the ratio of 10%:90%) by addition of PEGylated **356**. At the ratio of 30%:70%, TLP1 presented neutralized zeta potential value and diameter of ~127 nm. Similarly, TLP2 displayed zeta potential value of + 0.1 mV and size of ~90 nm (Table 3.3.3) at the ratio of 30%:70%, while TLP3 exhibited shielded surface charge (+9.2 mV) and size of ~198 nm at the ratio of 20%:80% (Table 3.3.4). Consistent among the TLPs, the morphology of formulations assessed by TEM indicated the TLPs were homogeneous spherical nanoparticles with size in a range similar to the DLS measurements (Figure 3.3.1C). Additionally, when the ratio approached 50%:50%, probably the hydrophilicity/hydrophobicity balance between two classes of oligomers was unstable, the increased particle heterogeneity and even agglomeration were observed from the DLS results.

To evaluate the siRNA binding ability of TLPs at different mixing ratios, we performed gel shift assays (Figure 3.3.4-3.3.6). When the fraction of lipo-oligomers was increased in the TLPs, the siRNA binding was greatly potentiated. Notably, complete siRNA binding was observed between the ratio of 10%:90% and 30%:70% for TLPs. Compared to **356** polyplexes, the results indicated that the presence of the lipo-oligomer in TLP formulations resulted in much improved siRNA binding efficiency, while tyrosine-modified **454** in the TLP1 had highest capacity from these formulations to stabilize the siRNA polyplexes [37]. In conclusion, by co-formulating two functional oligomers, the successful modification of polyplexes was accompanied by distinct changes in the physicochemical properties with tunable sizes, surface shielding and improved siRNA binding. According to these results, the molar ratios of two oligomers for TLPs were optimized (30%:70% for TLP1 and TLP2; 20%:80% for TLP3) for the following *in vitro* and *in vivo* studies.

Table 3.3.2. Size and zeta potential of TLP1 at N/P 16 by DLS measurements. Folate-PEG_{24}-K(Stp_4-C)$_2$ (**356**) as targeted PEG oligomer and C-Y_3-Stp_2-[(OleA)$_2$-K]K-Stp_2-Y_3-C (**454**) as lipo-oligomer were co-formulated according to different molar ratios to form siRNA polyplexes.

[Targeted PEG Oligomer / Lipo-oligomer] Molar Ratio		**Individual N/P Ratios**		**Size (nm)**	**PdI**	**Zeta Potential (mV)**
Targeted PEG Oligomer	Lipo-oligomer	Targeted PEG Oligomer	Lipo-oligomer			
-	100%	-	16	114.6±0.92	0.201±0.003	16.4±0.09
10%	90%	2.8	13.2	130.6±0.56	0.137±0.004	2.5±0.24
20%	80%	5.2	10.8	128.7±0.63	0.159±0.004	2±0.17
30%	70%	7.2	8.8	126.6±2.17	0.121±0.007	-0.1±0.18
40%	60%	9	7	1143±205.3	0.96±0.057	0.7±0
50%	50%	10.5	5.5	674±196.9	0.693±0.222	3.7±0.14
60%	40%	11.9	4.1	402±130.6	0.557±0.194	0.2±0.2
70%	30%	13.1	2.9	340±4.5	0.313±0.01	2.6±0.9
80%	20%	14.2	1.8	296±30.8	0.323±0.03	0.03±0.02
90%	10%	15.1	0.9	295±21.7	0.333±0.009	1.5±0.17

Table 3.3.3. Size and zeta potential of TLP2 at N/P 16 by DLS measurements. Folate-PEG_{24}-K(Stp_4-C)$_2$ (**356**) as targeted PEG oligomer and C-Stp_2-[$(OleA)_2$-K]K-Stp_2-C (**49**) as lipo-oligomer were co-formulated according to different molar ratios to form siRNA polyplexes.

[Targeted PEG Oligomer / Lipo-oligomer] Molar Ratio		**Individual N/P Ratios**		**Size (nm)**	**PdI**	**Zeta Potential (mV)**
Targeted PEG Oligomer	Lipo-oligomer	Targeted PEG Oligomer	Lipo-oligomer			
-	100%	-	16	90.8±0.4	0.256±0.014	13.6±1.4
10%	90%	2.8	13.2	125.7±1.1	0.126±0.021	17.5±0.6
20%	80%	5.2	10.8	93.5±0.7	0.182±0.003	18.2±0.5
30%	70%	7.2	8.8	90.3±1.5	0.193±0.011	0.1±0.2
40%	60%	9	7	2199±83.5	1±0	1.7±0.1
50%	50%	10.5	5.5	1562±435.4	1±0	4.1±0.5
60%	40%	11.9	4.1	2026±674.2	0.967±0	1±0.3
70%	30%	13.1	2.9	1196±300.1	0.933±0.047	4.3±
80%	20%	14.2	1.8	942±201.6	0.71±0.1	4±0.6
90%	10%	15.1	0.9	445±61.5	0.45±0.04	3.9±0.2

Table 3.3.4. Size and zeta potential of TLP3 at N/P 16 by DLS measurements. Folate-PEG_{24}-K(Stp_4-C)$_2$ (**356**) as targeted PEG oligomer and $(LinA)_2$-K-C-Stp_3-C (**229**) as lipo-oligomer were co-formulated according to different molar ratios to form siRNA polyplexes.

[Targeted PEG Oligomer / Lipo-oligomer] Molar Ratio		**Individual N/P Ratios**		**Size (nm)**	**PdI**	**Zeta Potential (mV)**
Targeted PEG Oligomer	Lipo-oligomer	Targeted PEG Oligomer	Lipo-oligomer			
-	100%	-	16	224±18.9	0.73±0.14	20.7±
10%	90%	3.8	12.2	183±2.5	0.277±0.04	15±0.5
20%	80%	6.6	9.4	198±4	0.293±0.02	9.2±0.6
30%	70%	8.7	7.3	1046±427.2	0.81±0.142	7.6±1.3
40%	60%	10.4	5.6	2636±1153.2	0.99±0.01	4.7±0.9
50%	50%	11.8	4.2	1096±149.9	0.89±0.08	3±0.6
60%	40%	12.9	3.1	806±135.5	0.66±0.08	2.9±0.2
70%	30%	13.9	2.1	630±122	0.617±0.11	4.2±0.9
80%	20%	14.7	1.3	890±52.2	0.55±0.07	-0.04±0
90%	10%	15.4	0.6	893±76.3	0.561±0.07	5.9±0.9

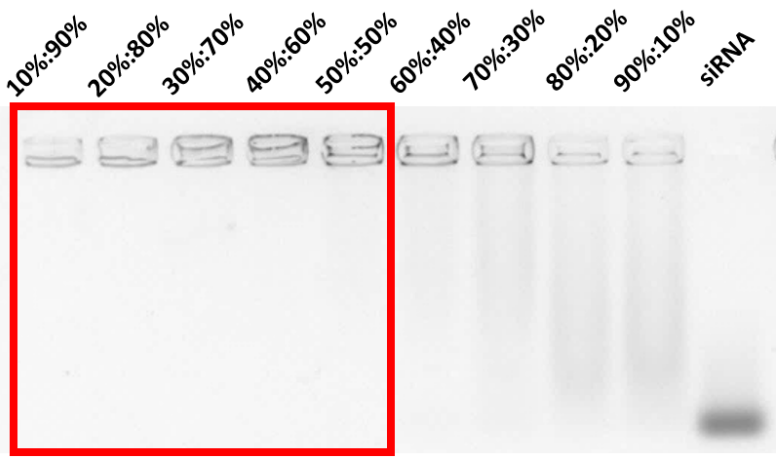

Figure 3.3.4. siRNA binding of TLP1 at N/P 16 determined by agarose gel shift assay. Folate-PEG_{24}-K(Stp_4-C)$_2$ (**356**) as targeted PEG oligomer and C-Y_3-Stp_2-[$(OleA)_2$-K]K-Stp_2-Y_3-C (**454**) as lipo-oligomer were co-formulated according to different [targeted PEG oligomer / lipo-oligomer] molar ratios to form siRNA polyplexes. Free siRNA was used as control. Complete siRNA binding was marked in red rectangle.

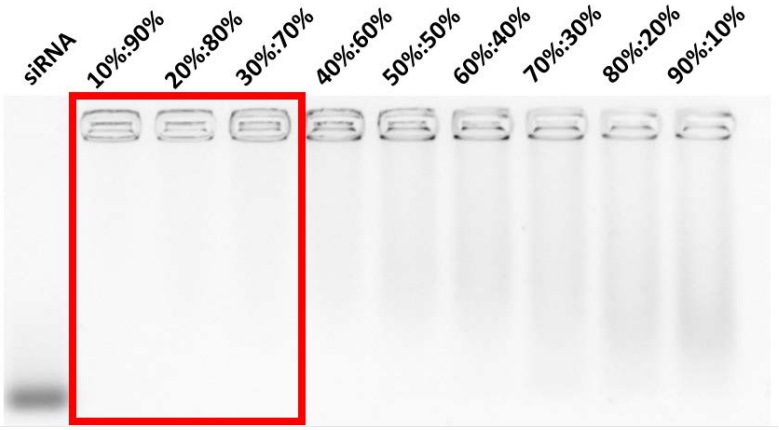

Figure 3.3.5. siRNA binding of TLP2 at N/P 16 determined by agarose gel shift assay. Folate-PEG_{24}-K(Stp_4-C)$_2$ (**356**) as targeted PEG oligomer and C-Stp_2-[$(OleA)_2$-K]K-Stp_2-C (**49**) as lipo-oligomer were co-formulated according to different [targeted PEG oligomer / lipo-oligomer] molar ratios to form siRNA polyplexes. Free siRNA was used as control. Complete siRNA binding was marked in red rectangle.

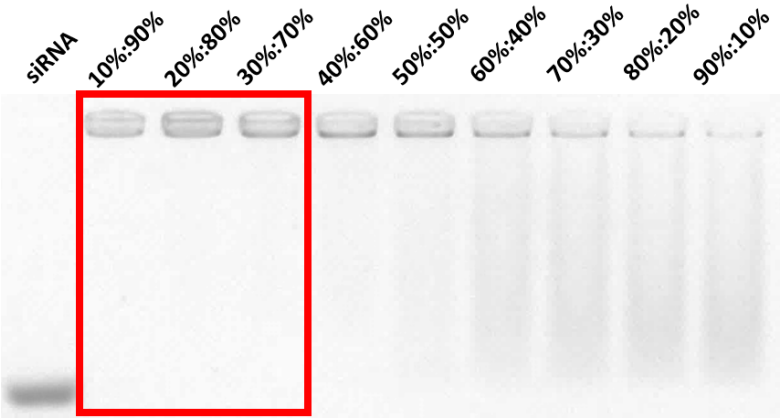

Figure 3.3.6. siRNA binding of TLP3 at N/P 16 determined by agarose gel shift assay. Folate-PEG_{24}-K(Stp_4-C)$_2$ (**356**) as targeted PEG oligomer and $(LinA)_2$-K-C-Stp_3-C (**229**) as lipo-oligomer were co-formulated according to different [targeted PEG oligomer / lipo-oligomer] molar ratios to form siRNA polyplexes. Free siRNA was used as control. Complete siRNA binding was marked in red rectangle.

3.3.2 Receptor-mediated internalization and intracellular distribution of TLPs

To verify targeting capacity of the folate-linked TLPs, fluorescent Cy5-labeled siRNA was exploited to study the cellular internalization profile by flow cytometry, and FR-rich tumor cell lines as L1210, M109 and KB cells, and FR-deficient cell line as MCF-7 cells [67, 76, 78, 79] were subjected for the following experiments.

The cells were treated with TLPs at N/P 16 for 4 h at 37 °C, and then the uptake levels of TLPs were analyzed by flow cytometry (Figure 3.3.7A). All the TLP formulations exhibited strong cellular internalization in FR-rich cells. The uptake levels for the TLPs in L1210 cells were similar (91-93% positive cells), which were higher than the levels in M109 cells (76-81% positive cells). On the contrary, all the TLP formulations barely entered FR-deficient MCF-7 cells. For control studies, alanine-substituted oligomer ***188*** and aforestated lipo-oligomers were co-formulated as non-targeted lipopolyplexes (NTLPs) (Table 3.3.5). In KB cells, the level of TLP1 (88% positive cells) was comparable as ***356*** polyplexes (91% positive cells), while NTLP1 mediated insufficient cellular uptake. In short, these results gave evidence that TLPs were internalized in a FR-specific manner, and the folate conjugates were required for association with the target tumor cells.

The crucial question about the membrane association, translocation into cells and the following trafficking of TLPs remained obscure. A powerful tool to elucidate the internalization mechanism of TLPs is TEM [81], which has been employed to examine the cell entry processes and intracellular distribution of various macromolecules and particles [88, 89]. Nevertheless, among these, few studies have focused on the targeted delivery of siRNA [76, 90]. To locate the receptor in relation to the plasma membrane and cellular organelles, the primary antibodies against FR were visualized with Protein G-gold conjugate (6 nm in diameter). To map the siRNA molecules, biotinylated siRNA was labeled with neutravidin-gold conjugate (10 nm in diameter). These studies were performed during a research visit at Institute of Molecular and Cell Biology, University of Tartu.

Table 3.3.5. TLP Formulations[a]

Formulation	Targeted PEG Oligomer	Lipo-Oligomer
NTLP1	A-PEG_{24}-K(Stp_4-C)$_2$ (**188**)	C-Y_3-Stp_2-[$(OleA)_2$-K]K-Stp_2-Y_3-C (**454**)
NTLP2		C-Stp_2-[$(OleA)_2$-K]K-Stp_2-C (**49**)
NTLP3		$(LinA)_2$-K-C-Stp_3-C (**229**)

[a] The sequence implies from C- terminal to N- terminal. C: cysteine; K: lysine; Y: tyrosine; PEG: polyethylene glycol; Stp: succinoyl-tetraethylene pentamine; OleA: oleic acid; LinA: linolic acid; K(and K[refer to branchings by α- and ε-amino modification of lysines.

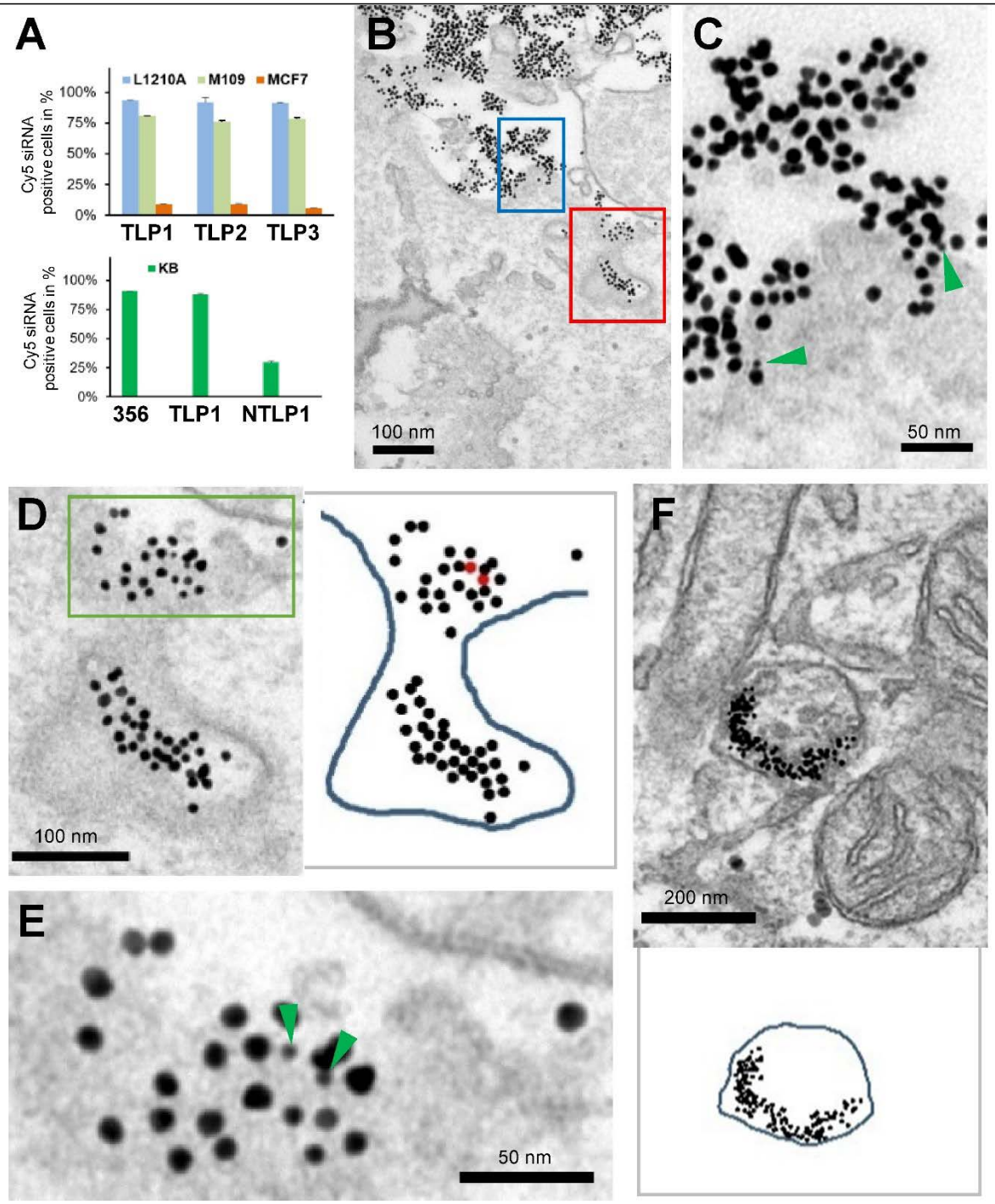

Figure 3.3.7. Folate receptor (FR)-mediated uptake and intracellular distribution of TLPs. (A) The cellular internalization capacity of TLPs was evaluated by comparing the uptake levels of siRNA polyplexes in FR-overexpressing L1210, M109 & KB vs. FR-deficient MCF-7 cells. siRNA polyplexes were prepared at N/P 16 with Cy5-labeled siRNA. The cells were incubated with siRNA polyplexes at 37 °C for 4 h before flow cytometric measurements. The amount of Cy5-positive cells was analyzed through excitation of the dye at 635 nm and detection of emission at 665/20 nm. (B-F) Immuno-TEM of FR-mediated endocytic pathway for TLP1 in FR-overexpressing KB cells. TLP1 was formed at N/P 16 with biotinylated-siRNA tagged with 10 nm neutravidin-gold particles. FR was visualized with anti-FR-α antibodies and Protein-G coupled to 6 nm gold particles (green arrowheads in the images or red dots in the scheme). The experiments were performed in collaboration with Dr. Kärt Padari (Institute of Molecular and Cell Biology, University of Tartu). (B) Association of siRNA polyplexes with the cell surface after incubation with siRNA polyplexes for 15 min. (C) The higher-magnification image of blue rectangle in (B) showed the association of siRNA polyplexes with FR. (D) The higher-magnification image of red rectangle in (B) showed membrane invagination. (E) The higher-magnification image of green rectangle in (D) indicated FR localizing in close proximity to siRNA polyplexes. (F) siRNA polyplexes localized inside the vesicular structure after 1 h.

As demonstrated in Figure 3.3.7B, after incubating FR-positive KB cells with 10 nm gold label-containing TLP1 for 15 min, siRNA polyplexes were detected prominently as electron dense particles and associated quickly with the cell surface. In the higher-magnification image, siRNA polyplexes seemed to be in close contact with the FR (6 nm gold tags indicated by arrowheads in Figure 3.3.7C). Subsequently, the colocalization of siRNA polyplexes and the FR (indicated by red dots in the scheme of Figure 3.3.7D and arrowheads in the enlarged image as Figure 3.3.7E) induced morphological changes in the plasma membrane, leading to the formation of membrane invaginations. Later at 1 h, siRNA polyplexes shifted deeper into the cytoplasm, being finally fully engulfed by the cell into vesicles (Figure 3.3.7F), which resembled the structures of endolysosomal pathway. Besides, NTLP1 were very rarely detected at the cell surface, and this correlated well with the inefficient uptake level measured by flow cytometry in KB cells (Figure 3.3.7A).

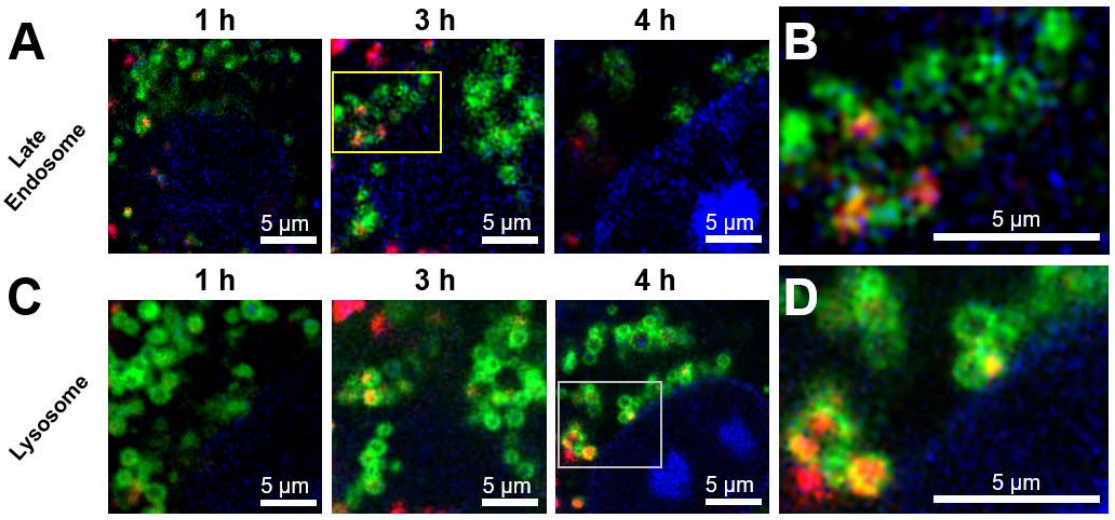

Figure 3.3.8. Time-lapse confocal laser scanning microscopy (CLSM) for TLP1 transduction in KB cells. TLP1 was prepared at N/P 16 with AF 647-labeled siRNA (red). The nuclei (blue) were stained with Hoechst 33342. The yellow and gray rectangles were enlarged as (B) and (D), respectively. (A) Endosomes (green) were visualized with CellLight Late Endosomes-RFP. (B) Lysosomes (green) were marked with CellLight Lysosomes-GFP. The experiments were performed in collaboration with Dr. Xueying Liu (Innovation Center of NanoMedicine).

As a next step, the involvement of endo-/lysosomal compartments in the transport of TLPs was further differentiated upon a collaborative research visit at Innovation Center of NanoMedicine and University of Tokyo. To gain more detailed insights into the dynamics of TLPs, we formulated TLP1 with AF 647-labeled siRNA, labeled late endosomes with CellLight Late Endosomes-RFP, and lysosomes with CellLight Lysosomes-GFP, and performed time-lapse confocal laser scanning microscopy (CLSM) with cultured KB cells. Within 1 h (Figure 3.3.8A), AF 647-labeled siRNA (red) polyplexes were gradually associated with late endosomes (green), and the colocalization of siRNA and late endosomes was obvious after incubation for 1 and 3 h. As shown in the enlarged

image (Figure 3.3.8B), the overlap of two signals suggested that TLP1 was entrapped in late endosomes. Between 3 and 4 h, the association with late endosomes diminished; and expectedly, at the same time, the colocalization of siRNA polyplexes and lysosomes (green) became excessive (Figure 3.3.8C). As shown in Figure 3.3.8D, the majority of siRNA polyplexes were found to be inside lysosomes at 4 h.

Hence, these findings validated that TLPs were capable of efficient tumor cell-specific uptake, and a particular emphasis is placed on the intracellular distribution of TLPs during FR-mediated endocytosis. FR appeared to serve as a docking point for TLPs, and the binding of TLPs to receptors shortly induced internalization of siRNA polyplexes within 15 min. Afterwards, at 1−3 h, late endosomes most often governed the transduction of TLP1, and the vesicles trafficked through the endolysosomal pathway experiencing a gradual drop of pH, then siRNA polyplexes were finally targeted to lysosomes.

3.3.3 siRNA release and reporter gene silencing by TLPs

As most of TLPs retained their dense packing inside endolysosomal compartments after cellular uptake, it is crucial to understand whether the cargo can be released from the endosomal entrapments, reach to the cytoplasm and be available for RNAi machinery for mediating gene silencing. To shed further light on the siRNA release from TLPs by immuno-TEM, we incubated KB cells with TLP1 (N/P 16) for 4 h (Figure 3.3.9). Generally, these TLP1-containing vesicles were intact and surrounded by a continuous membrane. Occasionally, some of these vesicles had a discontinuous membrane, and the electron density of the vesicle content was undistinguishable from that of cytosol (Figure 3.3.9A). Moreover, single (Figure 3.3.9B) or a small cluster (Figure 3.3.9C) of gold particles were spread apparently free in cytosol, often in the close proximity of vesicles with discontinuous membrane. As a key role in the delivery of TLPs, internalized FR proteins (arrowheads in Figure 3.3.9B and D) were still associated with siRNA polyplexes.

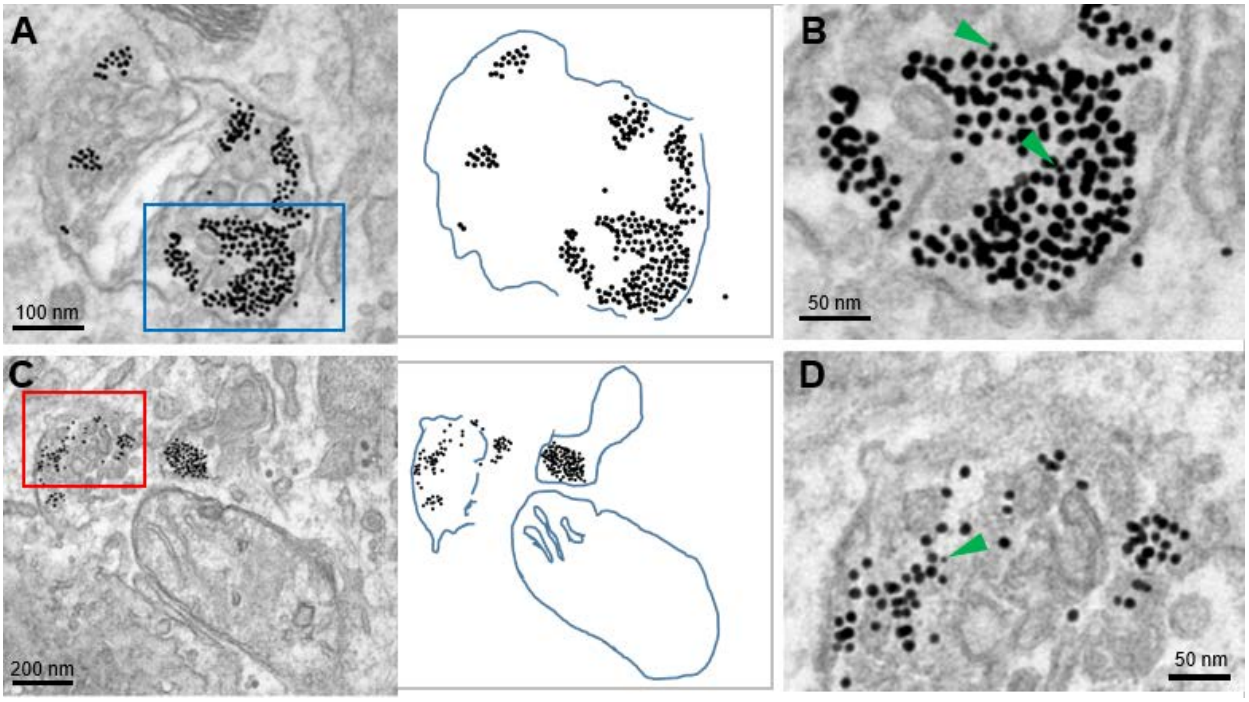

Figure 3.3.9. Morphological changes in TLP1-containing vesicles in FR-overexpressing KB cells at 4 h monitored by immuno-TEM. TLP1 was formed at N/P 16 with biotinylated-siRNA tagged with 10 nm neutravidin-gold particles. FR was visualized with anti-FR-α antibodies and Protein-G coupled to 6 nm gold particles (green arrowheads in the image). Discontinuous membrane of some endosomes resulted in endosomal escape of the siRNA molecules. (A) and (C) were accompanied by higher-magnification images, (B) and (D), respectively. The experiments were performed in collaboration with Dr. Kärt Padari (Institute of Molecular and Cell Biology, University of Tartu).

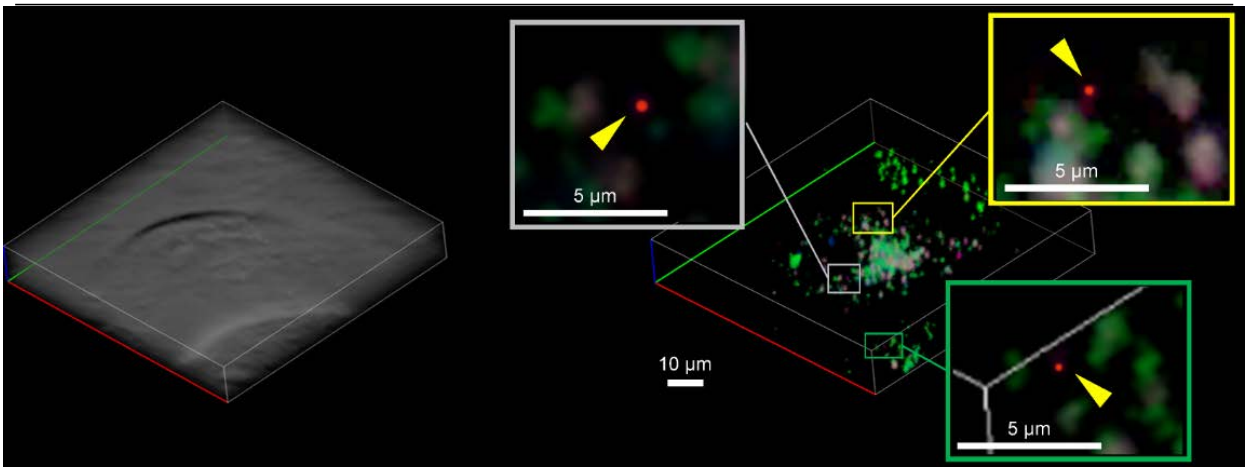

Figure 3.3.10. Reconstructed KB cell showing the distribution of siRNA, late endosomes and lysosomes based on CLSM. KB cells were incubated with TLP1 (N/P 16) containing AF 647-labeled siRNA (red) for 4 h. Late endosomes (blue) were visualized with CellLight Late Endosomes-RFP, and lysosomes (green) were marked with CellLight Lysosomes-GFP. The experiments were performed in collaboration with Dr. Xueying Liu (Innovation Center of NanoMedicine).

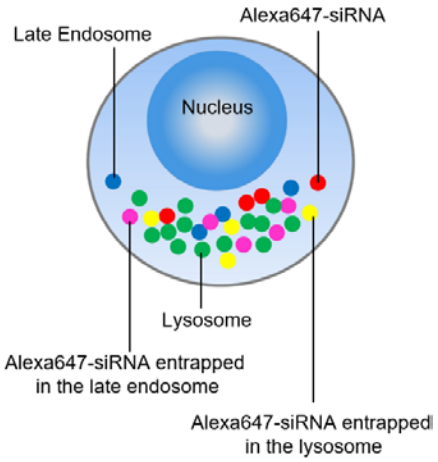

Figure 3.3.11. The scheme interpreting the distribution of siRNA, late endosomes and lysosomes in reconstructed KB cell using CLSM.

In an attempt to confirm the dislocation of siRNA from endolysosomal compartments, the results obtained by TEM were complemented by analogous experiments with CLSM. TLP1 was complexed with AF 647-labeled siRNA at N/P 16, and KB cells were stained with CellLight Late Endosomes-RFP and CellLight Lysosomes-GFP. To avoid misleading interpretation based on spatial limitations, 3D reconstruction of serial images from single cell was utilized (Figure 3.3.10 and 3.3.11). As shown in Figure 3.3.10, lysosomes (green) were dominant, and late endosomes (blue) were scarcely distributed in the cell. Similarly, siRNA molecules (red) were largely overlapped with late endosomes (purple) or lysosomes (yellow). Notably, although at low frequency, escaping siRNA molecules were detectable (yellow arrowheads in Figure 3.3.10), suggesting TLP1 managed to deliver siRNA into cytosol.

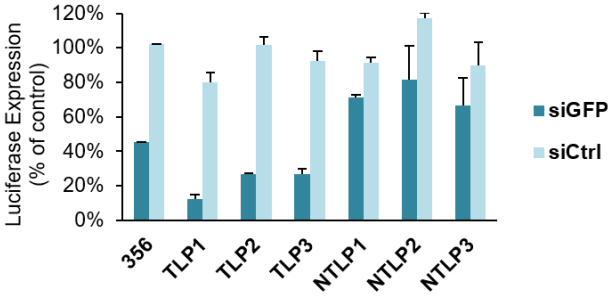

Figure 3.3.12. Gene silencing efficiency of TLPs in KB cells expressing eGFPLuc fusion protein (KB/eGFPLuc cells) measured by luminometer. The siRNA polyplexes were prepared at N/P 16 with different siRNA sequences: eGFP-targeted siRNA (siGFP) and control siRNA (siCtrl). After incubation of TLPs for 45 min, the luciferase expression was analyzed at 48 h, and presented as percentage in comparison to untreated control cells.

We next planned to estimate the ability of TLP formulations to induce target gene silencing in the cancer cell culture models. For this, we formulated siRNA targeting eGFP (siGFP) or control siRNA (siCtrl) within the different TLP formulations and carried out the transfections in the KB/eGFPLuc cells, which are stably expressing eGFP-Luciferase (eGFPLuc) fusion protein, and evaluated target gene silencing *via* luciferase activity by luminometric analysis. As shown in Figure 3.3.12, all the TLP formulations containing siGFP at N/P 16 mediated significant gene silencing efficiency in KB/eGFPLuc cells, as 73-88% of luciferase activity was downregulated. This effect was superior to the parent **356** polyplexes (55%). Among these TLP formulations, the most efficient gene silencing activity was achieved by TLP1 (88%). At the same time, polyplexes with siCtrl did not induce any unspecific gene silencing. Furthermore, non-targeted NTLPs formulations failed to reduce the reporter gene expression, highlighting that TLPs were taken up and able to invoke RNAi in the target cells by a specific manner. Very importantly, the parent oligomer **356** had limited ability for endosomal escape, and for robust pharmacological activity, it required the presence of the endosomolytic Inf7 peptide modification on siRNA [33]. As indicated by the studies above, the novel formulation strategy enabled us to overcome this limitation and achieve very efficient gene knockdowns with simply regular siRNA (without the need for additional endosmolytic modification).

To conclude, TEM and CLSM demonstrated the intracellular mode of trafficking of the TLPs and their ability to release siRNA from endosomes to cytosol (*i.e.* the site-of-action of siRNA). Furthermore, the gene silencing assay confirmed that TLPs allowed the siRNA to be released from polyplexes after FR-mediated endocytosis, and showed remarkable target gene silencing effect.

3.3.4 Receptor-dependent antitumoral activity by EG5 gene silencing

As aforementioned, TLPs mediated impressive functional gene silencing *in vitro*, and hence we next sought to investigate, whether by siRNA against EG5 (siEG5) we could achieve cell-targeted cytotoxicity in FR-expressing tumor cells. We formulated TLPs with siEG5 and treated both FR-positive KB cells and FR-negative MCF-7 cells for 45 min.

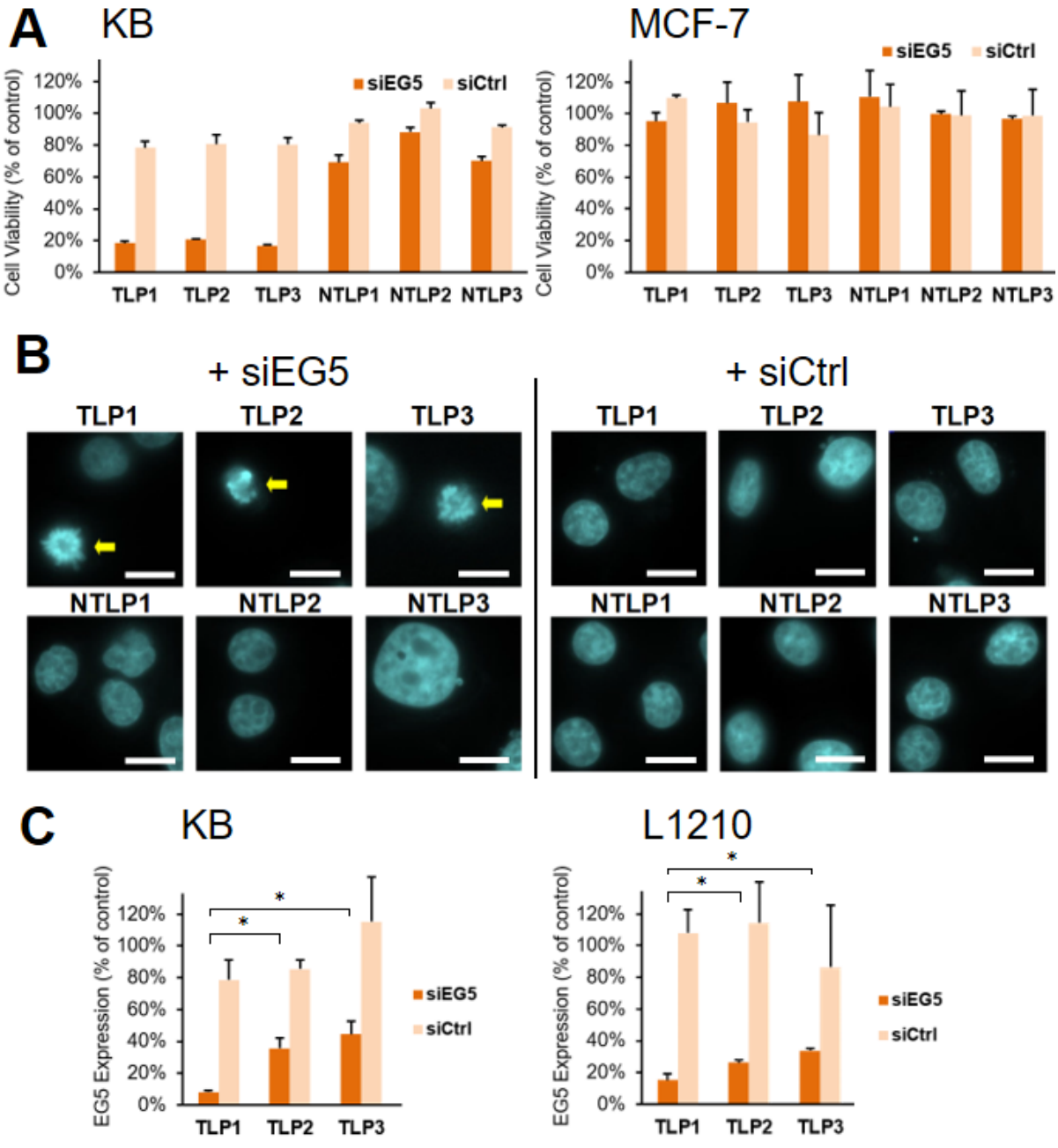

Figure 3.3.13. Treatments of TLPs containing EG5-targeted siRNA (siEG5) or control siRNA (siCtrl) at N/P 16. (A) Metabolic activity of FR-positive KB and FR-negative MCF-7 cells at 48 h after treatment with TLPs. (B) KB cells treated with TLPs observed by DAPI staining under the fluorescent microscope. The mitotic blockade that was induced by EG5 knockdown caused "aster formation" of nuclear DNA (yellow arrows). The scale bars represent 10 µm. (C) mRNA level of EG5 gene measured by qRT-PCR at 48 h after transfection of TLPs in FR-positive KB and L1210 cells. GAPDH was used as housekeeping gene.

After incubation for 48 h, a metabolic activity assay was used for assigning cell viability upon the treatments with the formulations, which reflected that all the siEG5 TLP formulations initiated effective cell killing in KB cells (Figure 3.3.13A). Besides, siCtrl TLPs did not affect cell viability in KB cells, indicating EG5-mediated effect was specific. Also, experiments in FR-negative MCF-7 cells confirmed that EG5-containing TLP formulations did not have any cytotoxic effect on non-target cells, indicating that uptake and cytotoxicity of the formulation was driven by the folate-FR interaction (Figure 3.3.13A). Moreover, siEG5-mediated cytotoxicity by EG5 was also confirmed in another FR-overexpressing cell line M109 (Figure 3.3.14). Moreover, it has been demonstrated that EG5 protein downregulation by RNAi leads to a monopolar spindle formation and arrest of cells in prometaphase with a phenotype as aster formation of nuclear DNA [53, 91]. After incubation with siEG5 TLPs, Figure 3.3.13B illustrated such typical mitotic asters (indicated by yellow arrows) in KB cells by DAPI staining. As expected, no aster formation was observed in case of siCtrl TLPs treatments.

EG5-specific gene silencing at mRNA level was further examined by qRT-PCR in FR-expressing KB and L1210 cells. As seen in Figure 3.3.13C, treatments with all siEG5 TLPs triggered pronounced degradation of EG5 mRNA expression levels in both cell lines. Moreover, siCtrl treatment remained on bar with untreated group, indicating the specificity of the EG5 knockdown without off-target effect. It is of notice that TLP2 and TLP3 had very similar gene silencing activity by qRT-PCR, in line with the preceding silencing experiments in the eGFPLuc assay (Figure 3.3.12). Interestingly, in both silencing models, TLP1 was significantly more potent than the rest of formulations (92% in KB cells; 85% in L1210 cells).

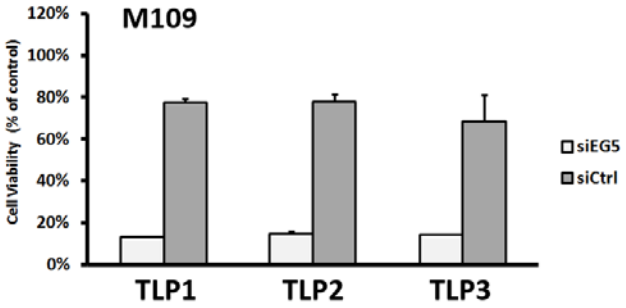

Figure 3.3.14. Metabolic activity of FR-postivie M109 cells after treatments of TLP containing EG5-targeted siRNA (siEG5) or control siRNA (siCtrl) at N/P 16 at 48 h.

These results provided clear evidence that folate-conjugated TLPs enabled efficient silencing of EG5 expression at mRNA level, followed by mitotic blockade and finally cell death, and these effects were mediated by the presence of the FR on the cancer cells. Whereas, further studies were required to discern the potential factors for the different gene silencing potencies of different TLPs.

3.3.5 siRNA release kinetics and stability in cells

Although all the TLPs induced comparably efficient cellular uptake in FR-expressing cells (Figure 3.3.7A), gene silencing ability for different TLPs varied for some reason (Figure 3.3.12 and 3.3.13C). To explore the underlying mechanisms, with a focus on molecular pharmacokinetics, we examined the translocation of siRNA from endosomes to cytosol after transfection to estimate endosomal escaping capability profile of each formulation. The intracellular distribution of AF 647-labeled siRNA polyplexes was analyzed by co-staining of late endosomes and lysosomes using LysoTracker Green in KB cells with CLSM. As presented in Figure 3.3.15A, colocalization (yellow) of AF 647-labeled siRNA (red) with late endosomes and lysosomes (green) was monitored at 2 and 4 h. As previously shown in Figure 3.3.8, the TLP-containing vesicles were actively shifted from late endosomes to lysosomes between 3 h and 4 h after transfection, where TLPs experienced gradual acidification.

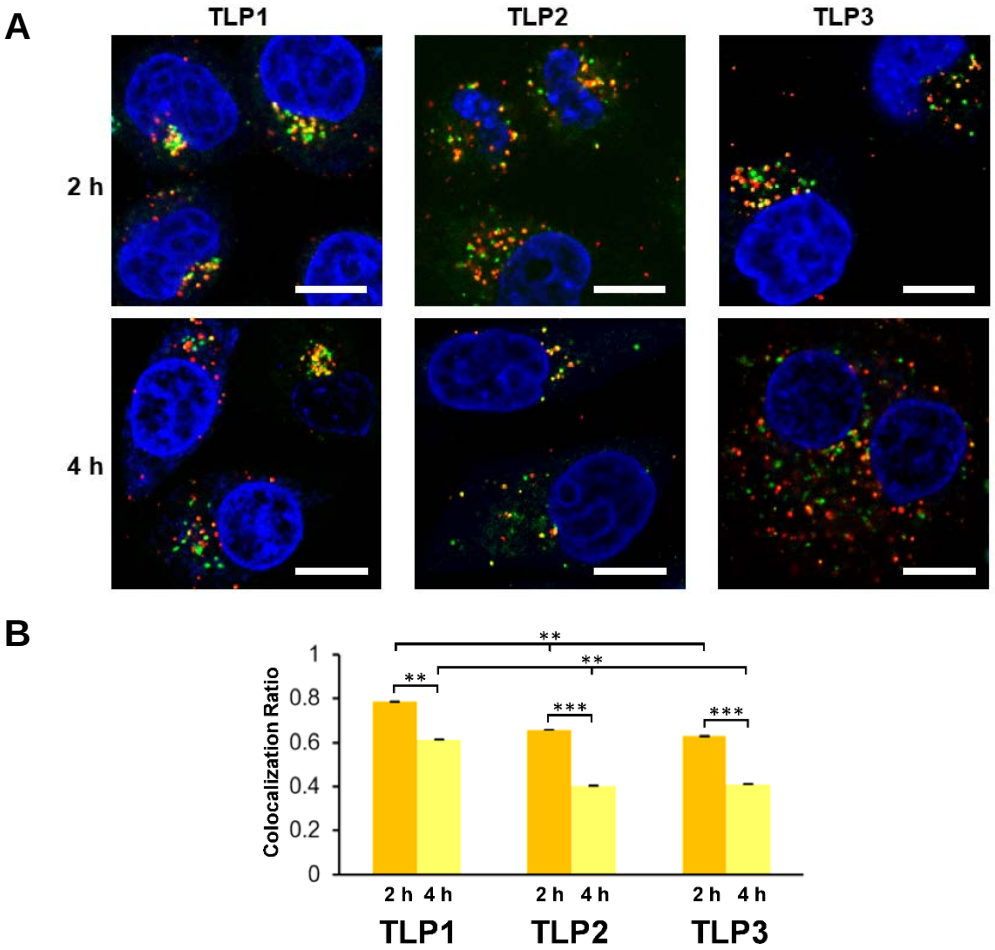

Figure 3.3.15. Colocalization of siRNA polyplexes with late endosomes and lysosomes was presented by CLSM. (A) Intracellular distribution of AF 647-labeled siRNA (red) polyplexes in KB cells at 2 and 4 h after transfection for 45 min. Late endosomes and lysosomes were stained with LysoTracker Green (green). Nuclei were stained with DAPI (blue). (B) After tranfection for 45 min, colocalization ratios of AF 647-labeled siRNA with late endosomes and lysosomes were calculated using ZEN 2.1 software at 2 and 4 h. The experiments were performed in collaboration with Dr. Xueying Liu (Innovation Center of NanoMedicine).

Furthermore, we observed a significant decrease in the colocalization ratios of all the TLPs in late endosomes and lysosomes (green) at 4 h after transfection (Figure 3.3.15B), indicating the onset of siRNA release from endosomes began during acidification of endolysosomal structures. Co-localization ratios of TLP1 were significantly higher than those of TLP2 and TLP3 at both 2 h and 4 h. This suggested that TLP2 and TLP3 had earlier endosomal escape capacity than TLP1. On the other hand, it seemed that sustained release of siRNA from endosomes to cytosol caused the enhanced gene silencing effect of TLP1, which corresponded with the results measured 48 h after transfection of TLPs (Figure 3.3.12 and 3.3.13C). As mentioned in literature, the decrease in intravesicular pH takes time along the endolysosomal pathway from pH 6.0−6.5 in early endosomes to pH 4.5−5.5 in late endosomes and lysosomes [92, 93], escaping of siRNA from vesicular compartments in response to dropping intravesicular pH for different TLP formulations may occur in different time courses.

In light of effective gene silencing effect, intracellular siRNA stability must also be taken into consideration. Through fluorescence resonance energy transfer (FRET) analysis, we aimed to track the stability and degradation of siRNA delivered by different TLP formulations in FR-expressing KB and L1210 cells. For this purpose, Cy5/TAMRA double-labeled siRNA was utilized: on the sense strand of siRNA, Cy5 was conjugated at the 5' end, and TAMRA was at 3’ end. After Cy5/TAMRA double-labeled siRNA transfection for 1, 4, and 48 h, FRET intensity of cells was analyzed with flow cytometry by exciting the cells with a 488 nm laser and monitoring the fluorescence emission through a 660/20 nm filter. The mean FRET intensity of each TLP formulation was calculated by using FACSDiva software (Figure 3.3.16).

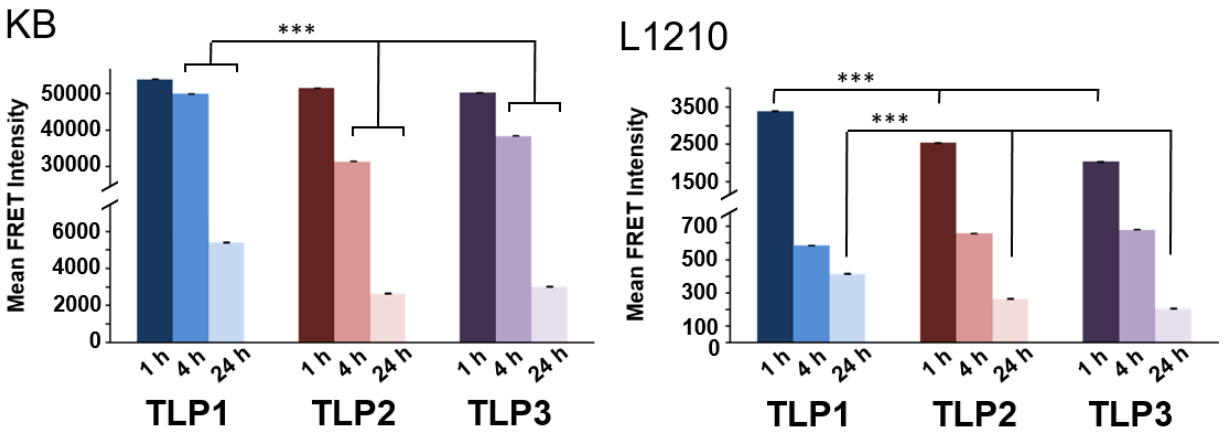

Figure 3.3.16. Intracellular fluorescence resonance energy transfer (FRET) signals were analyzed by flow cytometry at 1, 4 and 24 h after Cy5/TAMRA double-labeled siRNA transfection for 45 min in KB and L1210 cells. The samples were excited with a 488 nm laser, and their emission was monitored by using a 660/20 filter. The experiments were in collaboration with Naoto Yoshinaga (Department of Bioengineering, University of Tokyo).

Because FRET efficiency falls off as $1/R^6$, observation of FRET is typically limited to donor/acceptor distances of about 10 nm [94], and, therefore, FRET is only measurable when siRNA duplexes remain intact inside cells, otherwise the degradation of siRNA results in the loss of FRET. In KB cells, all the TLPs maintained high FRET intensity at 1 h. At 4 h, FRET intensity of TLP1 dropped only slightly by 7%, in contrast to TLP2 (loss by 39%) and TLP3 (loss by 24%), showing that siRNA remained intact in case of TLP1 formulation. Although FRET intensity of TLPs decreased up to 90-95% within 24 h, notably, FRET intensity of TLP1 remained 2-fold higher compared to TLP2 and TLP3. Similarly, in L1210 cells, FRET intensity of TLP1 was higher than those of TLP2 and TLP3 after incubation for 1 h, and similar trend was found at 24 h.

Additional proof of siRNA stability was obtained by CLSM in cultured KB cells transfected with Cy5 (red) and TAMRA (green) double-labeled siRNA. Lysosomes were labeled with CellLight Lysosomes-GFP (blue). As demonstrated by the representative examples in Figure 3.3.17, TLP1 showed extensive colocalization of the two fluorophores (yellow), *i.e.* intact siRNA, after incubating the cells for 1 h. Red or green pixels indicating the degraded siRNA molecules were also observed. Impressively, after 24 h, despite most of siRNA sequences were degraded by lysosomes, intact siRNA was still detectable. On the contrary, without **454**, **356** protected only few intact siRNA molecules at 1 h, and none at 24 h.

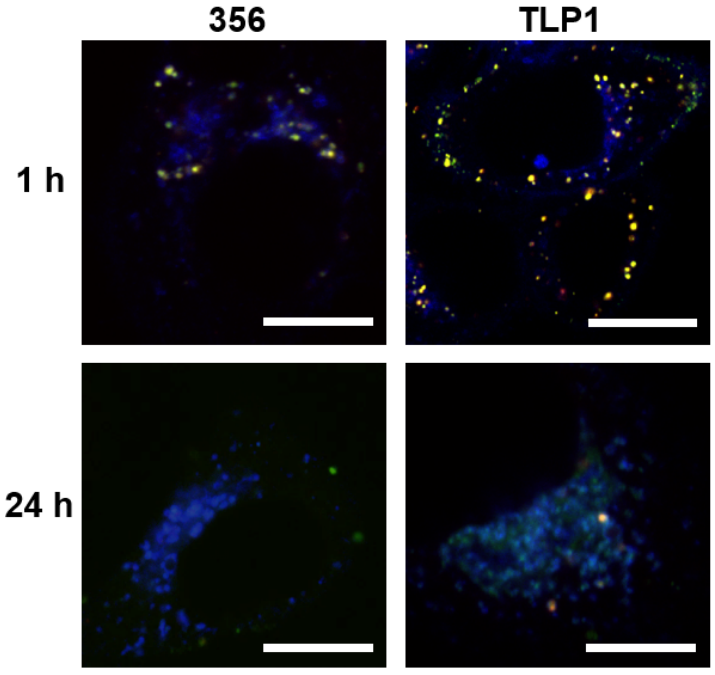

Figure 3.3.17. FRET imaging of Cy5 (red)/TAMRA (green) double-labeled siRNA at 1 and 24 h after transfection for 45 min in KB cells by CLSM. Colocalization of the two fluorophores (yellow) indicated intact siRNA. Lysosomes were labeled with CellLight Lysosome-GFP (blue). The scale bars represent 10 μm. The experiments were in collaboration with Dr. Xueying Liu (Innovation Center of NanoMedicine).

To conclude, on the condition that there was no significant difference for cellular internalization levels for TLPs, TLP1 is hypothesized to unload siRNA in a rather sustained manner based on the delayed shift in colocalization with late endosomes/lysosomes. Furthermore, TLP1 exhibited superior ability to confer the protection and stability of siRNA compared to the other formulation, as measured by a distance-dependent FRET-based approach. Since TLP2 and TLP3 did not show significant difference regarding endosomal escaping capability, siRNA stability and biological activity, it appeared that the modification of tyrosines to the fatty acid-based TLP1, which provides further stability to the polyplex, was essential for the increased activity of the formulations.

3.3.6 Tumoral delivery and gene silencing upon systemic administration

From the drug delivery standpoint, systemic delivery of siRNA poses a great challenge, since siRNA is readily degraded by serum endonucleases and is easily eliminated by glomerular filtration with a short plasma half-life of <10 min [95]. In order to understand whether TLPs could improve the distribution profile of siRNA, folate-conjugated TLP1, the most potent formulation *in vitro* with favorable size and surface charge, was selected for the further *in vivo* studies. The two single oligomer components of TLP1, *i.e*. PEGylated folate-equipped oligomer (**356**) and tyrosine-based oleic acid oligomer (**454**), were used for comparison. Non-targeted analogue NTLP1 and naked siRNA were also exploited as controls. FR-expressing L1210 tumor cells were implanted subcutaneously in nude mice. We formulated different Cy7-labeled siRNA (at the dose of 50 µg of siRNA) polyplexes at N/P 16, and administered these siRNA polyplexes intravenously (*i.v.*). The biodistribution of Cy7-labeled siRNA measured by near infrared (NIR) fluorescence imaging was demonstrated in Figure 3.3.18A. As Cy7-labeled siRNA spread throughout the whole body along with the blood circulation immediately after injection, Cy7 signal of naked siRNA lasted for merely 30 min. PEGylated folate-equipped oligomer **356** formed nanoparticles with a diameter of ~6 nm, approached the tumor site with small fraction of Cy7 signal at 15 min, and transiently disappeared after 30 min. Meanwhile, tyrosine-based **454** (100-130 nm in diameter) significantly improved the systemic retention of siRNA >4-fold over naked siRNA and **356**. For that the volume of blood circulates through the tumor is usually far less than that of the arteries, only the nanoparticles that are not rapidly cleared from the circulation will have a chance to encounter the leaky tumor vasculature for targeting [96]. Accordingly, TLP1, as an optimized co-formulation of **356** and **454**, has not only mediated comparably prolonged systemic retention as **454**, more advantageously, but also enhanced tumoral siRNA delivery within 2 h. Notably, Cy7 signal was detectable in harvested tumors only from TLP1-treated animals at 2 h, while there was no Cy7 signal in the rest of groups including folate-linked **356** (Figure 3.3.18B). As non-targeted

control, NTLP1 resulted in similar circulation profile as TLP1 but siRNA barely reached the tumor site, thus it revealed an explicit difference for the functionality of folate ligands.

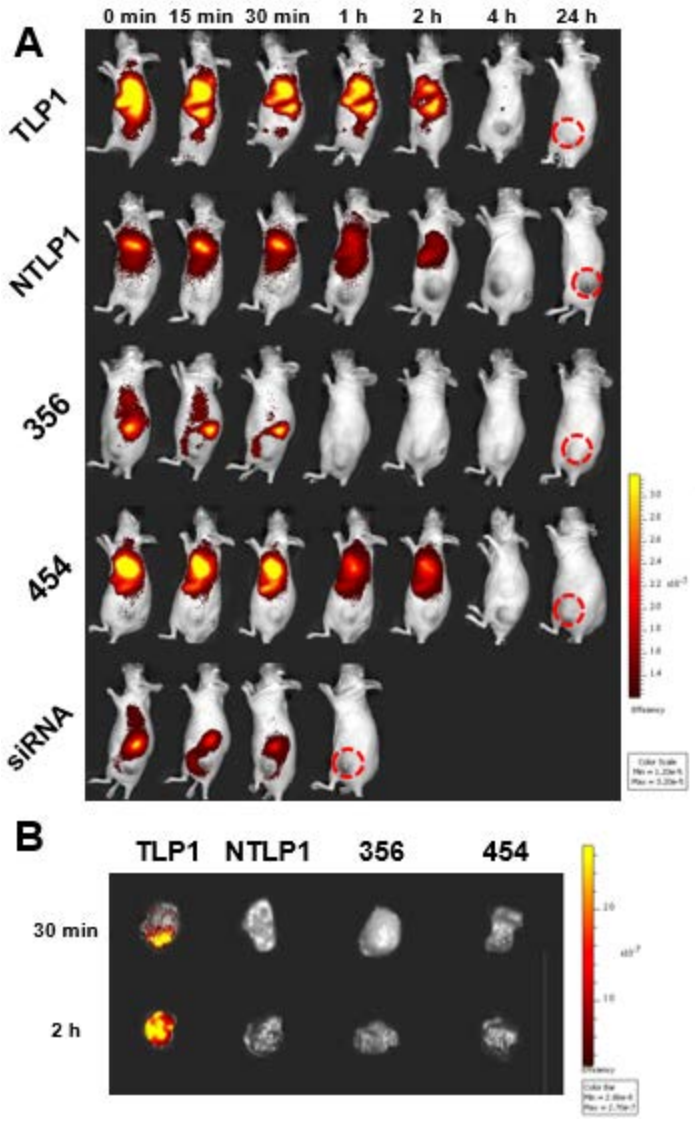

Figure 3.3.18. Biodistribution of TLP1 at N/P 16 in NMRI-nude mice bearing L1210 tumors *via i.v.* administration determined by NIR fluorescence bioimaging. 50 µg of Cy7-labeled siRNA was foumulated with TLP1, NTLP1, PEGylated folate-conjugated oligomer **356**, or tyrosine-conjugated oleic acid oligomer **454** as carrier. Experiments were performed with 3-4 animals per group; a representative animal of each group is shown. (A) Time-dependent tumoral retention of siRNA polyplexes over 24 h. Lateral views of animals were shown to present the tumor sites (dotted circles). (B) Tumors harvested 30 min and 2 h after injection of siRNA polyplexes. The experiments were performed in collaboration with Eva Kessel (Dr. med. vet. study, Department of Pharmacy, Ludwig-Maximilians-Universität München).

Upon systemic administration of siRNA polyplexes, the elimination profiles were presented in Figure 3.3.19. It is known that despite the formulation can be modified to prolong blood circulation, but non-specific distribution in the highly perfused organs including liver, kidneys and lung has thus far been inevitable [86]. In addition, several *in vivo* studies have reported that kidneys are prevailing in siRNA elimination [95], and the pore size of the glomerular filtration barrier is roughly 8 nm [97]. Not surprisingly, due to small particle size of **356** (6 nm in diameter), Cy7-siRNA immediately passed through glomeruli and was excreted into the urinary bladder within 1 h. For the purpose of circumventing rapid renal clearance, siRNA polyplexes should have a particle size of about 50-300 nm [98]. Interestingly, TLP1, with a diameter of 127 nm, seemed to take advantage of it component **454** to greatly reduce kidney uptake and increase systemic retention of siRNA for 4 h. Identical impact of **454** on the distribution profile can be also found in case of NTLP1.

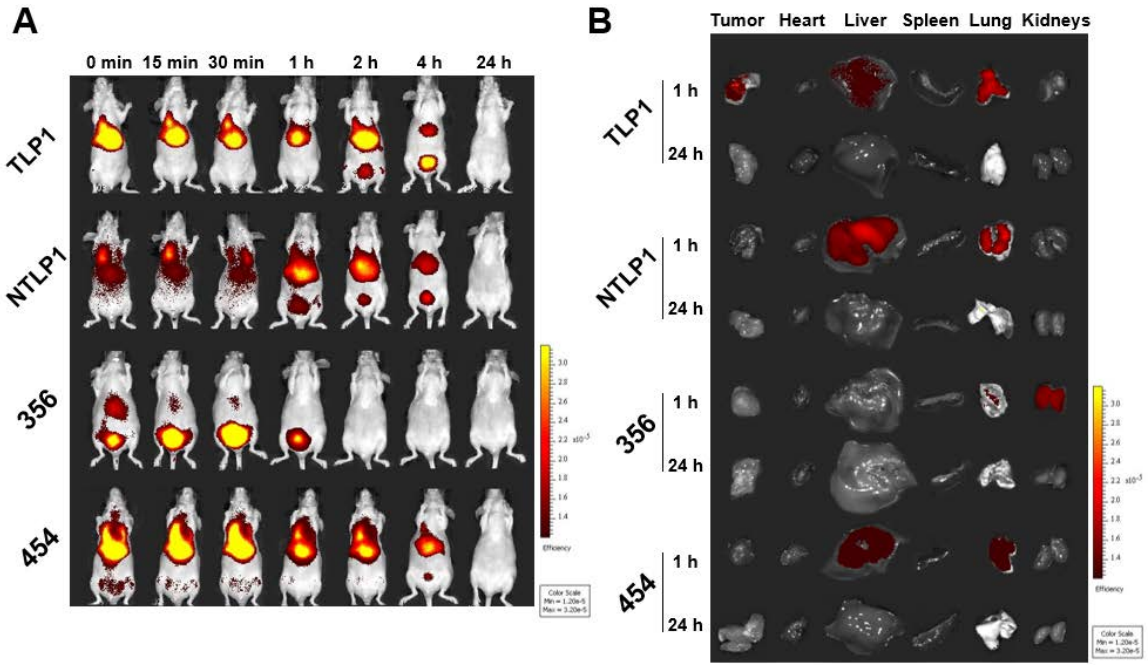

Figure 3.3.19. Biodistribution of TLP1 at N/P 16 in NMRI-nude mice bearing L1210 tumors *via i.v.* administration determined by NIR fluorescence bioimaging. 50 μg of Cy7-labeled siRNA was foumulated with TLP1, NTLP1, PEGylated folate-conjugated oligomer **356**, or tyrosine-conjugated oleic acid oligomer **454** as carrier. Experiments were performed with 3-4 animals per group; a representative animal of each group is shown. (A) Distribution and elimination of siRNA polyplexes over 24 h. Animals were presented in the ventral view. (B) Tumors and organs harvested 1 h and 24 h after injection of siRNA polyplexes. The experiments were in collaboration with Eva Kessel (Dr. med. vet. study, Department of Pharmacy, Ludwig-Maximilians-Universität München).

After clarifying that FR-specific TLP1 successfully delivered siRNA to the tumor *via i.v.* injection, we sought to validate the functional gene silencing of TLP1 *in vivo*. For this aim, we formulated TLP1 with siEG5 or siCtrl (50 µg of siRNA), and administered these siRNA polyplexes *i.v.* in the L1210 tumor-bearing mice twice. 24 h after the last treatment, we harvested the tumor, extracted RNA and measured the EG5 mRNA levels by qRT-PCR (Figure 3.3.20A). Compared to untreated controls, the siEG5 TLP1 induced significant downregulation of EG5 expression by 65%. Importantly, siCtrl TLP1 showed negligible effects on mRNA level of EG5 as compared with untreated tumors.

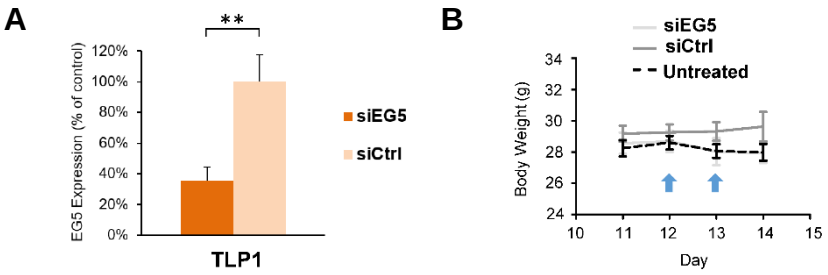

Figure 3.3.20. Gene silencing effect of TLP1 at N/P 16 in NMRI-nude mice bearing L1210 tumors *via i.v.* administration. (A) mRNA level of EG5 gene after two-fold *i.v.* injections of TLP1 with 50 µg of siEG5 or siCtrl. Experiments were performed with 5 animals per group. (B) Body weight development over treatment period. The *i.v.* injections were performed on day 12 and 13 as indicated by blue arrows. The body weight curves of TCP-treated animals were compared to that of untreated animals over the same time after tumor inoculation. Experiments were performed with 5 animals per group. The experiments were in collaboration with Eva Kessel (Dr. med. vet. study, Department of Pharmacy, Ludwig-Maximilians-Universität München).

Systemic circulation of siRNA polyplexes might also lead to exposure to non-target tissues which might cause potential side effects; we therefore monitored the body weights and carried out blood biochemistry examinations to help us realize the biocompatibility of TLP1. As shown in Figure 3.3.20B, the body weight curves indicated that the treatments were well-tolerated compared to untreated controls. The blood samples were collected 24 h after the treatments to determine four relevant clinical biochemistry parameters (ALT, AST, BUN and creatinine). Increased liver enzymes (ALT and AST) would indicate formulation-associated liver damage or acute hepatitis, while elevated BUN or creatinine would be related to renal malfunctions. As presented in Table 3.3.6, in the treatment groups, the levels of ALT and AST were in a range equivalent to the untreated control group. In context of creatinine and BUN, there was no significant difference, either.

Table 3.3.6. Clinical biochemistry parameters (ALT, AST, BUN and creatinine). Plasma was obtained from the treated animals 24 h after the second injection (n = 5) compared to untreated tumor-bearing mice (n = 3) that were euthanized on the same day.

	ALT (U/L)	AST (U/L)	Creatinine (mg/dL)	BUN (mg/dL)
TLP1 + siEG5	39 ± 2	120 ± 31	0.09 ± 0.01	40 ± 8
TLP1 + siCtrl	57.4 ± 25	130 ± 46	0.09 ± 0.01	39 ± 7
Untreated	46 ± 15	113 ± 23	0.07 ± 0.01	38 ± 7

To draw a conclusion, these encouraging results suggested that TLP1 delivered siRNA to the tumor within 2 h *via i.v.* injection, inducing specific RNAi-mediated degradation of EG5 mRNA in the tumor tissue. Moreover, no indication for potential side effects was given based on the body weight analysis and in clinical chemistry measurements from the blood.

4 Discussion

4.1 Oligoglutamyl-MTX-conjugated nanoplexes

One effective approach in cancer therapy is the use of a combination therapy with different therapeutic agents, allowing to tackle the disease from different angles. While such approaches with standard chemotherapeutic drugs are effectual and usually decrease the likelihood for chemoresistance, they still lack specificity and are associated with considerable toxicity. Novel gene therapeutic tools, such as RNAi, offer very interesting alternatives for modulating such therapy as they process sequence-specific gene silencing implicated in cell division, and importantly, may be used in combination with classical chemotherapeutic drugs. Another crucial aspect in cancer therapy is to be able to overcome or significantly decrease the side effects and associated toxicities of the therapeutics. The aim in this work was to combine two different antitumoral agents (the chemical DHFR inhibitor MTX and the mitosis-inhibiting EG5 siRNA) into one nanoparticle drug. Therein we took advantage of the bifunctional MTX which has been recently shown to possess potential as both cytotoxic drug and targeting ligand in a cancer combination therapy approach for the co-delivery of cytotoxic poly(I:C) [50]. As part of a multifunctional nanoplex, MTX was also supposed to facilitate targeted delivery of antitumoral EG5 siRNA to the tumor cells.

The structure of the used oligoaminoamides is based on analogous folate-containing two-arm branched oligomers with receptor-targeted gene silencing capacity *in vitro* and *in vivo* [33]. The artificial oligoamino acid succinoyl tetraethylene pentamine (Stp) together with natural amino acids (lysine, cysteine) serve as siRNA binding carriers, a PEG chain provides nanoplex shielding. In the current work, MTX derivatives acted as targeting ligand. As measured by FCS (Table 3.1.2), AFM (Figure 3.1.4) and TEM (Figure 3.1.5), these MTX conjugates electrostatically complexed siRNA and formed compact homogeneous spherical nanoparticles with hydrodynamic diameter of ~6 nm. The branched two-arm structure containing several Stp units provided the positive charge for siRNA binding, and two cysteines further stabilized the polyplex *via* disulfide crosslinking. As a result of the PEGylation, the surface charges of polyplexes were almost neutralized, which not only prevented aggregation, but also shielded the particles from unspecific cationic association and allowed for specifically presenting the targeting ligand to the cells. Considering that these polyplexes were only ~1.3 fold larger than free siRNA, it indicated that these PEGylated glutamyl-MTX conjugates were associated with single siRNA in a

monomolecular fashion, in line with the previous results with the PEGylated folate-conjugated oligomer **356** [33].

The cellular uptake studies demonstrated that the MTX oligomer conjugates were taken up into cells in a FR-specific fashion, as the polyplexes were avidly binding to FR-expressing KB cells while only negligible staining was seen in FR-negative A549 cells. Furthermore, in the competition assay, binding of polyplexes was blocked by preincubation with excess free folate or MTX. We also verified FR-specific targeting effect of MTX conjugates by a series of functional siRNA-mediated gene silencing assays in comparison between KB and FR-deficient MCF-7 cell lines. In the literature, the relationship between tumor response to MTX and FR expression has been extensively investigated. First, KB cell sublines with below-wildtype FR expression show resistance for MTX [99], while the cell lines lacking functional RFC are also commonly resistant to MTX [100]. Second, the IC_{50} of MTX for the cells co-expressing RFC after transfection with FR-α is the same as for the wild type [101], whereas MTX is active in cell lines that are RFC-deficient but overexpress FR-α [102, 103]. In addition, it has been reported that transfection of MCF-7 cells which do not express FR with FR cDNA increases MTX uptake and cytotoxicity [78]. It has been also shown that FR-mediated transport of MTX is highly energy-requiring and ceases rapidly when energy metabolism is blocked [104]. Moreover, MTX has been coupled to many natural and synthetic carriers, resulting in either amide or ester bond formation. The use of either conjugation or encapsulation approaches could change the cellular transport characteristics, pharmacokinetics and pharmacodynamics of the parent drug, resulting in increased or decreased cytotoxicity, along with altered *in vivo* distribution [105, 106]. For example, the uptake of a PAMAM dendrimers covalently conjugated with MTX is taking place in a FR-dependent manner in KB cells [71], and a polyvalent dendrimer-MTX conjugate is not toxic to FR-negative cells [107]. More importantly, polyglutamylation of the MTX at its γ-carboxylic acid is known to prevent transport of MTX across the membrane by RFC [108], and the oxidized pteridine ring as well as a glutamate tail are required for the greatest FR-α affinity [109]. In contrast to free MTX which could also enter the cell through the RFC, our findings confirmed a FR-specific uptake of MTX conjugated siRNA polyplexes.

Following FR-mediated internalization, the siRNA-linked endosomolytic Inf7 peptide is supposed to enhance endosomal escape into the cytosol, where the crosslinking disulfide bridges of the oligomer coat are thought to be cleaved within the reductive intracellular environment in order to release the siRNA and glutamylated MTX conjugates. In KB/eGFPLuc cells, all of these

polyplexes (**638**-**642**) mediated successful gene silencing potency with Inf7-modified siGFP (Figure 3.1.9). Among the MTX conjugates, **640** exhibited the best performance, and higher N/P ratios further enhanced the transfection efficiency. Lack of Inf7 peptide in the siRNA construct reduced the gene silencing potency (Figure 3.1.10). Consistent with prior work with free oligomer conjugates and poly(I:C) complexes [50], oligo-glutamyl MTX conjugates (**639**, **640** and **641**) were found to be more cytotoxic than free MTX (Figure 3.1.12). One explanation is that conjugated MTX could be internalized in higher quantities than free MTX in this model. Moreover, the glutamylation degree of MTX conjugates correlates to DHFR inhibition potency [50], which results in suppression of downstream effects on thymidylate and purine synthesis, and might be responsible for enhanced potency. In the experiments directly comparing the EG5 siRNA-mediated cytotoxicity in KB cells, it showed that in general MTX conjugates elicited considerably higher cytotoxicity levels compared to the folate analogue **356**. Also, the inhibitory efficacy of the conjugates seemed to be related to the increasing degree of polyglutamylation from **638** (MTX-Stp) to **641** (6E-MTX-Stp). The tetraglutamylated **640** and hexaglutamylated **641** siRNA polyplexes induced the most significant cytotoxicity, therefore this might indicate that the degree of polyglutamylation not only increased the MTX cytotoxicity but also potentiated the siEG5-dependent cytotoxicity in KB cells (Figure 3.1.12).

In the present study, upon *i.t.* administration of MTX-based **640** polyplexes showed significantly increased intratumoral retention time and achieved levels comparable or even exceeding the folate-based **356** polyplexes, and the remaining Cy7 signal in the **640**-treated tumor was higher than **356**-treated tumor after 168 h (Figure 3.1.15). *In vivo* distribution of siRNA polyplexes is dependent on (1) the physicochemical properties of the carrier, (2) the nature of the siRNA, and (3) the anatomy and physiology of the drug distribution site. Once the siRNA polyplexes have been injected into the interstitial space in the tumor, they have to avoid interactions with the extracellular matrix (including collagens, proteoglycans, hyaluronic acid, fibronectin, and other glycoproteins) such as binding, dissociation, or aggregation. MTX-conjugated **640**, folate-conjugated **356** and alanine-substituted **188** polyplexes were all PEGylated, which decreased the surface charge close to neutrality, and consequently avoided associating with these components. PEG molecules as hydrophilic domains were also vital for particle stabilization to prevent aggregation of polyplexes. Moreover, the particle size is known to be intrinsically related to the rate of clearance from the blood circulation. Nanosized **356** or **640** polyplexes are as small as abundant pores present in normal tissue endothelium [110], allowing good tissue penetration and slower removal from the circulation compared to free siRNA. Furthermore, considering that

the interstitial or extracellular pH in solid tumors is generally acidic, and the FR-α transport route has an affinity for folate that is comparable to that of MTX at low pH [111], such environment is beneficial for MTX conjugate **640** to compete with endogenous folate (*N*-5-methyltetrahydrofolate) for receptor binding and the following cellular internalization in KB xenograft tumors.

This study developed a molecule-defined nanoplex with bifunctional MTX ligand for effective intratumoral delivery of siRNA, which represents a challenging hurdle for the widespread application of RNAi in cancer research and therapy. First, the tetraglutamylated MTX of **640** showed greater *in vivo* KB tumor inhibition compared to equivalent free MTX (Figure 3.1.20A), validating the potentiated efficacy resulting from the degree of polyglutamylation. Second, **640** siRNA polyplexes (with siEG5-Inf7 or siCtrl-Inf7) led to significantly improved tumor suppression over free **640** (Figure 3.1.17A), which was expected to diffuse quickly after the administration because free **640** in the absence of siRNA failed to form nanoparticles. In addition, the endosomolytic Inf7 peptide contained within the siRNA polyplexes may facilitate the cytosolic delivery of polyplex-linked MTX molecules, enhancing their toxicity. In this respect, the co-delivery of siRNA/drug combinations by chemical or physical linkage into the same nanoparticle may present a therapeutic advantage in cancer treatment [112]. Encouragingly, the dual antitumoral mechanisms consisting of MTX-conjugated **640** and EG5 siRNA have shown enhanced antitumoral potency with 50% of recurrence-free survival (Figure 3.1.17C).

4.2 Targeted combinatorial polyplexes (TCPs)

By co-formulation strategy, TCP formulations presented different particle sizes and reduced surface charges as measured by DLS. These siRNA polyplexes were uniform compact nanoparticles without aggregates observed by TEM (Figure 3.2.3A), and siRNA complexation was verified by agarose gel shift assay (Figure 3.2.3B).

Measured by flow cytometry, the folate-based TCPs bound to FR-expressing L1210 and M109 cells in a receptor-specific pattern (Figure 3.2.4A). Characterization of the cellular uptake of TCPs in FR-positive KB cells by immuno-TEM further revealed the interaction of the siRNA polyplexes with FR at the plasma membrane and induction of their internalization *via* FR-mediated endocytosis. After internalization, the siRNA polyplexes mainly distributed in endocytic vesicles, where the FR remained in contact with TCPs and retained the colocalization. Upon longer incubation time, the membrane of TCP-containing vesicles became unstable and discontinuous, the tight clusters of siRNA polyplexes started to dissociate. Consequently, the occasional escape from endosomes and single TCP distribution to the cytosol was noted (Figure 3.2.4).

Endosomal entrapment is widely recognized as the main obstacle that limits the application of therapeutic nanocomplexes, whose target is in the cytoplasm or in the nucleus. It is of notice that oligoaminoamides were designed to act as PEI-like proton sponge motifs; by becoming increasingly protonated during acidification of endolysosomal structures, and to cause osmotic swelling of endosomes and release of the siRNA molecules upon vesicle rupture [42, 113, 114]. Published studies in the field of FR-targeted therapeutics have mainly focused on their role in bioactivity, but exact cellular trafficking has not been well studied so far. To our knowledge, this is the first time when immuno-TEM was applied to clarify the interactions of siRNA polyplexes and FR.

As shown in Figure 3.2.5, Inf7 peptide is necessary for efficient transfection of siRNA for TCPs and **356**. Besides, recently we verified that the uptake of 100-200 nm FR-targeted polyplexes could be blocked completely by excess free folate, while the agglomerated large particles (>200 nm) might partially undergo receptor-independent uptake and gene silencing [115]. The luciferase activity in KB/eGFPLuc cells treated with controls, including siCtrl polyplexes and siCtrl-Inf7 polyplexes were similar to untreated cells, suggesting that there's no intrinsic cytotoxicity of TCPs. Taken together, the gene silencing assay further showed that folate-containing TCPs allowed the Inf7-modifed siRNA polyplexes to access the cytosol, and showed not only gene-specific

silencing ability but also lack of cytotoxicity mediated by TCPs in KB/eGFPLuc cells.

After systemic administration, there are many ways by which siRNA carriers leave the bloodstream, including redistribution into the liver, spleen, kidneys and lung, nonspecific distribution has thus far been unavoidable; however, entering kidneys is the most common pathway [86]. The glomeruli in kidneys work as a filtration barrier that removes water and small molecules as urine while larger molecules are retained in the blood stream [116]. For mice, the excretion through kidneys typically occurs for molecules less than 30 kDa in size [117]; the molecular weight of naked siRNA is about 13 kDa [6], which readily passes glomerular fenestration and accumulates in urine. Aimed to avoid immediate glomerular filtration, we increased the particle size by introducing 3-arm Stp oligomers with larger size, and showed preliminary improvement on circulation time and therefore increased chance for TCPs to extravagate into the FR-expressing tumor.

In addition, to overcome steric hindrance surrounding the FR on the cell surface [118], a PEG linker was utilized to conjugate the oligomer to folate. PEGylation can minimize the protein binding and possibly attributes to the low clearance by the reticuloendothelial system or accumulation in related organs especially the liver [119], as extremely low Cy7 signal in liver and spleen was detected (Figure 3.2.7D). On the other hand, the hydrophilic nature of PEG might facilitate the renal excretion of TCPs [120].

Therefore, encouragingly, these results suggested that siEG5-Inf7 TCP1 successfully reached the target tissue *via* i.v. injection, rendering gene silencing in the tumor. It is considered that low toxicity is as important as functional activity; if siRNA delivery provoked unacceptable toxicity on either a cellular or systemic level, even the most effective siRNA delivery system would be vainness [121]. Thus it is important that the blood analysis gave no indication for toxicity affecting vital organs like liver or kidneys regarding TCPs.

4.3 Targeted lipopolyplexes (TLPs)

By co-formulation strategy, TCP formulations presented different particle sizes and reduced surface charges as measured by DLS. These siRNA polyplexes were uniform compact nanoparticles without aggregates observed by TEM (Figure 3.2.3A), and siRNA complexation was verified by agarose gel shift assay (Figure 3.2.3B).

In addition, the size of the administered siRNA polyplexes is one of the most important characteristics because it might affect uptake efficacy, kinetics, and internalization mechanisms [122]. The size limit for nanoparticles to undergo receptor-mediated endocytosis is about 100−200 nm [123, 124]. Shape can also affect the cellular uptake of nanoparticles, for example, spherical particles are taken up by cells more efficiently compared with the rod-shaped particles [122].

Notably, escaping siRNA molecules from endosomes were detected by TEM and CLSM (Figure 3.3.8), suggesting TLP1 managed to deliver siRNA into cytosol. One reasonable assumption is that the oligoaminoamides may act as proton sponge motifs to become increasingly cationized during endolysosomal acidification and, supported by the attached fatty acid domains, destabilize the lipid membrane [42, 125].

Most transfection reagents, *e.g*. RNAiMAX, Ribojuice, and Hiperfect, have a disassembly half-life of siRNA that falls in the range of 30 min to 2 h in HeLa cells [126], suggesting the intracellular milieu is challenging to siRNA integrity. It has been revealed that reactive oxygen species (ROS) and reactive nitrogen species (RNS) serve as messengers in cell signaling but also pose a potential oxidative damage to macromolecules, including nucleic acids [127]. And different FRET intensity profiles for certain TLP formulation in KB and L1210 cells may result from different reducing environments in different cell lines [128-130]. For that the rapid decrease of FRET intensity may relate to rapid degradation of siRNA delivered by TLP2 and TLP3, this effect was possibly attributed to the less potent gene knockdown. In contrast, TLP1 as the only formulation with **454** containing stabilizing tyrosine trimers [36, 37] improved the siRNA stability and thus might foster the access to the RNAi machinery.

PEG as the shielding agent has been proven to be valuable in preventing non-specific interactions and avoiding immune recognition in the circulation [131]; however, another major barrier, liver, still accumulates the most of PEGylated nanoparticles [98]. In the liver, Kupffer cells recognize the opsonized nanoparticles *via* the scavenger receptor [119]. In accordance with the literature,

abundant Cy7-siRNA of TLP1 ended up in the liver (Figure 3.3.19); besides, it is also possible that these fatty acid-containing siRNA polyplexes with larger size (**454**, TLP1 and NTLP1) were prone to be further metabolized by liver. In the end, recent efforts have focused on the impact of particle stability on the pharmacokinetic profile and gene silencing efficiency *in vivo* [132]. It is believed that the biodistribution of siRNA polyplexes is the deciding factor for better efficacy, thus there is an ongoing need to improve the formulation stability and following circulation time in the future.

5 Summary

It is now widely recognized that efficient intracellular siRNA delivery to target sites in the body is the most important hurdle for clinical applications of RNAi [31]. Hence, to formulate siRNA molecules with an appropriate biocompatible delivery system is necessary for improving biological stability, targeted cellular uptake, and the pharmacokinetics of siRNA [133]. Herein different siRNA formulations were delevloped to target folate receptor (FR)-overexpressing tumors.

In the first part, the antifolate drug methotrexate (MTX), a well-established chemotherapeutic agent, serves as both targeting ligand and anticancer agent, was conjugated with glutamyl units to the PEGylated Stp backbone. The oligomers formed uniform spherical siRNA polyplexes with a hydrodynamic diameter of approximately 6.5 nm. These polyplexes accessed KB cells by binding to the folate receptor in a MTX-dependent manner and induced efficient gene silencing activity *in vitro*. Impressively, by *i.t.* administration, MTX-conjugated polyplexes significantly increased the intratumoral retention (168 h) of the siRNA, as compared to alanine-substituted non-targeted control polyplexes (48 h). The combination of MTX-conjugated polyplexes and EG5 siRNA provided enhanced antitumoral potency with 50% of recurrence-free survival of KB tumor-bearing mice.

In the next part, we sought to improve the pharmacokinetic profile of siRNA polyplexes. To achieve this, we optimized the physicochemical properties of polyplexes by combinatorial optimization of PEGylated folate-conjugated oligomer (for FR targeting and shielding of surface charges) and 3-arm oligomer (for size modification and particle stability). For uni-directional fast coupling between the two groups of oligomers, we activated the cysteine thiol groups of one of the oligomers with 5,5’-dithio-bis(2-nitrobenzoic acid) to achieve a fast chemical linkage through disulfide formation with the free thiol groups of the other oligomer. These targeted combinatorial polyplexes (TCPs) were homogeneous spherical particles with favorable size and surface charge, which showed strong siRNA binding activity. TCPs were internalized into cells by FR-mediated endocytosis, triggered significant eGFP-luciferase marker gene silencing, and transfection with antitumoral EG5 siRNA suppressed cell proliferation in FR-expressing tumor cells. Moreover, the most promising formulation TCP1 after *i.v.* administration in L1210 tumor-bearing mice exhibited siRNA delivery into the tumor, resulting in 46% EG5 gene silencing at mRNA level without noticeable side effects.

Furthermore, by co-formulation of a targeted PEGylated oligomer and a lipo-oligomer, folate-equipped targeted lipopolyplexes (TLPs) for targeted siRNA delivery were generated. TLPs formed spherical homogenous particles with neutralized surface charge in complex with siRNA. After active tumor-specific uptake *via* FR-mediated endocytosis, TLPs effectively unpacked siRNA between 2 and 4 h in response to dropping intravesicular pH, and mediated significant gene silencing efficiency in the target cells, as 73-88% of luciferase activity was suppressed. TLPs loaded with siEG5 further triggered profound EG5 gene suppression, leading to mitotic arrest and following strong cytotoxicity in FR-expressing tumor cells. In these formulations, tyrosine-modified TLP1 with a diameter of 127 nm, has been proven to enable the best intracellular stabilization and sustained release of siRNA, thus inducing the superior gene silencing efficiency. By *i.v.* administration in L1210 tumor-bearing mice, TLP1 demonstrated tumoral retention of siRNA within 2 h and achieved EG5 gene silencing by 65% without noteworthy side effects.

Taken together, these siRNA formulations were generated based on precise chemistry, displayed excellent ability for tumor-targeted delivery and gene silencing upon *in vivo* application, and could be expected to facilitate the future translation of RNAi-based nanomedicine for cancer treatment.

6 Abbreviations

AGO	Argonaute
AF	Alexa Fluor
AFM	atomic force microscopy
ALT	alanine aminotransferase
AST	aspartate aminotransferase
BUN	blood urea nitrogen
CLSM	confocal laser scanning microscopy
DAPI	4',6-diamidino-2-phenylindole
DBU	1,8-diazabicyclo[5.4.0]undec-7-ene
d_h	hydrodynamic diameter
DIPEA	*N*,*N*-diisopropylethylamine
DLS	dynamic light scattering
DMEM	Dulbecco's modified Eagle's medium
DMSO	dimethylsulfoxide
DODT	3,6-dioxa-1,8-octanedithiol
DOPC	1,2-dioleoyl-sn-glycero-3-phosphocholine
DHFR	dihydrofolate reductase
DMF	dimethylformamide
DTNB	5,5-dithio-bis(2-nitrobenzoic acid)
EphA2	ephrin type-A receptor 2
FBS	fetal bovine serum
FCS	fluorescence correlation spectroscopy
FPGS	folylpolyglutamyl synthetase
FR	folate receptor
FRET	fluorescence resonance energy transfer
HA2	hemagglutinin subunit 2
HBG	20 mM HEPES buffered 5% glucose pH 7.4
HCC	hepatocellular carcinoma
HOBt	1-hydroxy-benzotriazole
i.t.	intratumorally
i.v.	intravenously
KRAS-G12D	Kirsten rat sarcoma viral oncogene homolog G12D mutation
LMW	low molecular weight
LODER	local drug eluter
LNP	lipid nanoparticle
MPS	mononuclear phagocyte system
mRNA	messenger RNA
MTT	3-(4,5-dimethylthiazol-2-yl)-2,5-diphenyltetrazolium bromide
MTX	methotrexate
N/P	pronatable amines of the oligomer/phosphates of the siRNA
NIR	near infrared
NMP	*N*-methyl-2-pyrrolidone
PAMAM	polyamidoamine
PEI	polyethylenimine
PLK1	polo-like kinase 1
PEG	polyethylene glycol
poly(I:C)	polyinosinic–polycytidylic acid
PRR	pattern recognition receptors
PTA	phosphotungstic acid
PyBOP	benzotriazol-1-yl-oxy-tris-pyrrolidino-phosphonium hexafluorophosphate
qRT-PCR	quantitative real-time polymerase chain reaction
RFC	reduced folate carrier
RISC	RNA-Induced Silencing Complex
RLU	relative light unit
ROS	reactive oxygen species
RNAi	RNA interference
RNS	reactive nitrogen species

s.c.	subcutaneously
siRNA	small interfering RNA
Sph	succinoyl-pentaethylene hexamine
Stp	succinoyl-tetraethylene pentamine
TCEP	tris(2-carboxyethyl)phosphine
TEM	transmission electron microscopy
TIS	triisopropylsilane
TCP	targeted combinatorial polyplex
TFA	trifluoroacetic acid
TLP	targeted lipopolyplex
TLR	toll-like receptor

7 References

[1] S. Kummar, H.X. Chen, J. Wright, S. Holbeck, M.D. Millin, J. Tomaszewski, J. Zweibel, J. Collins, J.H. Doroshow, Utilizing targeted cancer therapeutic agents in combination: novel approaches and urgent requirements, Nat Rev Drug Discov, 9 (2010) 843-856.
[2] A. Fire, S. Xu, M.K. Montgomery, S.A. Kostas, S.E. Driver, C.C. Mello, Potent and specific genetic interference by double-stranded RNA in *Caenorhabditis elegans*, Nature, 391 (1998) 806-811.
[3] S.M. Elbashir, J. Harborth, W. Lendeckel, A. Yalcin, K. Weber, T. Tuschl, Duplexes of 21-nucleotide RNAs mediate RNA interference in cultured mammalian cells, Nature, 411 (2001) 494-498.
[4] D. Castanotto, J.J. Rossi, The promises and pitfalls of RNA-interference-based therapeutics, Nature, 457 (2009) 426-433.
[5] R.L. Kanasty, K.A. Whitehead, A.J. Vegas, D.G. Anderson, Action and reaction: the biological response to siRNA and its delivery vehicles, Mol Ther, 20 (2012) 513-524.
[6] K.A. Whitehead, R. Langer, D.G. Anderson, Knocking down barriers: advances in siRNA delivery, Nat Rev Drug Discov, 8 (2009) 129-138.
[7] M. Jinek, J.A. Doudna, A three-dimensional view of the molecular machinery of RNA interference, Nature, 457 (2009) 405-412.
[8] E. Bernstein, A.A. Caudy, S.M. Hammond, G.J. Hannon, Role for a bidentate ribonuclease in the initiation step of RNA interference, Nature, 409 (2001) 363-366.
[9] J. Martinez, A. Patkaniowska, H. Urlaub, R. Luhrmann, T. Tuschl, Single-stranded antisense siRNAs guide target RNA cleavage in RNAi, Cell, 110 (2002) 563-574.
[10] J. Liu, M.A. Carmell, F.V. Rivas, C.G. Marsden, J.M. Thomson, J.J. Song, S.M. Hammond, L. Joshua-Tor, G.J. Hannon, Argonaute2 is the catalytic engine of mammalian RNAi, Science, 305 (2004) 1437-1441.
[11] J.J. Song, S.K. Smith, G.J. Hannon, L. Joshua-Tor, Crystal structure of Argonaute and its implications for RISC slicer activity, Science, 305 (2004) 1434-1437.
[12] K.S. Yan, S. Yan, A. Farooq, A. Han, L. Zeng, M.M. Zhou, Structure and conserved RNA binding of the PAZ domain, Nature, 426 (2003) 468-474.
[13] J.S. Parker, S.M. Roe, D. Barford, Structural insights into mRNA recognition from a PIWI domain-siRNA guide complex, Nature, 434 (2005) 663-666.
[14] B.L. Davidson, P.B. McCray, Jr., Current prospects for RNA interference-based therapies, Nat Rev Genet, 12 (2011) 329-340.
[15] L.M. Murrow, S.V. Garimella, T.L. Jones, N.J. Caplen, S. Lipkowitz, Identification of WEE1 as a potential molecular target in cancer cells by RNAi screening of the human tyrosine kinome, Breast Cancer Res Treat, 122 (2010) 347-357.
[16] V. Goidts, J. Bageritz, L. Puccio, S. Nakata, M. Zapatka, S. Barbus, G. Toedt, B. Campos, A. Korshunov, S. Momma, E. Van Schaftingen, G. Reifenberger, C. Herold-Mende, P. Lichter, B. Radlwimmer, RNAi screening in glioma stem-like cells identifies PFKFB4 as a key molecule important for cancer cell survival, Oncogene, 31 (2012) 3235-3243.
[17] R.E. Tiedemann, Y.X. Zhu, J. Schmidt, H. Yin, C.X. Shi, Q. Que, G. Basu, D. Azorsa, L.M. Perkins, E. Braggio, R. Fonseca, P.L. Bergsagel, S. Mousses, A.K. Stewart, Kinome-wide RNAi studies in human multiple myeloma identify vulnerable kinase targets, including a lymphoid-restricted kinase, GRK6, Blood, 115 (2010) 1594-1604.
[18] D.O. Azorsa, I.M. Gonzales, G.D. Basu, A. Choudhary, S. Arora, K.M. Bisanz, J.A. Kiefer, M.C. Henderson, J.M. Trent, D.D. Von Hoff, S. Mousses, Synthetic lethal RNAi screening identifies sensitizing targets for gemcitabine therapy in pancreatic cancer, J Transl Med, 7 (2009) 43.
[19] D. Haussecker, M.A. Kay, RNA interference. Drugging RNAi, Science, 347 (2015) 1069-

1070.
[20] Clinical Trials. U.S. National Institutes of Health, https://clinicaltrials.gov (2016).
[21] Y.D. Yao, T.M. Sun, S.Y. Huang, S. Dou, L. Lin, J.N. Chen, J.B. Ruan, C.Q. Mao, F.Y. Yu, M.S. Zeng, J.Y. Zang, Q. Liu, F.X. Su, P. Zhang, J. Lieberman, J. Wang, E. Song, Targeted delivery of PLK1-siRNA by ScFv suppresses Her2+ breast cancer growth and metastasis, Sci Transl Med, 4 (2012) 130ra148.
[22] M.L. Bobbin, J.J. Rossi, RNA Interference (RNAi)-Based Therapeutics: Delivering on the Promise? Annu Rev Pharmacol Toxicol, 56 (2016) 103-122.
[23] H. Shen, C. Rodriguez-Aguayo, R. Xu, V. Gonzalez-Villasana, J. Mai, Y. Huang, G. Zhang, X. Guo, L. Bai, G. Qin, X. Deng, Q. Li, D.R. Erm, B. Aslan, X. Liu, J. Sakamoto, A. Chavez-Reyes, H.D. Han, A.K. Sood, M. Ferrari, G. Lopez-Berestein, Enhancing chemotherapy response with sustained EphA2 silencing using multistage vector delivery, Clin Cancer Res, 19 (2013) 1806-1815.
[24] M.T. Valentine, P.M. Fordyce, S.M. Block, Eg5 steps it up! Cell Div, 1 (2006) 31.
[25] A.D. Judge, M. Robbins, I. Tavakoli, J. Levi, L. Hu, A. Fronda, E. Ambegia, K. McClintock, I. MacLachlan, Confirming the RNAi-mediated mechanism of action of siRNA-based cancer therapeutics in mice, J Clin Invest, 119 (2009) 661-673.
[26] D. Edinger, R. Kläger, C. Troiber, C. Dohmen, E. Wagner, Gene silencing and antitumoral effects of Eg5 or Ran siRNA oligoaminoamide polyplexes, Drug Deliv Transl Res, 4 (2014) 84.
[27] J. Harborth, S.M. Elbashir, K. Bechert, T. Tuschl, K. Weber, Identification of essential genes in cultured mammalian cells using small interfering RNAs, J Cell Sci, 114 (2001) 4557-4565.
[28] J.C. Burnett, J.J. Rossi, K. Tiemann, Current progress of siRNA/shRNA therapeutics in clinical trials, Biotechnol J, 6 (2011) 1130-1146.
[29] A.D. Judge, G. Bola, A.C. Lee, I. MacLachlan, Design of noninflammatory synthetic siRNA mediating potent gene silencing *in vivo*, Mol Ther, 13 (2006) 494-505.
[30] A.D. Judge, I. MacLachlan, Overcoming the innate immune response to small interfering RNA, Hum Gene Ther, 19 (2008) 111-124.
[31] E. Wagner, Biomaterials in RNAi therapeutics: *quo vadis*? Biomater. Sci., 1 (2013) 804-809.
[32] J.C. Burnett, J.J. Rossi, RNA-based therapeutics: current progress and future prospects, Chem Biol, 19 (2012) 60-71.
[33] C. Dohmen, D. Edinger, T. Fröhlich, L. Schreiner, U. Lächelt, C. Troiber, J. Rädler, P. Hadwiger, H.P. Vornlocher, E. Wagner, Nanosized multifunctional polyplexes for receptor-mediated siRNA delivery, ACS Nano, 6 (2012) 5198-5208.
[34] S. Singh, A. Sharma, G.P. Robertson, Realizing the clinical potential of cancer nanotechnology by minimizing toxicologic and targeted delivery concerns, Cancer Res, 72 (2012) 5663-5668.
[35] D. Schaffert, C. Troiber, E.E. Salcher, T. Fröhlich, I. Martin, N. Badgujar, C. Dohmen, D. Edinger, R. Kläger, G. Maiwald, K. Farkasova, S. Seeber, K. Jahn-Hofmann, P. Hadwiger, E. Wagner, Solid-phase synthesis of sequence-defined T-, i-, and U-shape polymers for pDNA and siRNA delivery, Angew Chem Int Ed, 50 (2011) 8986-8989.
[36] T. Fröhlich, D. Edinger, R. Kläger, C. Troiber, E. Salcher, N. Badgujar, I. Martin, D. Schaffert, A. Cengizeroglu, P. Hadwiger, H.P. Vornlocher, E. Wagner, Structure-activity relationships of siRNA carriers based on sequence-defined oligo (ethane amino) amides, J Control Release, 160 (2012) 532-541.
[37] C. Troiber, D. Edinger, P. Kos, L. Schreiner, R. Kläger, A. Herrmann, E. Wagner, Stabilizing effect of tyrosine trimers on pDNA and siRNA polyplexes, Biomaterials, 34 (2013) 1624-1633.
[38] M. Morille, C. Passirani, A. Vonarbourg, A. Clavreul, J.P. Benoit, Progress in developing cationic vectors for non-viral systemic gene therapy against cancer, Biomaterials, 29 (2008) 3477-3496.
[39] D. Edinger, E. Wagner, Bioresponsive polymers for the delivery of therapeutic nucleic acids, Wiley Interdiscip Rev Nanomed Nanobiotechnol, 3 (2011) 33-46.

[40] E.E. Salcher, P. Kos, T. Fröhlich, N. Badgujar, M. Scheible, E. Wagner, Sequence-defined four-arm oligo(ethanamino)amides for pDNA and siRNA delivery: impact of building blocks on efficacy, J Control Release, 164 (2012) 380-386.
[41] C. Scholz, E. Wagner, Therapeutic plasmid DNA versus siRNA delivery: common and different tasks for synthetic carriers, J Control Release, 161 (2012) 554-565.
[42] E. Wagner, Polymers for siRNA delivery: inspired by viruses to be targeted, dynamic, and precise, Acc Chem Res, 45 (2012) 1005-1013.
[43] T.M. Allen, Ligand-targeted therapeutics in anticancer therapy, Nat Rev Cancer, 2 (2002) 750-763.
[44] R. Zhao, N. Diop-Bove, M. Visentin, I.D. Goldman, Mechanisms of membrane transport of folates into cells and across epithelia, Annu Rev Nutr, 31 (2011) 177-201.
[45] N. Parker, M.J. Turk, E. Westrick, J.D. Lewis, P.S. Low, C.P. Leamon, Folate receptor expression in carcinomas and normal tissues determined by a quantitative radioligand binding assay, Anal Biochem, 338 (2005) 284-293.
[46] A.L. Jackman, D.S. Theti, D.D. Gibbs, Antifolates targeted specifically to the folate receptor, Adv Drug Deliv Rev, 56 (2004) 1111-1125.
[47] J.S. de Bono, A. Ashworth, Translating cancer research into targeted therapeutics, Nature, 467 (2010) 543-549.
[48] J.M. Kremer, Toward a better understanding of methotrexate, Arthritis Rheum, 50 (2004) 1370-1382.
[49] T.A. Garrow, A. Admon, B. Shane, Expression cloning of a human cDNA encoding folylpoly(gamma-glutamate) synthetase and determination of its primary structure, Proc Natl Acad Sci U S A, 89 (1992) 9151-9155.
[50] U. Lächelt, V. Wittmann, K. Müller, D. Edinger, P. Kos, M. Höhn, E. Wagner, Synthetic polyglutamylation of dual-functional MTX ligands for enhanced combined cytotoxicity of Poly(I:C) nanoplexes, Mol Pharm, 11 (2014) 2631-2639.
[51] H. Maeda, T. Sawa, T. Konno, Mechanism of tumor-targeted delivery of macromolecular drugs, including the EPR effect in solid tumor and clinical overview of the prototype polymeric drug SMANCS, J Control Release, 74 (2001) 47-61.
[52] P. Kos, U. Lächelt, D. He, Y. Nie, Z. Gu, E. Wagner, Dual-targeted polyplexes based on sequence-defined peptide-PEG-oligoamino amides, J Pharm Sci, 104 (2015) 464-475.
[53] D.J. Lee, E. Kessel, D. Edinger, D. He, P.M. Klein, L. Voith von Voithenberg, D.C. Lamb, U. Lächelt, T. Lehto, E. Wagner, Dual antitumoral potency of EG5 siRNA nanoplexes armed with cytotoxic bifunctional glutamyl-methotrexate targeting ligand, Biomaterials, 77 (2016) 98-110.
[54] S.D. Li, Y.C. Chen, M.J. Hackett, L. Huang, Tumor-targeted delivery of siRNA by self-assembled nanoparticles, Mol Ther, 16 (2008) 163-169.
[55] J. Schafer, S. Hobel, U. Bakowsky, A. Aigner, Liposome-polyethylenimine complexes for enhanced DNA and siRNA delivery, Biomaterials, 31 (2010) 6892-6900.
[56] D.J. Siegwart, K.A. Whitehead, L. Nuhn, G. Sahay, H. Cheng, S. Jiang, M. Ma, A. Lytton-Jean, A. Vegas, P. Fenton, C.G. Levins, K.T. Love, H. Lee, C. Cortez, S.P. Collins, Y.F. Li, J. Jang, W. Querbes, C. Zurenko, T. Novobrantseva, R. Langer, D.G. Anderson, Combinatorial synthesis of chemically diverse core-shell nanoparticles for intracellular delivery, Proc Natl Acad Sci U S A, 108 (2011) 12996-13001.
[57] S. Mitragotri, D.G. Anderson, X. Chen, E.K. Chow, D. Ho, A.V. Kabanov, J.M. Karp, K. Kataoka, C.A. Mirkin, S.H. Petrosko, J. Shi, M.M. Stevens, S. Sun, S. Teoh, S.S. Venkatraman, Y. Xia, S. Wang, Z. Gu, C. Xu, Accelerating the translation of nanomaterials in biomedicine, ACS Nano, 9 (2015) 6644-6654.
[58] D.J. Glover, H.J. Lipps, D.A. Jans, Towards safe, non-viral therapeutic gene expression in humans, Nat Rev Genet, 6 (2005) 299-310.
[59] J.C. Kasper, C. Troiber, S. Kuchler, E. Wagner, W. Friess, Formulation development of lyophilized, long-term stable siRNA/oligoaminoamide polyplexes, Eur J Pharm Biopharm, 85

(2013) 294-305.
[60] N. Penacho, S. Simoes, M.C. de Lima, Polyethylenimine of various molecular weights as adjuvant for transfection mediated by cationic liposomes, Mol Membr Biol, 26 (2009) 249-263.
[61] I.W. McLean, P.K. Nakane, Periodate-lysine-paraformaldehyde fixative. A new fixation for immunoelectron microscopy, J Histochem Cytochem, 22 (1974) 1077-1083.
[62] X.M. Xu, Y. Chen, J. Chen, S. Yang, F. Gao, C.B. Underhill, K. Creswell, L. Zhang, A peptide with three hyaluronan binding motifs inhibits tumor growth and induces apoptosis, Cancer Res, 63 (2003) 5685-5690.
[63] D. Schaffert, N. Badgujar, E. Wagner, Novel Fmoc-polyamino acids for solid-phase synthesis of defined polyamidoamines, Org Lett, 13 (2011) 1586-1589.
[64] M. Meyer, A. Philipp, R. Oskuee, C. Schmidt, E. Wagner, Breathing life into polycations: functionalization with pH-responsive endosomolytic peptides and polyethylene glycol enables siRNA delivery, J Am Chem Soc, 130 (2008) 3272-3273.
[65] A. Zintchenko, A. Philipp, A. Dehshahri, E. Wagner, Simple modifications of branched PEI lead to highly efficient siRNA carriers with low toxicity, Bioconjug Chem, 19 (2008) 1448-1455.
[66] C.Y. Zhang, P. Kos, K. Muller, W. Schrimpf, C. Troiber, U. Lächelt, C. Scholz, D.C. Lamb, E. Wagner, Native chemical ligation for conversion of sequence-defined oligomers into targeted pDNA and siRNA carriers, J Control Release, 180 (2014) 42-50.
[67] J.F. Ross, P.K. Chaudhuri, M. Ratnam, Differential regulation of folate receptor isoforms in normal and malignant tissues *in vivo* and in established cell lines. Physiologic and clinical implications, Cancer, 73 (1994) 2432-2443.
[68] H.S. Yoo, T.G. Park, Folate-receptor-targeted delivery of doxorubicin nano-aggregates stabilized by doxorubicin-PEG-folate conjugate, J Control Release, 100 (2004) 247-256.
[69] E.Q. Song, Z.L. Zhang, Q.Y. Luo, W. Lu, Y.B. Shi, D.W. Pang, Tumor cell targeting using folate-conjugated fluorescent quantum dots and receptor-mediated endocytosis, Clin Chem, 55 (2009) 955-963.
[70] Y. Wang, Y. Wang, J. Xiang, K. Yao, Target-specific cellular uptake of taxol-loaded heparin-PEG-folate nanoparticles, Biomacromolecules, 11 (2010) 3531-3538.
[71] A.K. Patri, J.F. Kukowska-Latallo, J.R. Baker, Jr., Targeted drug delivery with dendrimers: comparison of the release kinetics of covalently conjugated drug and non-covalent drug inclusion complex, Adv Drug Deliv Rev, 57 (2005) 2203-2214.
[72] C. Plank, B. Oberhauser, K. Mechtler, C. Koch, E. Wagner, The influence of endosome-disruptive peptides on gene transfer using synthetic virus-like gene transfer systems, J Biol Chem, 269 (1994) 12918-12924.
[73] J. Soutschek, A. Akinc, B. Bramlage, K. Charisse, R. Constien, M. Donoghue, S. Elbashir, A. Geick, P. Hadwiger, J. Harborth, M. John, V. Kesavan, G. Lavine, R.K. Pandey, T. Racie, K.G. Rajeev, I. Rohl, I. Toudjarska, G. Wang, S. Wuschko, D. Bumcrot, V. Koteliansky, S. Limmer, M. Manoharan, H.P. Vornlocher, Therapeutic silencing of an endogenous gene by systemic administration of modified siRNAs, Nature, 432 (2004) 173-178.
[74] P. Kos, U. Lächelt, A. Herrmann, F.M. Mickler, M. Döblinger, D. He, A. Krhac Levacic, S. Morys, C. Bräuchle, E. Wagner, Histidine-rich stabilized polyplexes for cMet-directed tumor-targeted gene transfer, Nanoscale, 7 (2015) 5350-5362.
[75] D. He, K. Müller, A. Krhac Levacic, P. Kos, U. Lächelt, E. Wagner, Combinatorial optimization of sequence-defined oligo(ethanamino)amides for folate receptor-targeted pDNA and siRNA delivery, Bioconjug Chem, 27 (2016) 647-659.
[76] D.J. Lee, D. He, E. Kessel, K. Padari, S. Kempter, U. Lächelt, J.O. Rädler, M. Pooga, E. Wagner, Tumoral gene silencing by receptor-targeted combinatorial siRNA polyplexes, J Control Release, 244 (2016) 280–291.
[77] S.D. Boss, T. Betzel, C. Müller, C.R. Fischer, S. Haller, J. Reber, V. Groehn, R. Schibli, S.M. Ametamey, Comparative studies of three pairs of α- and γ-conjugated folic acid derivatives labeled with Fluorine-18, Bioconjug Chem, 27 (2016) 74-86.

[78] K.N. Chung, Y. Saikawa, T.H. Paik, K.H. Dixon, T. Mulligan, K.H. Cowan, P.C. Elwood, Stable transfectants of human MCF-7 breast cancer cells with increased levels of the human folate receptor exhibit an increased sensitivity to antifolates, J Clin Invest, 91 (1993) 1289-1294.
[79] C.M. Paulos, J.A. Reddy, C.P. Leamon, M.J. Turk, P.S. Low, Ligand binding and kinetics of folate receptor recycling *in vivo*: impact on receptor-mediated drug delivery, Mol Pharmacol, 66 (2004) 1406-1414.
[80] P.C. Elwood, Molecular cloning and characterization of the human folate-binding protein cDNA from placenta and malignant tissue culture (KB) cells, J Biol Chem, 264 (1989) 14893-14901.
[81] H. Margus, K. Padari, M. Pooga, Insights into cell entry and intracellular trafficking of peptide and protein drugs provided by electron microscopy, Adv Drug Deliv Rev, 65 (2013) 1031-1038.
[82] G.F. Walker, C. Fella, J. Pelisek, J. Fahrmeir, S. Boeckle, M. Ogris, E. Wagner, Toward synthetic viruses: endosomal pH-triggered deshielding of targeted polyplexes greatly enhances gene transfer *in vitro* and *in vivo*, Mol Ther, 11 (2005) 418-425.
[83] K. Mechtler, E. Wagner, Gene transfer mediated by influenza virus peptides: the role of peptide sequence, New J Chem, 21 (1997) 105-111.
[84] E. Wagner, Effects of membrane-active agents in gene delivery, J Control Release, 53 (1998) 155-158.
[85] P.M. Klein, K. Müller, C. Gutmann, P. Kos, A. Krhac Levacic, D. Edinger, M. Höhn, J.C. Leroux, M.A. Gauthier, E. Wagner, Twin disulfides as opportunity for improving stability and transfection efficiency of oligoaminoethane polyplexes, J Control Release, 205 (2015) 109-119.
[86] F. Alexis, E. Pridgen, L.K. Molnar, O.C. Farokhzad, Factors affecting the clearance and biodistribution of polymeric nanoparticles, Mol Pharm, 5 (2008) 505-515.
[87] J.M. Layzer, A.P. McCaffrey, A.K. Tanner, Z. Huang, M.A. Kay, B.A. Sullenger, *In vivo* activity of nuclease-resistant siRNAs, RNA, 10 (2004) 766-771.
[88] G. Gaietta, T.J. Deerinck, S.R. Adams, J. Bouwer, O. Tour, D.W. Laird, G.E. Sosinsky, R.Y. Tsien, M.H. Ellisman, Multicolor and electron microscopic imaging of connexin trafficking, Science, 296 (2002) 503-507.
[89] A. Bennett, J. Liu, D. Van Ryk, D. Bliss, J. Arthos, R.M. Henderson, S. Subramaniam, Cryoelectron tomographic analysis of an HIV-neutralizing protein and its complex with native viral gp120, J Biol Chem, 282 (2007) 27754-27759.
[90] J. Gilleron, W. Querbes, A. Zeigerer, A. Borodovsky, G. Marsico, U. Schubert, K. Manygoats, S. Seifert, C. Andree, M. Stoter, H. Epstein-Barash, L. Zhang, V. Koteliansky, K. Fitzgerald, E. Fava, M. Bickle, Y. Kalaidzidis, A. Akinc, M. Maier, M. Zerial, Image-based analysis of lipid nanoparticle-mediated siRNA delivery, intracellular trafficking and endosomal escape, Nat Biotechnol, 31 (2013) 638-646.
[91] W. Zhang, K. Müller, E. Kessel, S. Reinhard, D. He, P.M. Klein, M. Höhn, W. Rödl, S. Kempter, E. Wagner, Targeted siRNA delivery using a lipo-oligoaminoamide nano-core with an influenza peptide and transferrin shell, Adv Healthc Mater, 5 (2016) 1493-1504.
[92] J. Gruenberg, The endocytic pathway: a mosaic of domains, Nat Rev Mol Cell Biol, 2 (2001) 721-730.
[93] A. Sorkin, M. Von Zastrow, Signal transduction and endocytosis: close encounters of many kinds, Nat Rev Mol Cell Biol, 3 (2002) 600-614.
[94] K.E. Sapsford, L. Berti, I.L. Medintz, Materials for fluorescence resonance energy transfer analysis: beyond traditional donor-acceptor combinations, Angew Chem Int Ed Engl, 45 (2006) 4562-4589.
[95] F.M. van de Water, O.C. Boerman, A.C. Wouterse, J.G. Peters, F.G. Russel, R. Masereeuw, Intravenously administered short interfering RNA accumulates in the kidney and selectively suppresses gene function in renal proximal tubules, Drug Metab Dispos, 34 (2006) 1393-1397.
[96] D. Brambilla, P. Luciani, J.C. Leroux, Breakthrough discoveries in drug delivery technologies: the next 30 years, J Control Release, 190 (2014) 9-14.

[97] J. Wartiovaara, L.G. Ofverstedt, J. Khoshnoodi, J. Zhang, E. Makela, S. Sandin, V. Ruotsalainen, R.H. Cheng, H. Jalanko, U. Skoglund, K. Tryggvason, Nephrin strands contribute to a porous slit diaphragm scaffold as revealed by electron tomography, J Clin Invest, 114 (2004) 1475-1483.
[98] Y.H. Bae, K. Park, Targeted drug delivery to tumors: myths, reality and possibility, J Control Release, 153 (2011) 198-205.
[99] Y. Saikawa, C.B. Knight, T. Saikawa, S.T. Page, B.A. Chabner, P.C. Elwood, Decreased expression of the human folate receptor mediates transport-defective methotrexate resistance in KB cells, J Biol Chem, 268 (1993) 5293-5301.
[100] R. Zhao, I.D. Goldman, Resistance to antifolates, Oncogene, 22 (2003) 7431-7457.
[101] D.S. Theti, A.L. Jackman, The role of alpha-folate receptor-mediated transport in the antitumor activity of antifolate drugs, Clin Cancer Res, 10 (2004) 1080-1089.
[102] G.R. Westerhof, S. Rijnboutt, J.H. Schornagel, H.M. Pinedo, G.J. Peters, G. Jansen, Functional activity of the reduced folate carrier in KB, MA104, and IGROV-I cells expressing folate-binding protein, Cancer Res, 55 (1995) 3795-3802.
[103] G.R. Westerhof, J.H. Schornagel, I. Kathmann, A.L. Jackman, A. Rosowsky, R.A. Forsch, J.B. Hynes, F.T. Boyle, G.J. Peters, H.M. Pinedo, et al., Carrier- and receptor-mediated transport of folate antagonists targeting folate-dependent enzymes: correlates of molecular-structure and biological activity, Mol Pharmacol, 48 (1995) 459-471.
[104] M.J. Spinella, K.E. Brigle, E.E. Sierra, I.D. Goldman, Distinguishing between folate receptor-alpha-mediated transport and reduced folate carrier-mediated transport in L1210 leukemia cells, J Biol Chem, 270 (1995) 7842-7849.
[105] O.L. Padilla De Jesus, H.R. Ihre, L. Gagne, J.M. Frechet, F.C. Szoka, Jr., Polyester dendritic systems for drug delivery applications: *in vitro* and *in vivo* evaluation, Bioconjug Chem, 13 (2002) 453-461.
[106] S. Gurdag, J. Khandare, S. Stapels, L.H. Matherly, R.M. Kannan, Activity of dendrimer-methotrexate conjugates on methotrexate-sensitive and -resistant cell lines, Bioconjug Chem, 17 (2006) 275-283.
[107] T.P. Thomas, B. Huang, S.K. Choi, J.E. Silpe, A. Kotlyar, A.M. Desai, H. Zong, J. Gam, M. Joice, J.R. Baker, Jr., Polyvalent dendrimer-methotrexate as a folate receptor-targeted cancer therapeutic, Mol Pharm, 9 (2012) 2669-2676.
[108] D.S. Rosenblatt, V.M. Whitehead, N. Vera, A. Pottier, M. Dupont, M.J. Vuchich, Prolonged inhibition of DNA synthesis associated with the accumulation of methotrexate polyglutamates by cultured human cells, Mol Pharmacol, 14 (1978) 1143-1147.
[109] B.A. Kamen, A.K. Smith, A review of folate receptor alpha cycling and 5-methyltetrahydrofolate accumulation with an emphasis on cell models *in vitro*, Adv Drug Deliv Rev, 56 (2004) 1085-1097.
[110] B. Rippe, B.I. Rosengren, O. Carlsson, D. Venturoli, Transendothelial transport: the vesicle controversy, J Vasc Res, 39 (2002) 375-390.
[111] L.H. Matherly, D.I. Goldman, Membrane transport of folates, Vitam Horm, 66 (2003) 403-456.
[112] M. Creixell, N.A. Peppas, Co-delivery of siRNA and therapeutic agents using nanocarriers to overcome cancer resistance, Nano Today, 7 (2012) 367-379.
[113] J.P. Behr, The proton sponge: a trick to enter cells the viruses did not exploit, Chimia, 51 (1997) 34-36.
[114] N.D. Sonawane, F.C. Szoka, Jr., A.S. Verkman, Chloride accumulation and swelling in endosomes enhances DNA transfer by polyamine-DNA polyplexes, J Biol Chem, 278 (2003) 44826-44831.
[115] K. Müller, E. Kessel, P.M. Klein, M. Hoehn, E. Wagner, Post-PEGylation of siRNA lipo-oligoamino amide polyplexes using tetra-glutamylated folic acid as ligand for receptor-targeted delivery, Mol Pharm, 13 (2016) 2332-2345.

[116] G. Jarad, J.H. Miner, Update on the glomerular filtration barrier, Curr Opin Nephrol Hypertens, 18 (2009) 226-232.
[117] T. Yamaoka, Y. Tabata, Y. Ikada, Distribution and tissue uptake of poly(ethylene glycol) with different molecular weights after intravenous administration to mice, J Pharm Sci, 83 (1994) 601-606.
[118] X. Zhao, H. Li, R.J. Lee, Targeted drug delivery via folate receptors, Expert Opin Drug Deliv, 5 (2008) 309-319.
[119] M.J. Ernsting, M. Murakami, A. Roy, S.D. Li, Factors controlling the pharmacokinetics, biodistribution and intratumoral penetration of nanoparticles, J Control Release, 172 (2013) 782-794.
[120] K. Park, To PEGylate or not to PEGylate, that is not the question, J Control Release, 142 (2010) 147-148.
[121] U. Lächelt, E. Wagner, Nucleic acid therapeutics using polyplexes: a journey of 50 years (and beyond), Chem Rev, 115 (2015) 11043-11078.
[122] B.D. Chithrani, W.C. Chan, Elucidating the mechanism of cellular uptake and removal of protein-coated gold nanoparticles of different sizes and shapes, Nano Lett, 7 (2007) 1542-1550.
[123] Y. Aoyama, T. Kanamori, T. Nakai, T. Sasaki, S. Horiuchi, S. Sando, T. Niidome, Artificial viruses and their application to gene delivery. Size-controlled gene coating with glycocluster nanoparticles, J Am Chem Soc, 125 (2003) 3455-3457.
[124] F. Osaki, T. Kanamori, S. Sando, T. Sera, Y. Aoyama, A quantum dot conjugated sugar ball and its cellular uptake. On the size effects of endocytosis in the subviral region, J Am Chem Soc, 126 (2004) 6520-6521.
[125] K. Miyata, N. Nishiyama, K. Kataoka, Rational design of smart supramolecular assemblies for gene delivery: chemical challenges in the creation of artificial viruses, Chem. Soc. Rev., 41 (2012) 2562-2574.
[126] C.A. Alabi, K.T. Love, G. Sahay, T. Stutzman, W.T. Young, R. Langer, D.G. Anderson, FRET-labeled siRNA probes for tracking assembly and disassembly of siRNA nanocomplexes, ACS Nano, 6 (2012) 6133-6141.
[127] J. Wang, L. Li, H. Cang, G. Shi, J. Yi, NADPH oxidase-derived reactive oxygen species are responsible for the high susceptibility to arsenic cytotoxicity in acute promyelocytic leukemia cells, Leuk Res, 32 (2008) 429-436.
[128] A.M. Oltra, F. Carbonell, C. Tormos, A. Iradi, G.T. Saez, Antioxidant enzyme activities and the production of MDA and 8-oxo-dG in chronic lymphocytic leukemia, Free Radic Biol Med, 30 (2001) 1286-1292.
[129] Y.M. Go, D.P. Jones, Redox compartmentalization in eukaryotic cells, Biochim Biophys Acta, 1780 (2008) 1273-1290.
[130] U.K. Udensi, P.B. Tchounwou, Dual effect of oxidative stress on leukemia cancer induction and treatment, J Exp Clin Cancer Res, 33 (2014) 106.
[131] R. Kanasty, J.R. Dorkin, A. Vegas, D. Anderson, Delivery materials for siRNA therapeutics, Nat Mater, 12 (2013) 967-977.
[132] X. Zhu, Y. Xu, L.M. Solis, W. Tao, L. Wang, C. Behrens, X. Xu, L. Zhao, D. Liu, J. Wu, N. Zhang, Wistuba, II, O.C. Farokhzad, B.R. Zetter, J. Shi, Long-circulating siRNA nanoparticles for validating Prohibitin1-targeted non-small cell lung cancer treatment, Proc Natl Acad Sci U S A, 112 (2015) 7779-7784.
[133] E. Wagner, Polymers for nucleic acid transfer-an overview, Adv Genet, 88 (2014) 231-261.

8 Publications

8.1 Original articles

1. Dian-Jang Lee, Eva Kessel, Daniel Edinger, Dongsheng He, Philipp M. Klein, Lena Voith von Voithenberg, Don C. Lamb, Ulrich Lächelt, Taavi Lehto, Ernst Wagner. Dual antitumoral potency of EG5 siRNA nanoplexes armed with cytotoxic bifunctional glutamyl-methotrexate targeting ligand, **Biomaterials** 2016;77:98-110
2. Dian-Jang Lee, Dongsheng He, Eva Kessel, Kärt Padari, Susanne Kempter, Joachim O. Rädler, Margus Pooga, Ernst Wagner. Tumoral gene silencing by receptor-targeted combinatorial siRNA polyplexes, **J Control Release** 2016;244: 280–291
3. Philipp M. Klein, Sören Reinhard, Dian-Jang Lee, Katharina Müller, Daniela Ponader, Laura Hartmann, Ernst Wagner. Precise redox-sensitive cleavage sites for improved bioactivity of siRNA lipopolyplexes. **Nanoscale** 2016;8:18098-18104

8.2 Book chapter

Dian-Jang Lee, Taavi Lehto, Ernst Wagner. Sequence-defined oligoaminoamides for the delivery of siRNAs, **Methods Mol Biol**. 2015;1206:15-27

8.3 Submitted manuscript

Dian-Jang Lee, Eva Kessel, Taavi Lehto, Xueying Liu, Naoto Yoshinaga, Kärt Padari, Yin-Chen Chen, Susanne Kempter, Satoshi Uchida, Joachim O. Rädler, Margus Pooga, Ming-Thau Sheu, Kazunori Kataoka, Ernst Wagner. Systemic delivery of folate-PEG siRNA lipopolyplexes with enhanced intracellular stability for gene silencing in leukemia, **submitted**.

8.4 Oral presentations

1. Dian-Jang Lee, Eva Kessel, Dongsheng He, Philipp M. Klein, Ulrich Lächelt, Ernst Wagner. Oligoaminoamide-based siRNA carriers for *in vivo* tumor targeting and gene silencing. **126th German Pharmaceutical Society (DPhG) Annual Meeting**, Oct 5-7, 2016, Munich, Germany
2. Dian-Jang Lee, Ulrich Lächelt, Daniel Edinger, Dongsheng He, Taavi Lehto, Ernst Wagner. siRNA nanocarriers with targeting ligand methotrexate. **Nanosystems Initiative Munich Summer School**, Jun 25-27, 2015, Kreuth, Germany

8.5 Poster presentations

1. Philipp M. Klein, Sören Reinhard, Dian-Jang Lee, Katharina Müller, Daniela Ponader, Laura Hartmann, Ernst Wagner. Precise integration of redox-sensitive cleavage sites for enhanced gene silencing and reduced toxicity of siRNA lipo-polyplexes. **22th German Society for Gene Therapy (DG-GT) Annual Meeting**, Sep 14-16, 2016, Heidelberg, Germany
2. Dian-Jang Lee, Dongsheng He, Eva Kessel, Ulrich Lächelt, Ernst Wagner. Folate-conjugated oligomer-based combinatorial nanocarrier for tumor-targeted siRNA delivery. **14th European Symposium on Controlled Drug Delivery (ESCDD)**, Apr 13-15, 2016, Egmond aan Zee, Netherlands
3. Dian-Jang Lee, Dongsheng He, Eva Kessel, Ulrich Lächelt, Ernst Wagner. Combinatorial siRNA polyplex for folate receptor-directed gene silencing efficiency and tumor targeting. **14th International Congress on Targeted Anticancer Therapies**, Mar 21-23, 2016, Washington DC, USA
4. Dian-Jang Lee, Eva Kessel, Dongsheng He, Philipp M. Klein, Ulrich Lächelt, Taavi Lehto, Ernst Wagner. Synergistic antitumoral potency mediated by EG5 siRNA nanoplexes with bifunctional glutamyl-MTX targeting ligand. **29th American Association of Pharmaceutical Scientists (AAPS) Annual Meeting**, Oct 25-29, 2015, Orlando, USA
5. Dian-Jang Lee, Eva Kessel, Dongsheng He, Philipp M. Klein, Ulrich Lächelt, Taavi Lehto, Ernst Wagner. Targeted Co-delivery of bifunctional glutamyl-methotrexate and EG5 siRNA using nanoplexes for combined antitumoral potency. **125th German Pharmaceutical Society (DPhG) Annual Meeting**, Sep 23-25, 2015, Düsseldorf, Germany
6. Dongsheng He, Katharina Müller, Petra Kos, Dian-Jang Lee, Ulrich Lächelt, Ernst Wagner. Cargo-specific optimization of sequence-defined non-viral nucleic acid carriers for folate receptor targeted pDNA and siRNA delivery. **20th German Society for Gene Therapy (DG-GT) Annual Meeting**, Mar. 20-22, 2014, Ulm, Germany

8.6 Honors

2016 Best Manuscript of the Year in Physical Pharmacy and Biopharmaceutics section (PPB), American Association of Pharmaceutical Scientists (AAPS)

2016 Jan Feijen Poster Prize certified by J Control Release,
14th European Symposium on Controlled Drug Delivery (ESCDD)

2016 German Research Foundation (DFG) Clusters of Excellence
Nanosystems Initiative Munich (NIM) Research Visit Grant

2015-2016 Elected Student Representative, Center for NanoScience (CeNS),
Ludwig-Maximilians-Universität München

2015 European Molecular Biology Organization (EMBO) Short-Term Fellowship

2015 Center for NanoScience (CeNS) Travel Award, Ludwig-Maximilians-Universität München

2013-2016 Bavarian Research Foundation (BFS) Research Fellowship, Germany

9 Acknowledgements

As a veterinary student, I finally took part in an actual clinic in a neat scrub suit, learning to be a professional veterinarian after all these years of training and waiting. I am fascinated by the effects and kinetics of drugs, which appeared to have the possibility of instant gratification from an act of therapeutic intervention, a clear separation of before and after, of then and now, of suffering and cure. And also, it arouses my motivation in pursuing advanced graduate training in pharmaceutical science.

My research experience in Germany dramatically broadens my horizons. First of all, I appreciate the supervision from Prof. Dr. Ernst Wagner, who is a very dedicated and energetic scientist with sharp precision. I will never forget the moments while we chattered along the way to Kühtai in his BMW M3 at >200 km/h, while we discussed about how combinatorial polyplexes form hypothetic nanogel structures, and while we won the poster prize at ESCDD meeting. Prof. Dr. Joachim O. Rädler as my NIM co-advisor, and Prof. Dr. Don C. Lamb are always supportive to my studies. In AK Rädler, I learned a lot from the productive discussions with physicists and TEM measurements with Susi. In AK Lamb, it was a successful collaboration with Lena to characterize nanoplexes using FCS and she especially prepared a cake to celebrate the publication of this MTX paper.

I appreciate such great guidance from my colleagues to help me get involved in this environment while I was a newcomer. Taavi supervised my initial projects, and together we had a lot of fun in D 3.017. Andi gave me gene safety instruction, and Miriam gave me cell culture instruction fitting AK Wagner. Katharina, Adam and Petra taught me a lot of *in vitro* assays, and their working efficiency really impressed me. Uli is the most experienced scientist with our oligomer systems beside Prof. Wagner in the lab, he is very insightful about my experiments and provides significant inputs in MTX and TCP projects. Xiaowen invited Dongsheng and me to his place for a welcome dinner. Annika taught me *in vivo* assays and put a lot of efforts in application of our animal experiment permission. Moreover, "Scholz, C. & Wagner, E. (2012) *Therapeutic plasmid DNA versus siRNA delivery: common and different tasks for synthetic carriers*" was an excellent guide for me at that time, and till now, it is still classic.

I have learned not to be afraid of the setbacks but to learn from the setbacks; I have learned to savor every small victory, every subtle moment of ongoing experiments in the lab. During my PhD years, Dongsheng has been striving with me to develop TCP formulations for 2.5 years. Together with Philipp K. and Sören, we also screened many oligomers in different cell lines. Eva is very skillful at *in vivo* studies but sometimes too busy to have lunch. In the animal room, we performed experiments also on weekends, we monitored clinical signs of mice, and we shared the disappointments and excitements about *in vivo* studies. In addition, discussions with Wei and Jonathan are definitely valuable to me.

Meanwhile, I would like to thank our powerful support team: Wolfgang (chemicals, instruments, IT…difficult to list them all), Markus (animal facility maintenance), Olga (secretarial assistance), Melinda (mycoplasma tests), Ursula and Anna (cell culture room maintenance). Through numerous lab events organized by colleagues, we had glittering memories together: ski trips, BBQ, Oktoberfest (it is noteworthy that drunken Dongsheng vomited in Oktoberfest 2013) and gifts for PhD graduates (mainly by Ruth, Katharina, Ines and Jasmin), hiking, Fasching and Christmas parties (by Martina), celebrations for new publications (I still kept the wine bottles as souvenirs) (by Prof. Wagner and Uli), football games (by Andi and Bojan), and lab dinners (Philipp K. is a big fan of Peking duck) (by Wei and Jonathan).

I feel privileged that Prof. Ming-Thau Sheu (Taipei Medical University, Taiwan) always supports me without restrictions. He co-advised TLP and intratumoral pharmacokinetics projects, and visited AK Wagner in 2014. His senior PhD student, Yen-Chen, also had a research visit for this collaboration in Munich in the same year.

At systemic level, the fact that tumor vascular supply may limit tumor drug uptake is surely one of my major concerns. Apart from that, I am also interested in morphology and intracellular pharmacokinetics of siRNA polyplexes at ultrastructural or molecular level. Using TEM with Susi (AK Rädler), and using AFM with Dr. Rong Zhu (AK Hinterdorfer, Johannes-Kepler-Universität Linz, Austria), eventually I was able to see "*these siRNA polyplexes which I have been working on for so long!*" Furthermore, using immuno-TEM with Dr. Kärt Padari (AK Pooga, University of Tartu, Estonia), and using time-lapse CLSM and FRET study with Dr. Xueying Liu and Naoto (AK Kataoka, iCONM and University of Tokyo, Japan), I could even visualize how siRNA polyplexes interacted with receptors and trafficked through the endolysosomal pathway. Interestingly, it reminds me that while I was a sophomore in Prof. Ling-Ling Que's class, she told us how delighted she was while she observed her research subject, *Salmonella* Typhimurium, under TEM, as a graduate student (in 1979). "*It is just like…after expecting for months, for the first time you finally see your own baby!*" So vividly, she said with full of joy. I couldn't understand her at that time, but now I really feel the similar sense of achievement. Almost 4 decades later, thanks to more advanced technology, I not only see "*my baby*", in this sense, but also see "*my baby crawling and playing toys*".

An essential aspect of CeNS is a broad array of research activities at the nanoscale that seek to develop next-generation devices, therapeutics or techniques. I'm glad to be elected as student representative together with Franzi and Luisa, and planned many events to facilitate interactions among colleagues with diverse expertise/from different faculties. With Susanne's indispensable help, we invited foreign speaker, and organized lab tour, BBQ, "Science in a Nutshell"/welcome party, and company visit.

Absolutely, it is my great honor to work with these talented colleagues, together we showed strong teamwork (also at interdisciplinary and international level), and encouragingly, our work has been recognized by representative journals and societies.

As John Donne said, "*no man is an island*." For these years living in Germany, I especially thank Yen-Chi, Cheng-Chang, Pang-Yen and Ching-Ning. I really cherish the time spending with them and warm supports from them. Without their presences, my daily life in Munich can be lonely and tasteless (or even miserable). I also enjoy lunch time with Yu-Kai, Chien-Sin, Tsai-Hsuan, Fang-Yu, Hung-En, Hsin-Yi and Liang-Yu on Wednesdays, and basketball games with Peng, Philipp K., Sören, Philipp H. and Stephan (it is an advantage that basketball courts are always available because it is not a popular sport here).

I sincerely thank my beloved parents for that I was born physiologically healthy, which is so essential for one's lifetime (though I am sure they never expected their son would guide them to visit Europe 29 years later). I appreciate that they carefully raised me up and cultivated me. I still remember my handwriting was strictly corrected by my father while I was in elementary school. My life philosophy (if anything positive) is deeply influenced by my mother. My lovely grandmother always worries about my diet and personal safety abroad. Also, I thank my younger brothers Wei-Ping and Wei-Jen for taking care of familial obligations for me in Taiwan. Wei-Jen as an IT engineer, particularly helped me to estimate the pharmacokinetic parameters using C program. Moreover, I often receive kind supports from other family members (uncles, aunts and cousins).

Finally, I have learned to appreciate the fact that although I don’t directly provide medical care for animals, my impact on animals and human beings through pharmaceutical research can be no less daunting and no less gratifying. Not only have I learned valuable knowledge and skills from these experiences, I realized how rewarding and meaningful a career for a pharmaceutical scientist can be. More importantly, I am clear that this is the type of career I seek.

I have learned so much, but I still have so much to learn.